Vortex statics and dynamics in anisotropic and/or magnetic superconductors.

Anton Bespalov

université de BORDEAUX

THÈSE PRÉSENTÉE

POUR OBTENIR LE GRADE DE

DOCTEUR DE

L'UNIVERSITÉ DE BORDEAUX

ÉCOLE DOCTORALE: SCIENCES PHYSIQUES ET DE L'INGENIEUR

SPÉCIALITÉ: Lasers, matière et nanosciences

Par Anton BESPALOV

VORTEX STATICS AND DYNAMICS IN ANISOTROPIC AND/OR MAGNETIC SUPERCONDUCTORS

Sous la direction de : Alexandre BOUZDINE
(co-directeur : Alexander MEL'NIKOV)

Soutenue le 29 Septembre 2014

Membres du jury:

M. HOUZET Manuel	Chercheur – CEA Grenoble	Rapporteur
M. RODITCHEV Dimitri	Professeur – Institut des NanoSciences de Paris	Rapporteur
M. TAMARAT Philippe	Professeur – Université de Bordeaux	President
M. VILLEGAS HERNANDES Javier Eulogio	Chercheur – Unité Mixte de Physique CNRS/Thales	Examinateur

Titre : STATIQUE ET DYNAMIQUE DES VORTEX DANS LES SUPRACONDUCTEURS ANISOTROPIQUES ET/OU MAGNÉTIQUES

Résumé : Récemment, les études des propriétés de vortex Abrikosov dans des systèmes fortement anisotropes et magnétiques ont été stimulées par la découverte des supraconducteurs à base de fer et des supraconducteurs ferromagnétiques. Dans cette thèse nous étudions la statique et la dynamique de vortex dans ces systèmes. D'abord, le problème de l'interaction de vortex avec un petit défaut a été examiné dans le cadre de la théorie de Ginzburg-Landau. Le potentiel de pinning pour une cavité cylindrique elliptique a été calculé. D'autre part, la conductivité d'un supraconducteur anisotrope à l'état mixte a été analysée en détail dans le cadre de la théorie de Ginzburg-Landau dépendant du temps.

Une partie significative de la thèse est consacrée à l'étude de l'interaction entre les ondes de spin (magnons) et vortex dans les supraconducteurs ferromagnétiques. Nous avons démontré que le spectre de magnon acquiert une structure de bande en présence d'un réseau de vortex idéal. En utilisant les équations phénoménologiques de London et de Landau-Lifshitz-Gilbert, nous avons étudié les réponses ac et dc de vortex dans les supraconducteurs ferromagnétiques. Enfin, nous avons examiné l'état de vortex dans des structures hybrides supraconducteur(S)-ferromagnétique(F) (par exemple, super-réseaux FS) avec une forte dispersion spatiale de la susceptibilité magnétique. Dans ces systèmes l'électrodynamique supraconductrice peut être fortement non locale, qui mène à l'attraction des vortex et à une transition de phase du premier ordre dans la phase de vortex.

Mots clés : Vortex Abrikosov, pinning, écoulement de vortex, supraconducteurs ferromagnétiques, ondes de spin

Title : VORTEX STATICS AND DYNAMICS IN ANISOTROPIC AND/OR MAGNETIC SUPERCONDUCTORS

Abstract :

Recently, the studies of the properties of Abrikosov vortices in strongly anisotropic and magnetic media have been stimulated by the discovery of the iron-based and ferromagnetic superconductors. In this thesis an analysis of vortex statics and dynamics in such systems has been carried out. Firstly, the problem of vortex pinning on a small defect has been considered. Within the Ginzburg-Landau theory the pinning potential for a cavity in the form of an elliptical cylinder has been derived. Secondly, the flux-flow conductivity of an anisotropic superconductor has been analyzed in detail within the time-dependent Ginzburg-Landau theory.

A significant part of the thesis is devoted to the study of interplay between spin waves (magnons) and vortices in ferromagnetic superconductors. We have demonstrated that the magnon spectrum acquires a Bloch-like band structure in the presence of an ideal vortex lattice. Using the phenomenological London and Landau-Lifshitz-Gilbert equations, we studied the ac and dc responses of vortices in ferromagnetic superconductors. Finally, we investigated the vortex state in superconductor-ferromagnet (FS) hybrid structures (e. g., FS superlattices) with strong spatial dispersion of the magnetic susceptibility. In such systems the superconducting electrodynamics may be strongly nonlocal, which leads to the attraction of vortices and to a first order phase transition at the lower critical field.

Keywords : Abrikosov vortices, pinning, flux-flow, ferromagnetic superconductors, spin waves

---

Unité de recherche

Laboratoire Ondes et Matière d'Aquitaine, UMR 5798, 351 cours de la Libération, 33405 TALENCE CEDEX

Résumé détaillé de la thèse

L'existence d'une résistance électrique non nulle dans les supraconducteurs de type II dans l'état mixte est reliée aux mouvements des vortex de flux magnétique. Dans un supraconducteur dans l'état mixte la conductivité σ est donnée par

$$\sigma = \frac{c^2 \eta}{B_0 \Phi_0},$$

où c est la vitesse de la lumière, B_0 le champ magnétique dans l'échantillon, Φ_0 le quantum de flux, et η est le coefficient de viscosité, qui figure dans l'équation de mouvement des vortex:

$$\frac{\Phi_0}{cB_0} \mathbf{j}_{\text{tr}} \times \mathbf{B}_0 - \eta \mathbf{V}_L = 0.$$

Dans cette relation, $\mathbf{j}_{\text{tr}}$ est la densité de courant de transport, et $\mathbf{V}_{\text{L}}$ la vitesse de flux. Dans le cas général σ et η sont des tenseurs. Les études théoriques sur les écoulements des vortex dans les matériaux anisotropes ont été stimulées par la découverte de supraconducteurs à haute température critique, qui possèdent une structure en couches. En outre, les supraconducteurs à base de fer découverts récemment sont également fortement anisotropes.

Toutefois, les caractéristiques courant-tension typiques des supraconducteurs de type II ne sont pas décrites par la loi d'Ohm. Le supraconducteur peut supporter sans dissipation une densité de courant n'excédant pas une valeur critique $\mathbf{j}_{\text{cr}}$. Ceci s'explique par la présence de défauts dans le supraconducteur, agissant comme des centres de piégeage. Ces défauts peuvent piéger les vortex, de sorte qu'ils restent immobiles quand un petit courant circule dans le supraconducteur. L'implantation des centres de piégeage colonnaires artificiels dans les supraconducteurs peut induire une augmentation drastique du courant critique, si les lignes de flux sont alignées le long de ces défauts.

Ainsi, pour interpréter quantitativement les données expérimentales sur la résistivité des supraconducteurs de type II, il est nécessaire d'estimer la force de fixation et la viscosité η.

La physique de vortex deviens beaucoup plus riche dans les hybrides supraconducteurs et magnétiques. Au cours des 14 dernières années, un certain nombre de composés très intéressants ont été découverts révélant la coexistence de la supraconductivité et du ferromagnétisme en volume: UGe_2 (température critique T_c = 0.7 K) , URhGe (T_c = 0.25 K), UCoGe (T_c = 0.8K), et $EuFe_2As_2$ dopé (T_c = 25 K). De plus, récemment des succès significatifs ont été obtenus dans la fabrication et la caractérisation des super-réseaux supraconducteur-ferromagnétique (SF). Dans ces systèmes différents effets intéressants peuvent résulter de l'interaction entre les vortex d'Abrikosov et les ondes de spin, ou les magnons. En particulier, il a été prédit que la viscosité de vortex η sera augmentée en raison de l'irradiation de magnons par des vortex mobiles.

La thèse présentée est consacrée à l'étude théorique des propriétés statiques et dynamiques des vortex d'Abrikosov dans les deux supraconducteurs ordinaires et ferromagnétiques. Ce travail utilise les approches analytiques suivantes:

- La théorie de London, les théories de Ginzburg-Landau ordinaires et dépendante du temps pour la description de la supraconductivité;
- L'équation de Landau-Lifshitz-Gilbert pour la dynamique de magnétisation.

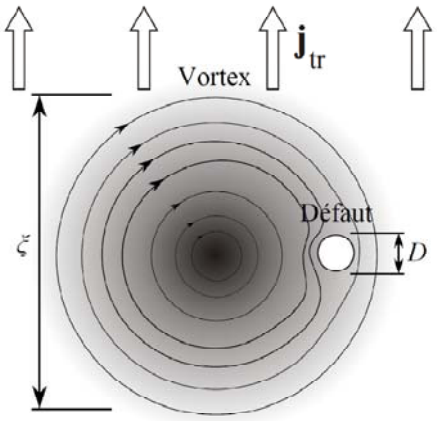

Fig. 1. La section transversale de l'un des systèmes étudiés dans cette thèse: un vortex en interaction avec un petit défaut. ξ est la longueur de cohérence.

Les principaux résultats obtenus dans cette thèse sont:

- Dans le cadre de la théorie de Ginzburg-Landau, une nouvelle approche pour le calcul du potentiel d'interaction de vortex avec un petit défaut isolant cylindrique a été développée. Le potentiel de piégeage pour un défaut cylindrique elliptique et le courant de «désencrage » d'un défaut cylindrique circulaire ont été déterminés. Nous avons prédit l'existence d'un état lié métastable, où le centre du vortex est situé hors du défaut (voir Fig. 1), bien que le vortex reste épinglé. Cet état peut être vu expérimentalement en utilisant la microscopie à effet tunnel ou un nano-SQUID.
- Le tenseur de viscosité $\hat{\eta}$ du vortex a été calculé pour un supraconducteur avec un décalage d'anisotropies de la masse de paire de Cooper et la conductivité normale. Nous avons prédit que l'anisotropie de la conductivité dans l'état mixte peut dépendre fortement de la température, même dans le proche voisinage de T_c. Ces résultats peuvent être utiles pour l'interprétation des données expérimentales sur la résistivité des supraconducteurs à base de fer et des supraconducteurs «cuprates», qui sont fortement anisotropes.
- Nous avons démontré que le spectre de magnons d'un supraconducteur ferromagnétique à l'état mixte a une structure de bande. Le spectre a été calculé analytiquement et numériquement (voir Fig. 2).
- Nous avons aussi calculé la force induite par les moments magnétiques agissant sur les vortex mobiles dans les structures SF hybrides dans les cas d'un courant de transport continu ou alternatif, et pour un réseau de vortex parfait ou désordonnée. Quand les vortex rayonnent des magnons, cette force est augmentée. Par conséquent, certains éléments résonants doivent apparaître sur la courbe I-V de l'échantillon et sur les dépendances de l'impédance de surface en fonction du champ magnétique et de la fréquence.
- Nous avons démontré que dans des systèmes SF avec une grande largeur de la paroi de domaine de Bloch la structure magnétique de vortex est sensiblement modifiée. En particulier, le champ d'un vortex peut changer de signe, qui peut être confirmé expérimentalement en utilisant la technique de rotation de spin de muonique. L'inversion de signe de champ des vortex mène à une interaction attractive entre les vortex et à une transition de phase du premier ordre dans la phase des vortex. Une

conséquence de ceci est la formation d'un état mixte intermédiaire dans une dalle (voir Fig. 3), qui peut être visualisé à l'aide de la technique de décoration de Bitter.

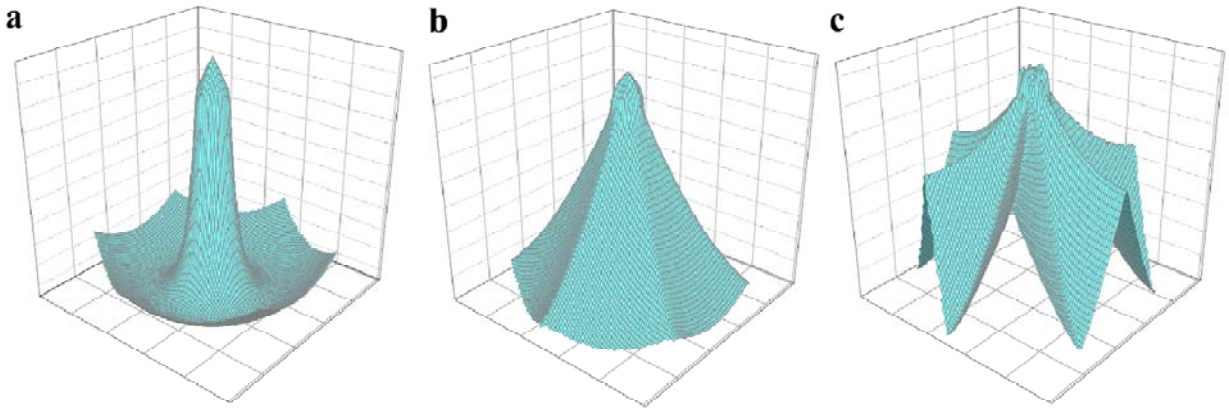

Fig. 2. Spectre des ondes de spin propageant perpendiculairement à l'axe de magnétisation facile dans un supraconducteur ferromagnétique dans l'état mixte. La première zone de Brillouin pour un réseau triangulaire de vortex est affiché. (a), (b) et (c) correspondent à la première, la deuxième et la troisième bande du spectre.

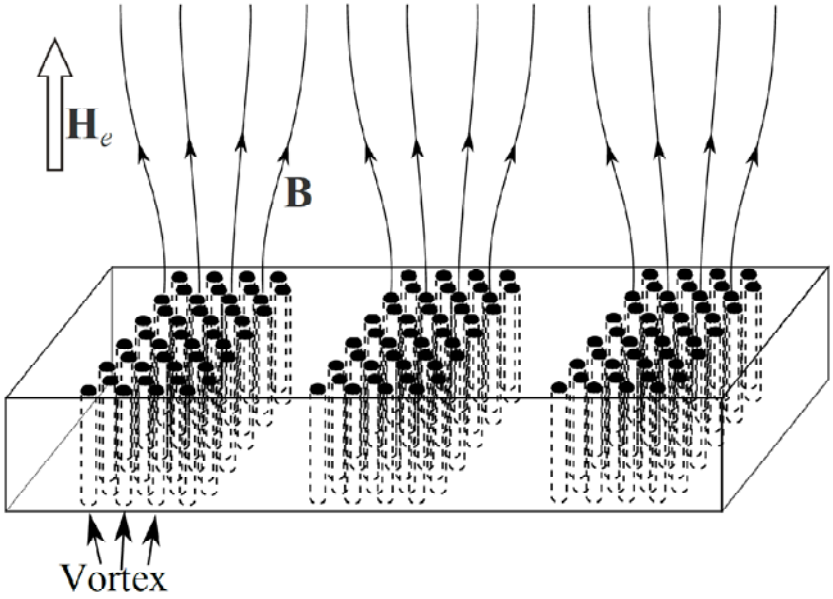

Fig. 3. Une dalle supraconductrice dans l'état mixte intermédiaire. $\mathbf{H}_e$ est le champ magnétique externe.

Acknowledgements

I am very grateful to my scientific advisors, Alexander I. Buzdin and Alexander S. Mel'nikov, for their patience and constant support. It was a great pleasure for me to work with them. The experience that I gained during this cooperation is priceless for me.

I am thankful to my "rapporteurs", Dimitri Roditchev and Manuel Houzet, for carefully reading my manuscript and for useful discussions. I would like to thank also other members of the jury, Javier E. Villegas Hernandes and Philippe Tamarat, for participating in the evaluation of my Thesis and for useful comments.

I am grateful to the members of LOMA, Joseph Leandri, Sébastien Burdin and Isabelle Guillaume, for helping me to resolve technical issues. My special appreciation goes to the librarian of LOMA, Bernadette Bergeret, for her friendship and help with finding necessary books and articles.

I want to express my gratitude to the members of the Institute for Physics of Microstructures RAS in Nizhny Novgorod, Vladislav V. Kurin, Denis Yu. Vodolazov, Iosif D. Tokman, Aleksei V. Samokhvalov and Andrei A. Fraerman, for their interest in my work and for their useful criticism and hints. I thank also Lev. N. Bulaevskii for fruitful discussions.

Finally, I am eternally grateful to my family and friends for their love and encouragement.

Contents

Introduction

The phenomenon of superconductivity, discovered by Kamerlingh Onnes in 1911, has two main hallmarks: a vanishing electrical resistance and the expulsion of the magnetic field, referred to as the Meissner-Ochsenfeld (or simply Meissner) effect [1]. For a long time an unequivocal explanation of these experimental facts had been lacking, until the advent of the Bardeen-Cooper-Schrieffer (BCS) theory [2] in 1957. According to this theory, the emergence of superconductivity is connected with the mutual attraction of electrons due to the exchange of virtual phonons. At low temperatures electrons with opposite spins and momenta form the so-called Cooper pairs, whose size equals the superconducting coherence length ξ. A finite energy is required to destroy these pairs, thereby the quasiparticle spectrum of a superconductor has an energy gap. The presence of this gap explains the zero resistance of the electron gas, as follows from the Landau superfluidity criterion [3]. Note that in the conventional BCS picture the Cooper pairs have a zero spin and angular momentum.

Before the establishment of the BCS theory several simple phenomenological descriptions of superconductivity had been proposed. Among them, the most well-known are the London [4] and Ginzburg-Landau (GL) theories [5]. These were especially successful in describing the perfect conductivity phenomenon and Meissner effect, and, in addition, concealed in themselves some fascinating predictions, which were later confirmed experimentally. In particular, the London theory asserts that an external magnetic field decays exponentially inside the superconductor over a length λ, which is called the London penetration depth. The GL theory predicts that all superconductors can be divided into two classes, based on the value of the GL parameter $\kappa = \lambda/\xi$. Materials with $\kappa < 1/\sqrt{2}$ have a positive superconductor-normal metal boundary energy. The phase diagram of these so-called type-I superconductors in the plane temperature (T)-magnetic field (H) is quite simple (see Fig. 1a): at $T < T_c$, where T_c is a critical temperature, when $H < H_c(T)$ the material is in the superconducting Meissner state (with a vanishing internal induction B), and at $H > H_c(T)$ it is in the normal state. The field $H_c(T)$, called the thermodynamic critical field, is given by [6]

$$H_c = \frac{\Phi_0}{2\sqrt{2}\pi\lambda(T)\xi(T)}, \tag{1}$$

where $\Phi_0 = \pi\hbar c/e \approx 2.06 \times 10^{-7}\mathrm{Gs}\cdot\mathrm{cm}^2$ is the magnetic flux quantum, c is the light velocity, and $e > 0$ is the elementary charge. Equation (1) is valid at $T_c - T \ll T_c$, where the Ginzburg-Landau theory is applicable.

In compounds with $\kappa > 1/\sqrt{2}$ — the type-II superconductors — the energy of the superconducting-normal phase interface is negative. At first, type-II superconductivity was believed to be unphysical. Abrikosov was the first to realize how in materials with

$\kappa > 1/\sqrt{2}$ the superconducting and normal phases may coexist. In his paper [7] he suggested that type-II superconductors may exhibit a mixed state. In this unusual state the magnetic field penetrates the sample in the form of flux lines, known as Abrikosov vortices, carrying one flux quantum Φ_0 each. The vortices have a normal core, which is separated from the rest of the superconductor by a circulating supercurrent. Thus, the boundary between the normal and superconducting phases becomes largely extended, allowing for a gain in the interface energy. In a homogeneous superconductor the vortices should form an ideal 2D-lattice. The field and order parameter profiles of a vortex are depicted in Fig. 1b, and the phase diagram of a type-II superconductor is shown in Fig. 1c. Apart from the Meissner and normal states, it contains the mixed state (or Shubnikov phase), which exists at $H_{c1}(T) < H < H_{c2}(T)$, where H_{c1} and H_{c2} are the lower and upper critical fields, respectively. The London theory in the high-κ limit ($\kappa \gg 1$) gives for H_{c1} the value

$$H_{c1} \approx \frac{\Phi_0}{4\pi\lambda^2} \ln \frac{\lambda}{\xi}. \tag{2}$$

The upper critical field, according to the GL theory [6], equals

$$H_{c2} = \frac{\Phi_0}{2\pi\xi^2}. \tag{3}$$

Note that in type-II superconductors $H_{c2} > H_c$, and in type-I superconductors $H_{c2} < H_c$. For this reason the vortex state is unstable in the latter.

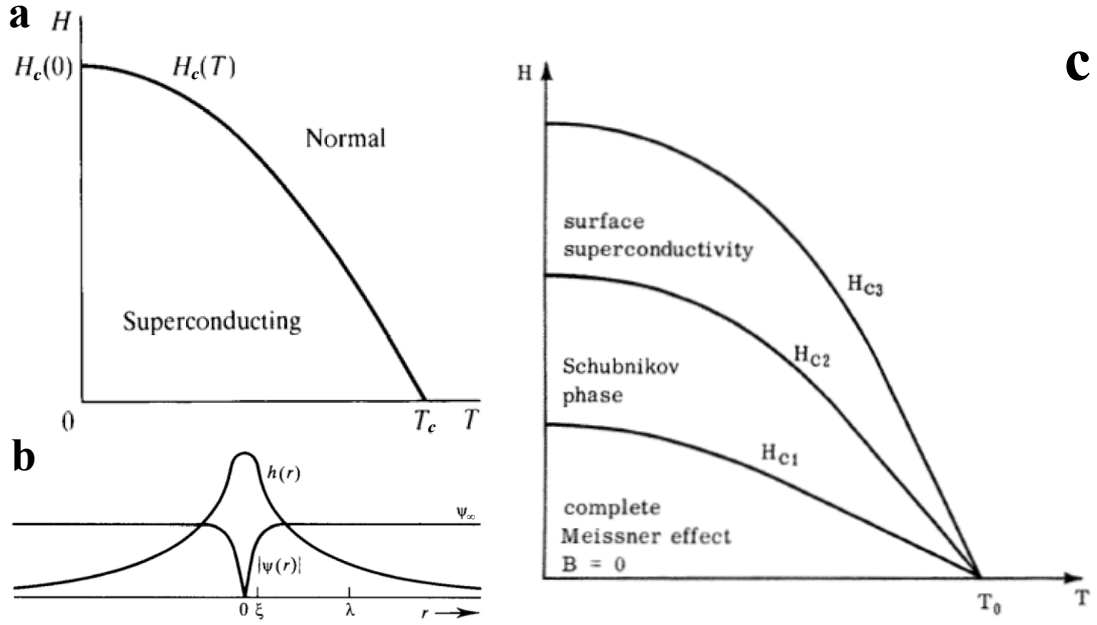

Figure 1: (a) Phase diagram of a type-I superconductor [6]. (b) The magnetic field ($h(r)$) and order parameter modulus ($|\psi(r)|$) profiles of a single Abrikosov vortex [6]. (c) Phase diagram of a type-II superconductor [8]. The third critical field, H_{c3}, and surface superconductivity are not discussed here.

An experimental confirmation of Abrikosov's prediction was obtained in 1964, when the vortex lattice was observed by neutron diffraction [9]. Later, the Bitter decoration technique allowed to see individual vortices [10].

One of the fundamental effects connected with the existence of Abrikosov vortices is the presence of a non-zero resistance in type-II superconductors in the mixed state. This fact is explained by the transport current exerting a force

$$\mathbf{F}_L = \frac{\Phi_0}{cB_0}\mathbf{j}_{\rm tr} \times \mathbf{B_0} \tag{4}$$

on the flux lines [6], setting them in motion. Here, $\mathbf{B}_0$ is the average magnetic field in the superconductor, and $\mathbf{j}_{\rm tr}$ is the transport current density. $\mathbf{F}_L$ is called the Lorentz force. In defect-free superconductors in the stationary flux-flow regime the Lorentz force is balanced by the viscous drag force:

$$\mathbf{F}_L - \eta \mathbf{V}_L = 0, \tag{5}$$

where $\mathbf{V}_L$ is the velocity of the vortices, and η is a viscosity coefficient. It follows from Faraday's law that the moving magnetic flux induces in the superconductor an average electric field

$$\mathbf{E} = \frac{1}{c}\mathbf{B}_0 \times \mathbf{V}_L. \tag{6}$$

The, from Eqs. (4) - (6) we obtain Ohm's law, $\mathbf{j}_{\rm tr} = \sigma \mathbf{E}$, where the conductivity is

$$\sigma = \frac{c^2 \eta}{B_0 \Phi_0}. \tag{7}$$

In anisotropic superconductors both σ and η are tensors. Then, Eq. (7) is generalized as follows:

$$\hat{\sigma} = \frac{c^2}{B_0 \Phi_0} \begin{pmatrix} \eta_{yy} & -\eta_{yx} \\ -\eta_{xy} & \eta_{xx} \end{pmatrix}, \tag{8}$$

when the z-axis is directed along the magnetic field. The peculiar structure of the conductivity tensor is explained by the fact that the x component of the electric field depends on the y component of the vortex velocity, and vice versa.

Typical current-voltage characteristics of type-II superconductors, however, are not described by the simple Ohm's law. The superconductor may support a dissipationless current density $j_{\rm tr}$ not exceeding some critical value $j_{\rm cr}$ [11]. A finite voltage must be applied to introduce in the sample a current density larger than $j_{\rm cr}$. This is explained by the presence of defects in the superconductor, acting as "pinning" centers. These defects may trap (pin) vortices, so that they remain immobile when a small current is flowing through the superconductor. The implantation of artificial columnar pinning centers into superconductors may lead to a drastic increase of the critical current $j_{\rm cr}$, if the flux lines are aligned along the defects (see [12, 13, 14, 15, 16, 17] and references therein). Nowadays, various techniques exist allowing to create disordered arrays of such defects [12, 13], as well as regular defect lattices [18, 19, 20].

When the applied current is sufficiently large ($j_{\rm tr} > j_{\rm cr}$), the Lorentz force will depin the vortices. Then the dissipative flux-flow regime sets in, where vortex motion is governed by Eq. (5), if the pinning force is negligible. Thus, for the quantitative interpretation of experimental data on the resistivity of type-II superconductors, estimates of the pinning force and of the viscosity η are required.

The theoretical investigation of collective pinning of the vortex lattice is known to be a quite complicated task. An extensive review of existing theories, which account for vortex-defect as well as vortex-vortex interactions, can be found in [11]. In order to deduce results which can be quantitatively compared with experimental data, these theories require the individual vortex pinning potential as input. It is known that the efficiency of a pinning array depends not only on the depth of the potential well for a vortex, but also on the shape of the well [21]. Thus, a detailed investigation of single vortex-single defect interactions provides the basis for considerations of many-vortex systems. The problem of individual vortex pinning has been solved exactly for insulating columnar defects of different shapes within the London theory [22, 23, 24, 25, 26, 27]. This approach allows to consider only relatively large defects, with the characteristic cross-section size $D \gg \xi$. In the case $D \lesssim \xi$, the Ginzburg-Landau theory may be applied. Analysis of the interaction of vortices with columnar defects with the size $D \sim \xi$ has been carried out in a number of papers [28, 29, 30, 31]. Due to the nonlinearity of the GL equation, its analytical solution presents a theoretical challenge, especially when the vortex is not centered at the defect. For that reason this equation has been mainly analyzed numerically. Exact expressions for the vortex pinning potential and the depinning current in the case $D \lesssim \xi$ have been lacking so far.

For the calculation of the viscosity η (and, correspondingly, the flux-flow conductivity) two theoretical approaches have been developed. The first method, proposed by Bardeen and Stephen (BS) [32], is based on the London theory and on the simplifying assumption of a step-like order parameter profile of a vortex. This approach usually allows to obtain a correct order-of-magnitude estimate for η. The second, more rigorous method for the calculation of the viscosity is based on the non-stationary generalization of the GL theory — the time-dependent Ginzburg-Landau (TDGL) equation [33, 34, 35]. Within this approach, the flux-flow conductivity has been evaluated for isotropic superconductors in several papers [36, 37, 38].

Theoretical studies of free flux flow in anisotropic materials have been stimulated by the discovery of high-temperature superconductors, which appeared to possess a rather strong anisotropy [39]. A number of papers have addressed this problem using the TDGL equation [40, 41]. It has been shown that the procedure of viscosity calculation can be significantly simplified in the limit of dirty uniaxial superconductors with the ratio $s_0 = m_c\sigma_c/m_{ab}\sigma_{ab}$ equal to unity. Here, σ_c, σ_{ab} and m_c, m_{ab} are the normal conductivities and Cooper-pair masses in the direction of the anisotropy axis c and in the perpendicular ab plane, respectively. The condition $s_0 = 1$ allows to reduce the problem of anisotropic vortex dynamics to an isotropic one by means of a scaling transformation [41]. Yet, this is not true in the case $s_0 \neq 1$, i.e, for a mismatch of anisotropies of Cooper-pair masses and normal conductivities. Such a mismatch is theoretically possible in the relatively clean limit [35] and it may have been experimentally observed in the Fe-based pnictide superconductors [42]. To estimate the parameter s_0 of these materials using given experimental data, we may use the fact that in the vicinity of the critical temperature

$$s_0 = \gamma_H^2/\gamma_\sigma,$$

where

$$\gamma_H = H_{c2,ab}/H_{c2,c}, \qquad \gamma_\sigma = \sigma_{ab}/\sigma_c,$$

and $H_{c2,c}$ and $H_{c2,ab}$ are the second critical fields along and perpendicular to the c axis, respectively. In literature we can find the values $\gamma_H = 1.15$ and $\gamma_\sigma = 3.3$ for LiFeAs [43], $\gamma_H = 5$ and $\gamma_\sigma = 30 - 45$ for $Tl_{0.58}Rb_{0.42}Fe_{1.72}Se_2$ [44], and $\gamma_H = 2$ and $\gamma_\sigma = 21$ for $Sr_{0.6}K_{0.4}Fe_2As_2$ [45]. For $BaFe_2As_2$ [46] and $PrFeAsO_{0.7}$ [47] very large values of the resistivity anisotropy have been reported — $\gamma_\sigma > 100$ — as counterposed to the relatively low anisotropies of the upper critical field ($\gamma_H \sim 1$), typical for Fe-based superconductors [42]. It should be noted that existing experimental data on the pnictides are somewhat contradictory: in [48] and [49] relatively low values $\gamma_\sigma \lesssim 10$ for $BaFe_2As_2$ and $Ba(Fe_{1-x}Co_x)_2As_2$ are given. Still, we can see that there is experimental evidence of a Cooper-pair mass-normal conductivity anisotropy mismatch in the Fe-based superconductors.

Previous calculations of the viscous drag tensor within the TDGL theory accounted for the anisotropy mismatch only on the basis of a simplified model of a step-like order parameter profile in the vortex core [40] (see also [50] for a study using the BS approach). Of course, a detailed comparison with experimental data demands these calculations to be generalized for a more realistic order parameter profile.

Vortex physics becomes much richer in superconducting and magnetic hybrids. Magnetism and superconductivity are known to be antagonistic phenomena: magnetic moments destroy Cooper pairs in two ways [51]. First, the induction $\mathbf{B}$ affects the orbital motion of electrons, tearing apart the Cooper pairs. This so-called electromagnetic mechanism completely suppresses superconductivity when B exceeds the upper critical field H_{c2}. Second, the exchange field in the magnetic material tends to align the electron spins in the same direction, thus preventing the formation of spin-singlet Cooper pairs. This is called the paramagnetic effect. Because of it, in materials with the Curie temperature Θ smaller than T_c spin-singlet superconductivity exists only in a small temperature window below Θ [51], and in the case $T_c \lesssim \Theta$ a nonuniform Fulde-Ferrel-Larkin-Ovchinnikov phase is expected to form [52, 53].

Within the last 14 years, a number of fascinating compounds have been discovered, revealing the coexistence of ferromagnetism and superconductivity in the bulk (see [54] for review): UGe_2 [55] ($T_c = 0.7$ K) , URhGe [56] ($T_c = 0.25$ K), UCoGe [57, 58] ($T_c = 0.8$ K), and doped $EuFe_2As_2$ [59] ($T_c = 25$ K). Remarkably, in most of these compounds $T_c \ll \Theta$. It is believed that superconductivity in these materials is of spin-triplet type, with electron spins in a Cooper pair pointing in the same direction. This allows the Cooper pairs to survive in the strong exchange field. Another interesting property of the ferromagnetic superconductors is the incomplete ac Meissner effect [56, 57, 59], indicating that these materials are in the spontaneous vortex state even in the absence of an external magnetic field.

Magnetic materials support a special type of collective excitations — the spin waves [60]. These waves, being essentially oscillations of the magnetization, are also called magnons. Typically, the spin-wave frequency $\omega(\mathbf{q})$ in ferro- and antiferromagnets depends monotonically on the wave-vector modulus $|\mathbf{q}|$. In superconducting and magnetic hybrids the spin-wave spectrum is significantly influenced by the additional superconducting order. It has been shown that in antiferromagnetic [61] and ferromagnetic superconductors [62, 63] the magnon spectrum in the Meissner state becomes nonmonotonic. A more realistic model of the ferromagnetic superconductor should take into account that the sample is the mixed state. Ng and Varma [62] studied the coupled magnetic moment-vortex dynamics in the limit of long wavelength $\lambda_w \gg a_v$, where where a_v is the inter-vortex

distance. The magnon spectrum within the continuous medium approximation has been determined. The opposite limit, $\lambda_w \lesssim a_v$, has not been studied previously.

The reverse influence of magnetism on vortex dynamics has been considered by Bulaevskii et al. [64, 65, 66, 67, 68, 69, 70, 71]. It has been demonstrated theoretically that the vortex viscosity in magnetic superconductors is enhanced due to the radiation of magnons by moving vortices [66, 69, 71]. This affects the current-voltage characteristics of the sample, allowing to extract the spin-wave spectrum from these characteristics [64, 68]. In [69] the occurrence of vortex-vortex attraction and formation of vortex clusters in materials with a large magnetic susceptibility has been predicted. It should be noted that the preceding papers [64, 65, 68] concentrated on the interaction of vortices with magnons in antiferromagnetic compounds. Thus, an extension of the theory for ferromagnetic superconductors is required.

The present thesis is devoted to the study of static and dynamic properties of Abrikosov vortices in both ordinary and ferromagnetic superconductors. This work fills the outlined above gaps in theory, namely:

- the exact vortex pinning potential for a small columnar defect ($D \ll \xi$) with an elliptic cross-section is evaluated. For a defect with a circular cross-section the depinning current is determined.

- the viscosity tensor $\hat{\eta}$ in an anisotropic superconductor with the parameter $s_0 \neq 1$ is calculated using the exact order parameter profile of a vortex;

- the short-wavelength ($\lambda_w \lesssim a_v$) magnon spectrum of a ferromagnetic superconductor in the mixed state is determined;

- the damping force connected with the generation of magnons, acting on moving vortices in ferromagnetic superconductors is calculated.

In addition, several new effects are predicted:

- in the presence of a small transport current, a metastable bound state of a vortex and a small columnar defect should occur;

- in anisotropic superconductors with the parameter $s_0 \neq 1$ the flux-flow conductivity anisotropy should depend significantly on temperature even in the close vicinity of T_c, where the TDGL theory is applicable;

- in superconducting (S) and ferromagnetic (F) hybrid systems with a large GL parameter the nonlocal electrodynamics may lead to vortex-vortex attraction. Then, the transition from the Meissner to the mixed state will be a first order phase transition.

The structure of the thesis is as follows. In Chapter 1 the problem of vortex pinning on a small columnar defect is considered within the Ginzburg-Landau theory. The new results are compared with those obtained previously within the London theory. In Chapter 2 the vortex viscosity $\hat{\eta}$ for an anisotropic superconductor with the parameter $s_0 \neq 1$ is calculated using the TDGL theory. Several asymptotic expressions for $\hat{\eta}$ are derived, and a variational principle is proposed to evaluate $\hat{\eta}$ for superconductors with arbitrary

parameters m_{ab}, m_c, σ_{ab} and σ_c. Chapter 3 is devoted to the study of the interplay between magnons and Abrikosov vortices in SF hybrid systems. The spin-wave spectrum of a ferromagnetic superconductor in the mixed state is determined using the phenomenological London and Landau-Lifshitz-Gilbert equations [72]. The damping force acting on moving vortices in ferromagnetic superconductors and SF-superlattices is calculated. The cases of both a dc and ac driving force acting on vortices are considered. Finally, the surface impedance of a ferromagnetic superconductor is determined. In Chapter 4 the interaction of vortices in high-κ SF-hybrids with strong spatial dispersion of the magnetic susceptibility is studied. It is shown that the vortices may be attracted to each other at certain distances. Experimental consequences of this fact are discussed. In the conclusion of the thesis the main results are summarized.

Chapter 1

Abrikosov vortex pinning on a small cylindrical cavity

1.1 Introduction

The problem of single-vortex pinning is generally formulated as follows. The system (see Fig. 1.1a and b) contains a vortex and a defect, which is typically assumed to be of cylindrical shape. The task is to determine the vortex energy as a function of its position, and the depinning current density. The first theoretical study of individual vortex pinning on a cylindrical cavity was carried out by Mkrtchyan and Schmidt [22], who analyzed the problem using the London theory. Within this approach, the field of a vortex in a superconductor is determined by the equation

$$-\nabla^2\mathbf{B}+\frac{\mathbf{B}}{\lambda^2}=\frac{\Phi_0}{\lambda^2}\mathbf{z}_0\delta^{(2)}(\boldsymbol{\rho}-\mathbf{R}_0) \tag{1.1}$$

with the boundary condition $\mathbf{B}=\text{const}$ on the boundary of the superconductor. Here, $\mathbf{z}_0$ is a unit vector along the z-axis, and the vector $\mathbf{R}_0$ specifies the position of the vortex in the xy plane. The London equation (1.1) is suitable for the description of the vortex field in high-κ superconductors, and may be used for the calculation of the pinning potential in the situation depicted in Fig. 1.1a: the defect size D and the vortex-defect distance w must be much larger than the coherence length.

In the mentioned paper [22] the pinning potential was determined for a defect with a radius $a \ll \lambda$. Later [23, 27], this analysis was extended to the case of larger cavities. Buzdin and Feinberg [24] pointed out that the term $\mathbf{B}/\lambda^2$ in Eq. (1.1), responsible for London screening, can be neglected when $w \ll \lambda$ and $D \ll \lambda$. This observation allowed them to establish an electrostatic analogy and to simplify considerably the solution for a vortex interacting with a circular cavity: it was demonstrated that the full magnetic field can be presented as the sum of the vortex self-field and the field of image vortices, situated inside the cavity. Using the conformal transformation technique, pinning potentials for more tricky columnar cavities have been derived [25, 26]. However, in the calculation of the pinning potential for non-circular defects, only the field of the image vortices has been transformed, while the modification of the self-field of the real vortex has not been taken into account. This mistake has been corrected in [A2] by the author of the thesis.

For considerations of small defects, with $D \lesssim \xi$, the Ginzburg-Landau equation may

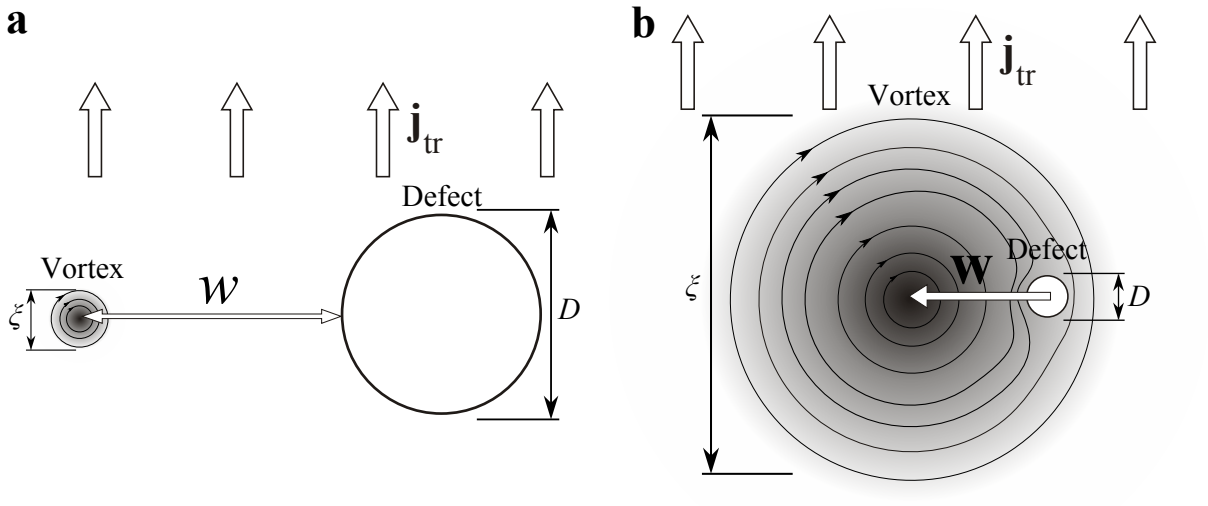

Figure 1.1: The cross-section of the system. (a) The case when the London theory can be applied: the defect size D and vortex-defect distance w are large as compared to the coherence length. (b) The case studied in this Chapter: the defect is small ($D \ll \xi$) and may be situated inside the vortex core.

be used. The GL theory is based on the general Landau theory of second-order phase transitions. Thus, the free energy of a superconductor in the GL approximation has the form [6]

$$F = \frac{H_c^2}{4\pi n_0} \int \left(\xi^2 \left| \left(\nabla + \frac{2ie}{\hbar c} \mathbf{A} \right) \psi \right|^2 - |\psi|^2 + n_0^{-1} \frac{|\psi|^4}{2} \right) d^3\mathbf{r} + \int \frac{(\mathrm{rot}\, \mathbf{A})^2}{8\pi} d^3\mathbf{r}. \qquad (1.2)$$

Here, n_0 is the Cooper pair concentration in the bulk of the superconductor (far from the vortex), $\mathbf{A}$ is the vector potential, and ψ is the superconducting order parameter. The equilibrium functions $\psi(\mathbf{r})$ and $\mathbf{A}(\mathbf{r})$ minimize the free energy. Equating to zero the first variation of F, we obtain the two equations

$$-\xi^2 \left(\nabla + \frac{2ie}{\hbar c} \mathbf{A} \right)^2 \psi - \psi + n_0^{-1} |\psi|^2 \psi = 0, \qquad (1.3)$$

$$\mathrm{rot}\, \mathrm{rot}\, \mathbf{A} = \frac{4\pi}{c} \mathbf{j}_S, \qquad (1.4)$$

where $\mathbf{j}_S$ is the supercurrent:

$$\mathbf{j}_S = -\frac{c}{4\pi\lambda^2} \frac{|\psi|^2}{n_0} \left(\mathbf{A} + \frac{\Phi_0}{2\pi} \nabla\theta_S \right). \qquad (1.5)$$

Here, $\theta_S = \arg\psi$, and $\lambda = \Phi_0/(2\sqrt{2}\pi H_c \xi)$ (compare with Eq. (1)). The GL boundary condition is

$$\mathbf{n} \left(\nabla + \frac{2ie}{\hbar c} \mathbf{A} \right) \psi = 0, \qquad (1.6)$$

where $\mathbf{n}$ is the normal to the surface of the superconductor.

Vortex pinning on a cylindrical defect within the GL theory has been studied in a number of papers [11, 28, 29, 30, 31]. In the review by Blatter et al. [11] an analytical estimate for the single-vortex pinning energy is given. The authors applied the variational principle, taking into account the suppression of the order parameter inside the defect and ignoring the local vortex distortion, induced by the boundary condition (1.6). This estimate will be discussed below. In subsequent papers the GL equation was mostly solved numerically. Maurer et al. [28] calculated the pinning energy for a vortex centered on a circular insulating or metallic inclusion. Later [29], the depinning current for defects with radii of 0.25ξ and larger was determined. Priour and Fertig [30] analyzed the interaction of a vortex with a cylindrical hole with a square cross-section. In [31] the critical current for a vortex lattice pinned on a set of defects with reduced critical temperature was determined using numerical simulations and a variational procedure.

The present Chapter of the thesis is based on the paper [A2]. It is devoted to the study of vortex pinning on a small cylindrical cavity, or insulating inclusion, with the characteristic size of the cross-section D lying in the range $\xi_0 \ll D \ll \xi$. Here, ξ_0 is the zero-temperature coherence length (in the case $D \sim \xi_0$ the correct description can be obtained only on the basis of a microscopic theory [73, 74, 75, 76]). In Sec. 1.2.1 the general form of the pinning potential within the GL theory is derived. In Sec. 1.2.2 this result is used to evaluate the exact pinning potential and depinning current for a cavity with a circular cross-section. In Sec. 1.2.3 the pinning potential for a defect in the form of a general elliptic cylinder is determined. Finally, in Sec. 1.3 the GL results are compared with the result obtained previously using the London theory [24, 25, 26]. The correct pinning potential for an elliptic cavity with the size $D \gg \xi$, $D \ll \lambda$ is presented.

1.2 Vortex pinning within the Ginzburg-Landau theory

1.2.1 General form of the pinning potential

When solving Eqs. (1.3) - (1.6) we shall restrict ourselves to the case of a high-κ superconductors. Then these equations can be significantly simplified. At small distances $r \ll \lambda$ from the vortex center the vector potential can be neglected in Eqs. (1.3) and (1.6) (see [77]). To prove this, let us make a simple estimate. The vortex field (in the absence of the defect) is given by [6]

$$\mathbf{B} = \mathbf{z}_0 \frac{\Phi_0}{2\pi\lambda^2} \mathrm{K}_0(r/\lambda), \qquad (r \gg \xi) \tag{1.7}$$

where K_0 is the modified Bessel function of the second kind. Let us choose the gauge where the order parameter phase coincides with the polar angle φ, and the vector potential in the center of the vortex vanishes. In this gauge $\mathbf{A}$ has only the A_φ component, which equals

$$A_\varphi(r) = \frac{1}{2\pi r} \int_{\rho<r} B_z d^2\boldsymbol{\rho} \approx \frac{\Phi_0 r}{4\pi\lambda^2} \ln\frac{\lambda}{r}, \qquad r \ll \lambda. \tag{1.8}$$

At $r \gg \xi$ $\psi \approx \sqrt{n_0} e^{i\varphi}$, and $|\nabla\psi| \approx |\psi|/r$. Hence, at $r \ll \lambda$

$$|\nabla\psi| \gg \left|\frac{2e}{\hbar c}\mathbf{A}\psi\right|. \tag{1.9}$$

In this Chapter defects with the size $D \ll \xi$ are considered. It will be shown below that the distortion of the vortex by such small pinning centers is very weak, so that Eq. (1.9) holds even in the presence of the defect. Thus, further on we may neglect the vector potential and consider the simplified GL equation

$$-\xi^2\nabla^2\psi - \psi + n_0^{-1}|\psi|^2\psi = 0 \tag{1.10}$$

instead of Eq. (1.3). The boundary condition (1.6) takes the form

$$\mathbf{n}\nabla\psi\Big|_{\partial S} = 0, \tag{1.11}$$

where S is the cross-section of the cavity, ∂S denotes the boundary of S, and $\mathbf{n}$ is the outward normal to ∂S. The origin of coordinates is placed inside the defect. The second boundary condition for Eq. (1.10) specifies the transport current density $\mathbf{j}_{\rm tr}$ far from the vortex core:

$$-\frac{c\Phi_0|\psi|^2\nabla\theta_S}{8\pi^2\lambda^2 n_0}\Big|_{\rho\to\infty} = \mathbf{j}_{\rm tr}. \tag{1.12}$$

Finally, since our system must contain one vortex, the following condition for the order parameter phase arises:

$$\oint \nabla\theta_S d\mathbf{l} = 2\pi, \tag{1.13}$$

where integration is over a wide contour surrounding the defect.

We expect that the equations (1.10) - (1.13) can be solved when $j_{\rm tr}$ does not exceed some value j_d, and no solution exists when $j_{\rm tr} > j_d$. Then it is natural to consider j_d as a depinning current.

We will solve Eqs. (1.10) - (1.13) in the case $j_{\rm tr} < j_d$. If the transport current is much smaller than the depairing current, the order parameter has the following asymptotics at infinity:

$$\psi \approx \sqrt{n_0} e^{i\varphi' + i\mathbf{q}\boldsymbol{\rho}}, \tag{1.14}$$

where φ' is the polar angle measured from an axis passing through the center of the vortex (φ' will be explicitly defined below), and $\mathbf{q} = -8\pi^2\lambda^2\mathbf{j}_{\rm tr}/c\Phi_0$. This asymptotics can be derived from Eqs. (1.10), (1.12) and (1.13) if one expands ψ in powers of ρ^{-1} and neglects terms proportional to $j_{\rm tr}^2$.

Now we make two assumptions concerning the behavior of the order parameter in the vicinity of the defect.

(A) The order parameter phase reaches its asymptotic behavior at sufficiently small distances from the origin: $\theta_S \approx \varphi' + \mathbf{q}\boldsymbol{\rho}$ when $\rho \geq R$, where R is some radius in the range $\xi \ll R \ll q^{-1}, \lambda$.

(B) The vortex is weakly distorted by a small defect and a small current. This means that the solution of equations (1.10) - (1.13) can be presented in the form $\psi = \psi_0 + \psi_1$, where ψ_0 corresponds to an unperturbed vortex shifted from the origin by a vector $\mathbf{w}$ (see Fig. 1.1b), and ψ_1 is a small perturbation: $|\psi_1(\rho)| \ll \sqrt{n_0}$ when $\rho < R$.

The assumption (B) is justified by the fact that the unperturbed vortex corresponds to a local minimum of the free energy, so large distortions are not energetically favorable. Both statements (A) and (B) can be verified by numerical calculations. In terms of the vector $\mathbf{w}$, the angle φ' is defined as

$$\tan\varphi' = \frac{y - w_y}{x - w_x}.$$

Let us write down the equations for the function ψ_1. Linearization of Eq. (1.10) yields

$$-\xi^2\nabla^2\psi_1 - \psi_1 + 2n_0^{-1}\left|\psi_0\right|^2\psi_1 + n_0^{-1}\psi_0^2\psi_1^* = 0. \tag{1.15}$$

Far from the vortex core, when the characteristic scale of the order parameter is much larger than ξ, we may obtain from the GL equation

$$\psi \approx \sqrt{n_0}\left(1 - \frac{\xi^2}{2}(\nabla\theta_S)^2\right)e^{i\theta_S}.$$

Hence, according to the statement (A), the perturbation $\psi_1 = \psi - \psi_0$ of the order parameter is given by

$$\psi_1(\boldsymbol{\rho}) = \sqrt{n_0}ie^{i\varphi'}(\mathbf{q}\boldsymbol{\rho}) + O\left(\frac{\sqrt{n_0}\xi^2 q}{\rho}\right), \quad \rho \sim R. \tag{1.16}$$

The boundary condition for ψ_1 at the defect border follows from Eq. (1.11):

$$(\nabla\psi_1 + \nabla\psi_0)\mathbf{n}\Big|_{\partial S} = 0. \tag{1.17}$$

Thus, equations (1.15) - (1.17) are to be solved. Here, for clarity, we would like to stress that the boundary condition (1.17) accounts for both the variations of the order parameter modulus and phase. It is reduced to the London theory boundary condition, $\nabla\theta_S\mathbf{n} = 0$, only if the vortex is far from the defect, i.e. $w \gg \xi$.

To derive the solvability condition for the system (1.15) - (1.17) we may use a method analogous to the one used in [77] to determine the viscous drag force acting on a moving vortex. First, we introduce the auxiliary function $\psi_d = \mathbf{d}\nabla\psi_0$, where $\mathbf{d}$ is an arbitrary constant unit vector, lying in the xy plane. ψ_d satifies the equation

$$-\xi^2\nabla^2\psi_d - \psi_d + 2n_0^{-1}\left|\psi_0\right|^2\psi_d + n_0^{-1}\psi_0^2\psi_d^* = 0. \tag{1.18}$$

Let us multiply Eq. (1.15) by ψ_d^* and subtract Eq. (1.18) multiplied by ψ_1^* from it. When we add the complex conjugate to the resulting equation we obtain

$$\operatorname{div}\left(-\psi_d^*\nabla\psi_1 + \psi_1\nabla\psi_d^* - \psi_d\nabla\psi_1^* + \psi_1^*\nabla\psi_d\right) = 0.$$

Now we integrate this relation over the region $\boldsymbol{\rho} \notin S$, $|\boldsymbol{\rho} - \mathbf{w}| < R$ and apply the Gauss theorem:

$$\begin{aligned} &\int_{|\boldsymbol{\rho}-\mathbf{w}|=R} \left(-\psi_d^* \nabla\psi_1 + \psi_1 \nabla\psi_d^* - \psi_d \nabla\psi_1^* + \psi_1^* \nabla\psi_d\right) \mathbf{n}_1 d\ell \\ &- \int_{\partial S} \left(-\psi_d^* \nabla\psi_1 + \psi_1 \nabla\psi_d^* - \psi_d \nabla\psi_1^* + \psi_1^* \nabla\psi_d\right) \mathbf{n} d\ell = 0, \end{aligned} \tag{1.19}$$

where $\mathbf{n}_1$ is the outward unit normal to the circle $|\boldsymbol{\rho} - \mathbf{w}| = R$. The first integral can be calculated with the help of Eq. (1.16):

$$\int_{|\boldsymbol{\rho}-\mathbf{w}|=R} \left(-\psi_d^* \nabla\psi_1 + \psi_1 \nabla\psi_d^* - \psi_d \nabla\psi_1^* + \psi_1^* \nabla\psi_d\right) \mathbf{n} d\ell \approx \frac{32\pi^3 \lambda^2 n_0}{c\Phi_0} \left[\mathbf{d} \cdot (\mathbf{z}_0 \times \mathbf{j}_{\rm tr})\right]. \tag{1.20}$$

Here, we neglected terms of the order of ξ^2/R^2, which appear due to variations of the order parameter modulus. Note that the z axis is directed opposite to the magnetic field.

The second integral in Eq. (1.19) can be transformed using (1.17) and the Gauss theorem:

$$\begin{aligned} &\int_{\partial S} \left(-\psi_d^* \nabla\psi_1 - \psi_d \nabla\psi_1^* + \psi_1 \nabla\psi_d^* + \psi_1^* \nabla\psi_d\right) \mathbf{n} d\ell \\ &\approx S \cdot \mathrm{div} \left(\psi_d^* \nabla\psi_0 + \psi_d \nabla\psi_0^*\right)\Big|_{\boldsymbol{\rho}=0} + \int_{\partial S} \left(\psi_1 \nabla\psi_d^*(0) + \psi_1^* \nabla\psi_d(0)\right) \mathbf{n} d\ell. \end{aligned} \tag{1.21}$$

Here and further we neglect terms which are much smaller than $n_0 D^2/\xi^3$.

To proceed we have to determine the value of ψ_1 at the defect boundary. Note that near the cavity the characteristic scale of ψ_1 is much smaller than ξ (since $D \ll \xi$), so at $\rho \ll \xi$ in (1.15) the dominating terms are those containing the derivatives of ψ_1. Hence, in the close vicinity of the cavity Eq. (1.15) is reduced to Laplace's equation

$$\nabla^2 \psi_1 = 0. \tag{1.22}$$

The boundary condition can also be simplified:

$$\nabla\psi_1 \mathbf{n}\Big|_{\partial S} = -\nabla\psi_0(0)\mathbf{n}. \tag{1.23}$$

Such simplification is acceptable since we are not interested in small corrections of the order of $\sqrt{n_0} D^2/\xi^2$ to ψ_1. Equations (1.22) and (1.23) are equivalent to an electrostatic problem where ψ_1 plays the role of the electric potential of a charged cylinder. Note that these equations can not be derived within the electrostatic approximation for the London theory [24], where variations of the superconducting phase are taken into account, but the order parameter modulus is assumed to be constant.

The relation

$$\oint_{\partial S} \nabla\psi_1 \mathbf{n} d\ell = 0,$$

can be interpreted as a vanishing total "charge" of the cylinder. It provides that a solution of equations (1.22) and (1.23) exists that decays like ρ^{-1} at infinity. This solution, which we denote as $\psi_1^{(d)}$, represents the irregular part of ψ_1: it has singularities inside the defect. We define the regular component of ψ_1 as

$$\psi_1^{(i)} = \psi_1 - \psi_1^{(d)}. \tag{1.24}$$

It is proved in Appendix A that the contribution of $\psi_1^{(i)}$ to the integral in the right-hand side of equation (1.21) is negligible.

Combining Eqs. (1.19) - (1.21) and using the fact that ψ_0 satisfies Eq. (1.10) we obtain

$$-\tfrac{4\pi n_0\Phi_0}{H_c^2 c}\left[\mathbf{d}\cdot(\mathbf{z}_0\times\mathbf{j}_{\rm tr})\right]+S(\mathbf{d}\nabla)\left(\xi^2\left|\nabla\psi_0\right|^2-\left|\psi_0\right|^2+\tfrac{\left|\psi_0\right|^4}{2n_0}\right)\Bigg|_{\boldsymbol{\rho}=0}$$
$$+\xi^2\int_{\partial S}\left[\psi_1^{(d)}\nabla\psi_d^*(0)+\psi_1^{(d)*}\nabla\psi_d(0)\right]\mathbf{n}d\ell\approx 0. \tag{1.25}$$

Owing to the linearity of Eqs. (1.22) and (1.23) the solution can be presented in the form

$$\psi_1^{(d)}=\mathbf{g}(\boldsymbol{\rho})\cdot\nabla\psi_0(0), \tag{1.26}$$

where $\mathbf{g}$ is a real vector field defined by the relations

$$\nabla^2\mathbf{g}=0,\qquad (\mathbf{n}\nabla)\mathbf{g}\Big|_{\partial S}=-\mathbf{n},\qquad \mathbf{g}\Big|_{\rho\to\infty}=0. \tag{1.27}$$

Then

$$\int_{\partial S}\left[\psi_1^{(d)}\nabla\psi_d^*(0)+\psi_1^{(d)*}\nabla\psi_d(0)\right]\mathbf{n}d\ell=(\mathbf{d}\nabla)\left(\nabla\psi_0\hat{G}\nabla\psi_0^*\right)\Big|_{\boldsymbol{\rho}=0},$$

where $\hat{G}$ is a real symmetric matrix with components

$$G_{ij}=\int_{\partial S}g_i n_j d\ell=\int_{\boldsymbol{\rho}\notin S}\nabla g_i\nabla g_j\,d^2\boldsymbol{\rho}. \tag{1.28}$$

Equation (1.25) transforms into

$$\frac{\Phi_0}{c}\left[\mathbf{d}\cdot(\mathbf{z}_0\times\mathbf{j}_{\rm tr})\right]-(\mathbf{d}\nabla_{\mathbf{w}})U_p=0. \tag{1.29}$$

Here, $\nabla_{\mathbf{w}}=\partial/\partial\mathbf{w}$, and

$$U_p=-S\frac{H_c^2}{4\pi n_0}\left(\xi^2\left|\nabla\psi_0\right|^2-\left|\psi_0\right|^2+\frac{\left|\psi_0\right|^4}{2n_0}\right)\Bigg|_{\boldsymbol{\rho}=0}-\xi^2\frac{H_c^2}{4\pi n_0}\nabla\psi_0(0)\hat{G}\nabla\psi_0^*(0). \tag{1.30}$$

Since $\mathbf{d}$ is an arbitrary vector, it can be dropped, and we finally obtain the force balance equation, connecting the vortex displacement $\mathbf{w}$ with the transport current $\mathbf{j}_{\rm tr}$:

$$\frac{\Phi_0}{c}\left(\mathbf{z}_0\times\mathbf{j}_{\rm tr}\right)-\nabla_{\mathbf{w}}U_p=0. \tag{1.31}$$

Here, the first term is the Lorentz force (compare with Eq. (4)) and the second term is the pinning force: $\mathbf{F}_p=-\nabla_{\mathbf{w}}U_p(\mathbf{w})$. Thus, we may conclude that U_p is the pinning potential. This potential has two components. The first one,

$$-S\frac{H_c^2}{4\pi n_0}\left(\xi^2\left|\nabla\psi_0\right|^2-\left|\psi_0\right|^2+\frac{\left|\psi_0\right|^4}{2n_0}\right)\Bigg|_{\boldsymbol{\rho}=0}, \tag{1.32}$$

appears due to the suppression of the order parameter inside the cavity ($\psi = 0$). Note that the expression (1.32) is given in the review [11] as an estimate of the pinning potential. The second component of U_p,

$$-\xi^2 \frac{H_c^2}{4\pi n_0} \nabla\psi_0(0) \hat{G} \nabla\psi_0^*(0), \tag{1.33}$$

is connected with the distortion of the vortex in the vicinity of the cavity. Generally, the contributions (1.32) and (1.33) to U_p are of the same order of magnitude.

Before we determine some pinning potentials explicitly, we would like to note that our consideration can be easily generalized for the anisotropic case. Indeed, the GL free energy of an anisotropic superconductor can be presented in the form

$$F = \frac{H_c^2}{4\pi n_0} \int \left(\xi_x^2 \left| \frac{\partial\psi}{\partial x} \right|^2 + \xi_y^2 \left| \frac{\partial\psi}{\partial y} \right|^2 + \xi_z^2 \left| \frac{\partial\psi}{\partial z} \right|^2 - |\psi|^2 + \frac{|\psi|^4}{2n_0} \right) d^3\mathbf{r}, \tag{1.34}$$

where ξ_x, ξ_y and ξ_z are the coherence lengths for different directions. The scaling transformation $\tilde{x} = x$, $\tilde{y} = y\xi_x/\xi_y$, and $\tilde{z} = z\xi_x/\xi_z$ reduces the free energy to the isotropic form. Thus, we again arrive at Eqs. (1.10) - (1.12).

Now we will consider two types of defects.

1.2.2 A defect in the form of a circular cylinder

Let the defect be a circular cylinder with the radius a. When the origin is placed on the axis of the cylinder, the decaying solution of equations (1.22) and (1.23) is

$$\psi_1^{(d)} = \frac{a^2(\nabla\psi_0 \cdot \boldsymbol{\rho})}{\rho^2}, \tag{1.35}$$

and the pinning potential is

$$U_p(\mathbf{w}) = -\frac{H_c^2 a^2}{4n_0} \left(2\xi^2 |\nabla\psi_0|^2 - |\psi_0|^2 + \frac{|\psi_0|^4}{2n_0} \right) \Bigg|_{\boldsymbol{\rho}=0}. \tag{1.36}$$

The function ψ_0 can be determined numerically from the GL equation (1.15), using standard methods for the solution of ordinary differential equations. The details of these simple calculations are omitted for brevity. A detailed numerical analysis of the function ψ_0 can be found in [37].

Equation (1.36) allows us to determine the pinning energy, E_p:

$$E_p = U_p(\infty) - U_p(0) = 0.47 H_c^2 a^2,$$

This value coincides with the numerical result given in [28] up to a factor of the order of unity.

The profiles of the pinning potential and the pinning force are plotted in Fig 1.2. The pinning force reaches its maximum at $w = w_{\rm cr} = 0.84\xi$, where $F_p = F_{\rm cr} = 0.252 H_c^2 a^2/\xi$. When $j_{\rm tr} > cF_{\rm cr}/\Phi_0$, the force balance equation (1.31) has no solutions, hence

$$j_d = cF_{\rm cr}/\Phi_0 = 0.252 \frac{cH_c^2 a^2}{\Phi_0 \xi} \tag{1.37}$$

is the depinning current. Note that j_d is much smaller than the depairing current density

$$J_c = \frac{2c\xi H_c^2}{3\sqrt{3}\Phi_0},$$

if $a \ll \xi$.

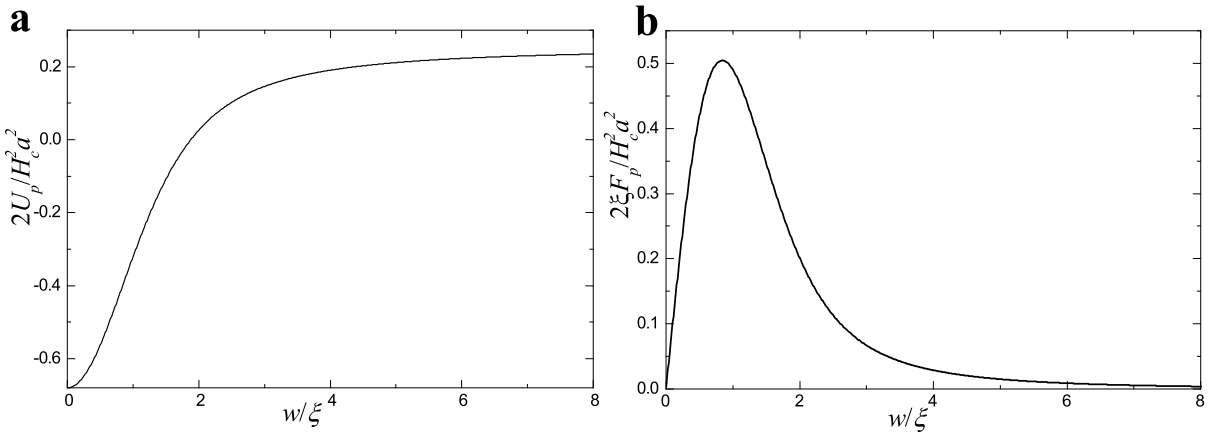

Figure 1.2: Profiles of the pinning potential (a) and the pinning force (b) for a circular defect.

When $j < j_d$ Eq. (1.31) has two solutions due to the nonmonotonic behavior of the function $F_p(w)$, but the solution with the larger vortex displacement is thermodynamically unstable. Indeed, it can be easily proved that it corresponds to a saddle point of the correction ΔF to the free energy of a vortex connected with the presence of the defect and the transport current:

$$\Delta F = U_p - \frac{\Phi_0}{c}\left[(\mathbf{z}_0 \times \mathbf{j}_{\rm tr})\mathbf{w}\right].$$

Equation (1.37) predicts that the depinning current grows like a^2 when the defect size is increased. Obviously, this quadratic growth rate must slow down when the defect size is of the order of the coherence length (otherwise, the depinning current would eventually exceed J_c). Thus, for $a \sim \xi$ equation (1.37) should give an upper estimate for j_d. This argument is well confirmed by the fact that the numerical value of the depinning current for the defect radius 0.25ξ,

$$j_d = 0.01\frac{H_c^2\xi c}{\Phi_0}, \tag{1.38}$$

given in [29], is 1.5 times smaller than our estimate.

An important conclusion following from the force balance equation (1.31) is the existence of a metastable bound state at $j < j_d$, when the vortex center is situated outside the cavity. In [29] this state has not been detected numerically. This disagreement with our result may be due to the relatively large size of defects considered in the paper ($a \geq 0.25\xi$), and also due to the strong influence of the outer periphery of the cell where the GL equation has been integrated.

1.2.3 The case of an elliptic cylinder

Consider an elliptic defect with the cross-section

$$\frac{x^2}{a^2}+\frac{y^2}{b^2}<1,$$

where $a > b$. We shall determine the vector field $\mathbf{g}$ and the pinning potential. It is convenient to use the elliptic coordinates (ζ, ϑ):

$$x=\sqrt{a^2-b^2}\cosh\zeta\cos\vartheta, \qquad y=\sqrt{a^2-b^2}\sinh\zeta\sin\vartheta.$$

The border of the defect corresponds to the value $\zeta = \zeta_0$, where

$$\sinh\zeta_0=\frac{b}{\sqrt{a^2-b^2}}, \qquad \cosh\zeta_0=\frac{a}{\sqrt{a^2-b^2}}.$$

Equations (1.27) in the new coordinates read

$$\frac{\partial^2\mathbf{g}}{\partial\zeta^2}+\frac{\partial^2\mathbf{g}}{\partial\vartheta^2}=0, \qquad \mathbf{g}\Big|_{\zeta\to\infty}=0, \qquad \frac{\partial g_x}{\partial\zeta}\Big|_{\zeta=\zeta_0}=-b\cos\vartheta, \qquad \frac{\partial g_y}{\partial\zeta}\Big|_{\zeta=\zeta_0}=-a\sin\vartheta. \quad (1.39)$$

The solution is

$$g_x=be^{\zeta_0-\zeta}\cos\vartheta, \qquad g_y=ae^{\zeta_0-\zeta}\sin\vartheta. \quad (1.40)$$

Using (1.28), we obtain the components of the matrix $\hat{G}$:

$$G_{xx}=\pi b^2, \qquad G_{yy}=\pi a^2, \qquad G_{xy}=G_{yx}=0. \quad (1.41)$$

According to equation (1.30), the pinning potential is

$$U_p=-\frac{H_c^2}{4n_0}\left[ab\left(\xi^2\left|\nabla\psi_0\right|^2-\left|\psi_0\right|^2+\frac{\left|\psi_0\right|^4}{2n_0}\right)+\xi^2b^2\left|\frac{\partial\psi_0}{\partial x}\right|^2+\xi^2a^2\left|\frac{\partial\psi_0}{\partial y}\right|^2\right]\Bigg|_{\boldsymbol{\rho}=0}. \quad (1.42)$$

The potential well for the vortex now does not have cylindrical symmetry. As a result, the vortex displacement w and the depinning threshold j_d will depend on the direction of the transport current.

1.3 Comparison with the London theory

In the paper [25] the pinning potential in the presence of a circular and elliptic cavity has been derived within the London theory. This approach is applicable when the defect size is much larger than the temperature-dependent coherence length, i.e., $D \gg \xi(T)$. Under certain conditions, the results from Section 1.2 can be extended to the case $D \gg \xi(T)$. Indeed, the calculations in Section 1.2 based on the following two statements: (i) $|\psi_1| \ll \sqrt{n_0}$ and (ii): the quantity $\nabla\psi_0$ is approximately constant in the area occupied by the cavity. These two conditions are satisfied when

$$D\gg\xi \text{ and } w\gg D, \quad (1.43)$$

so for a large defect and large vortex-defect distance the pinning potential (1.30) should coincide with the one obtained within the London theory.

At large vortex-defect distances, $w \gg a$, for a circular defect Eq. (1.36) gives

$$U_p = -\left(\frac{\Phi_0}{4\pi\lambda}\right)^2 \frac{a^2}{w^2} + \text{const.} \tag{1.44}$$

This result is in good agreement with equation (5) from [25]. For an elliptic hole Eq. (1.42) yields in the $w \gg a$ limit

$$U_p = -\left(\frac{\Phi_0}{4\pi\lambda}\right)^2 \frac{1}{2}\left(\frac{ab}{w^2} + \frac{b^2 w_y^2}{w^4} + \frac{a^2 w_x^2}{w^4}\right) + \text{const}, \tag{1.45}$$

whereas the potential from [25] is

$$U_p = -\left(\frac{\Phi_0}{4\pi\lambda}\right)^2 \left(\frac{a+b}{2}\right)^2 \frac{1}{w^2}, \tag{1.46}$$

which, obviously, does not coincide with (1.45). The reason of this discrepancy is explained below.

The derivation of the interaction energy between a vortex and a cavity in the London approximation is based on the equation

$$U_p = \frac{\Phi_0 B_{\text{im}}(\mathbf{w})}{8\pi}, \tag{1.47}$$

where B_{im} is the z projection of the field created by image vortices. This field can be expressed as

$$B_{\text{im}} = B_z - \frac{\Phi_0}{2\pi\lambda^2} \ln\left|\frac{\lambda^2}{\zeta - \zeta_0}\right|, \tag{1.48}$$

where $\zeta = x + iy$, $\zeta_0 = w_x + iw_y$, and B_z is the full magnetic field, satisfying the Poisson equation

$$\nabla^2 B_z = -\frac{\Phi_0}{\lambda^2}\delta(\boldsymbol{\rho} - \mathbf{w}). \tag{1.49}$$

The second term in the right-hand side of Eq. (1.48) represents the self field of the vortex with the opposite sign. The image vortices are placed in such a way to provide the fulfillment of the condition $B_z = \text{const}$ on the boundary of the cavity. For a circular defect with the radius a_0 the image field at the position of the vortex is [24]

$$B^{\text{c}}_{\text{im}}(\zeta_0) = \frac{\Phi_0}{2\pi\lambda^2} \ln\left(1 - \frac{a_0^2}{|\zeta_0|^2}\right), \tag{1.50}$$

To obtain the magnetic field in the presence of a non-circular defect, we may apply a conformal transformation $W = W(\zeta)$ to the ζ plane. Since the form of Poisson's equation is not modified by such a transformation, the field distribution in the W plane is given by

$$B_z(W) = B^{\text{c}}_z(\zeta(W)),$$

where $B_z^{\rm c}(\zeta)$ is the solution of Eq. (1.49) in the presence of a circular defect. Using the definition (1.48) of the image field, we obtain

$$B_{\rm im}(W_0) = B_{\rm im}^{\rm c}(\zeta(W_0)) + \left[\frac{\Phi_0}{2\pi\lambda^2}\ln\left|\frac{\lambda}{\zeta(W)-\zeta_0}\right| - \frac{\Phi_0}{2\pi\lambda^2}\ln\left|\frac{\lambda}{W-W_0}\right|\right]\Bigg|_{W=W_0}, \quad (1.51)$$

where $W_0 = W(\zeta_0)$ specifies the position of the vortex in the W-plane. Hence, the pinning potential equals

$$U_p = \left(\frac{\Phi_0}{4\pi\lambda}\right)^2\left[\ln\left(1-\frac{a_0^2}{|\zeta(W_0)|^2}\right) - \ln\left|\frac{d\zeta}{dW}(W_0)\right|\right]. \quad (1.52)$$

Here, the first logarithmic term originates from the transformation of the image field (1.50), while the second term is connected with the modification of the self field of the vortex. In [25] this term has not been taken into account. As a result, the isotropic potential (1.46) has been obtained. In order to determine the correct pinning potential for an elliptic cavity, we apply the modified Joukovsky transformation [25]:

$$W(\zeta) = \frac{a+b}{2}\frac{\zeta}{a_0} + \frac{a-b}{2}\frac{a_0}{\zeta}; \quad (1.53)$$

$$U_p(W_0) = \left(\frac{\Phi_0}{4\pi\lambda}\right)^2\left[\ln\left(1-\left|\frac{a+b}{W_0+\sqrt{W_0^2-a^2+b^2}}\right|^2\right) - \ln\left|1+\frac{W_0}{\sqrt{W_0^2-a^2+b^2}}\right|\right] + \text{const.} \quad (1.54)$$

For $|W_0| \gg a$ this expression is in good agreement with the result obtained within the GL theory (Eq. (1.45)).

1.4 Summary

The central results of this Chapter are the equations (1.27), (1.28) and (1.30), defining the interaction energy of a vortex and a small cylindrical cavity ($D \ll \xi$) with an arbitrary cross-section. The problem of the pinning potential evaluation is reduced to a linear Neumann problem for Laplace's equation (for the solution of the latter various standard procedures exist [78]). It should be noted that the method developed here can be applied not only to bulk superconductors, but also to thin films with the vortices directed normal to the film.

On the basis of Eqs. (1.27), (1.28) and (1.30) the exact pinning potential for a cavity with an elliptic cross-section has been calculated (see Eq. (1.42)). The occurrence a metastable bound state of the vortex and the defect (Fig. 1.1b) at low transport currents has been predicted. This bound state may be observed, for example, using scanning tunneling microscopy or a nano-SQUID [79]. For a cavity in the form of a circular cylinder the depinning current has been determined.

The vortex-defect interaction was also considered within the London theory. The relation (1.52) has been derived, allowing to calculate the pinning potential for complex cavities, using the conformal transformation technique. The pinning potentials obtained within the GL and London theories coincide with each other in the range of parameters where both approaches are applicable.

The results of this Chapter comprise an important basis for estimates of the critical current in superconductors with small columnar defects. In addition, the present analysis is relevant to recent experimental studies of the vortex ratchet effect [80, 81, 82, 83, 84, 85], where an anisotropic pinning structure is a key element. Note that the experimental conditions in [85] almost perfectly match the model used here: the antidots embedded into the thin Al films represent insulating inclusions, and the typical temperatures are very close to the critical temperature, so that the coherence length is larger than the defect size. Thus, the obtained relations for the anisotropic pinning potential may be useful for vortex ratchet design and for interpretation of future experiments in this field.

Chapter 2

Resistivity of an anisotropic type-II superconductor in the mixed state

2.1 Introduction

In the previous Chapter the case of a relatively low transport current has been studied, when the vortex is pinned. In the opposite limiting case, when the current is sufficiently strong, the interaction of vortices with defects becomes inessential, and the stationary flux-flow regime sets in. In the first theoretical papers devoted to the study of the flux-flow conductivity it has been pointed out that vortex motion is accompanied by dissipation, having two origins: losses due to relaxation of the order parameter [86] and ohmic losses associated with normal currents flowing through the vortex core [32]. Both these mechanisms contribute to the vortex viscosity η (see Eq. (7)). A rigorous approach to the evaluation of this quantity has been proposed by Schmid [33], and was later developed by Gor'kov and Kopnin [34]. Their method is based on the time-dependent Ginzburg-Landau (TDGL) equation

$$\Gamma\left(\hbar\frac{\partial\psi}{\partial t}-2ie\Phi\psi\right)=-\frac{\delta F}{\delta\psi^*}. \tag{2.1}$$

Here, Γ is a relaxation constant, Φ is the electric potential, and F is the GL free energy. Using this approach, the viscosity η of an isolated vortex in an isotropic superconductor has been calculated in the papers [36, 37, 38]. A study of the flux-flow conductivity in the anisotropic (uniaxial) case, relevant to the cuprates [39] and Fe-pnictide superconductors [42], is given in [40] and [41] (see also the book [35]). When the parameter $s_0 = m_c\sigma_c/m_{ab}\sigma_{ab}$ is equal to unity, the problem can be reduced to the isotropic form [41]. The more complicated case of a Cooper pair mass-normal conductivity anisotropy mismatch ($s_0 \neq 1$) has been considered in [40] on the basis of a simplified step-like order parameter profile in a vortex.

The present Chapter of the thesis is mainly devoted to the study of the viscosity tensor $\hat{\eta}$ in the case $s_0 \neq 1$ using a realistic (sometimes, even exact) order parameter profile of a vortex. In Sec. 2.2 the initial equations are given. In Sec. 2.3 some exact asymptotic expressions for the vortex viscosity are derived. In Sec. 2.4 a variational principle is established, which allows to obtain a universal approximate expression for $\hat{\eta}$.

Finally, in Sec. 2.5 the temperature dependence of the flux-flow conductivity anisotropy is considered within a generalized TDGL theory.

2.2 Basic equations

The GL free energy of a uniaxial superconductor is given by

$$F = \int \left[\hbar^2 \nabla\psi^* \frac{\hat{m}^{-1}}{2} \nabla\psi + a_{GL} |\psi|^2 + \frac{1}{2} b_{GL} |\psi|^4 \right] d^3\mathbf{r}. \tag{2.2}$$

Here, a_{GL} and b_{GL} are parameters that do not depend on coordinates, $\hat{m}$ is the Cooper pair mass tensor with the components $m_{ij} = m_{ab}(\delta_{ij} + \mu e_i e_j)$, where $\mathbf{e}$ is a unit vector directed along the anisotropy axis, and μ is a dimensionless constant. The Cooper pair concentration in the uniform state n_0 equals $|a_{GL}|/b_{GL}$. Like in the previous Chapter, we neglect the vector potential, assuming that the superconductor is in the high-κ limit. Equations (2.1) and (2.2) are supplemented by the charge conservation law

$$\frac{\partial \rho_e}{\partial t} + \operatorname{div} \mathbf{j} = 0, \tag{2.3}$$

where the full current density is

$$\mathbf{j} = -2e\hbar |\psi|^2 \hat{m}^{-1} \nabla\theta_S - \hat{\sigma}_n \nabla\tilde{\Phi}. \tag{2.4}$$

Here, ρ_e is the electric charge density, $\hat{\sigma}_n$ is the normal conductivity tensor with the components $\sigma_{nij} = \sigma_{ab}\delta_{ij} + (\sigma_c - \sigma_{ab}) e_i e_j$, and $\tilde{\Phi}$ is the electrochemical potential. When the Thomas-Fermi screening length is much smaller than all characteristic length scales of the problem, one can neglect the difference between $\nabla\Phi$ and $\nabla\tilde{\Phi}$ [36, 77]. The Thomas-Fermi screening length is typically of the order of the interatomic distance, so we will henceforth assume that $\nabla\Phi \approx \nabla\tilde{\Phi}$.

Let us consider the orientation of the internal magnetic field at an angle φ_0 to the crystallographic c axis. We choose the coordinate frame (x, y, z) with the z axis coinciding with the vortex axis and with the c axis lying in the xz plane (see Fig. 2.1). In this frame the functions ψ and Φ do not depend on z, and the tensor $\hat{\eta}$ is diagonal.

The derivation of the force balance equation (5) and of the explicit expression for the viscous drag tensor may be found in [77] and [40]. However, in Appendix B, the calculations are outlined for the reader's convenience.

The full viscosity can be presented as the sum of the ohmic (Bardeen-Stephen [32]) and relaxational [86] contribution: $\hat{\eta} = \hat{\eta}_{oh} + \hat{\eta}_{p0}$. The latter is given by

$$(\eta_{p0})_{xx} = 2\pi\hbar\Gamma n_0 \alpha_1 \left(\frac{m(\varphi_0)}{m_{ab}} \right)^{1/2}, \qquad (\eta_{p0})_{yy} = 2\pi\hbar\Gamma n_0 \alpha_1 \left(\frac{m_{ab}}{m(\varphi_0)} \right)^{1/2}, \tag{2.5}$$

where

$$m(\varphi_0) = \frac{m_{ab}(1+\mu)}{1 + \mu \cos^2 \varphi_0}, \tag{2.6}$$

and the constant α_1 is given by Eq. (B20).

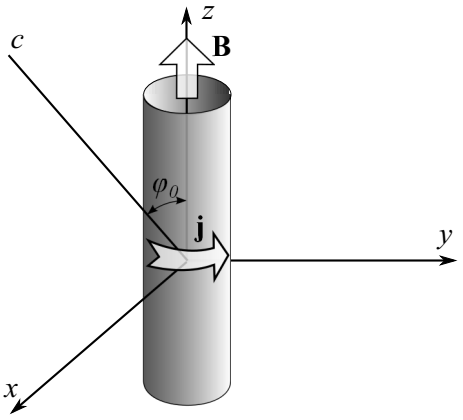

Figure 2.1: The coordinate frame.

The components of the Bardeen-Stephen contribution, $\hat{\eta}_{\rm oh}$, are

$$\eta_x \equiv [m_{ab}/m(\varphi_0)]^{1/2}(\eta_{\rm oh})_{xx} = -2n_0\Gamma\hbar \int f^2(\rho_1)\frac{y_1}{\rho_1^2}\left(u^2\Phi_x - \frac{y_1}{\rho_1^2}\right) dx_1 dy_1, \tag{2.7}$$

$$\eta_y \equiv [m(\varphi_0)/m_{ab}]^{1/2}(\eta_{\rm oh})_{yy} = -2n_0\Gamma\hbar \int f^2(\rho_1)\frac{x_1}{\rho_1^2}\left(u^2\Phi_y - \frac{x_1}{\rho_1^2}\right) dx_1 dy_1. \tag{2.8}$$

where $u = \xi_{ab}/l_{Eab}$,

$$(x_1, y_1) = \xi_{ab}^{-1}\left(\sqrt{\frac{m(\varphi_0)}{m_{ab}}}x, y\right), \qquad \rho_1 = \sqrt{x_1^2 + y_1^2}, \tag{2.9}$$

ξ_{ab} and l_{Eab} are the coherence length and the electric field penetration depth in the ab-plane:

$$\xi_{ab} = \sqrt{\frac{\hbar^2}{2m_{ab}\left|a_{GL}\right|}}, \qquad l_{Eab} = \left[\hbar\sigma_{ab}/\left(8e^2\Gamma n_0\right)\right]^{1/2}. \tag{2.10}$$

In a similar way the quantities ξ_c and l_{Ec}, related to the c-axis, may be introduced. The function $f(\rho)$ in Eqs. (2.7) and (2.7) is the dimensionless order parameter in an isotropic vortex (see Eq. (B17)). It satisfies the equation

$$\frac{1}{\rho}\frac{d}{d\rho}\left(\rho\frac{df}{d\rho}\right) - \frac{f}{\rho^2} + f - f^3 = 0, \tag{2.11}$$

which follows from Eq. (B8). The boundary conditions are $f(0) = 0$, $f(\infty) = 1$. The functions Φ_x and Φ_y in Eqs. (2.7) and (2.8) should be determined from the linear equations

$$s(\varphi_0)\frac{\partial^2\Phi_x}{\partial x_1^2} + \frac{\partial^2\Phi_x}{\partial y_1^2} = \left(u^2\Phi_x - \frac{y_1}{\rho_1^2}\right) f^2(\rho_1), \tag{2.12}$$

$$s(\varphi_0)\frac{\partial^2\Phi_y}{\partial x_1^2} + \frac{\partial^2\Phi_y}{\partial y_1^2} = \left(u^2\Phi_y - \frac{x_1}{\rho_1^2}\right) f^2(\rho_1), \tag{2.13}$$

where

$$s(\varphi_0) = 1 + \left(\frac{m_c \sigma_c}{m_{ab} \sigma_{ab}} - 1 \right) \frac{\sin^2 \varphi_0}{1 + \mu \cos^2 \varphi_0} > 0. \tag{2.14}$$

The electric potential can be expressed in terms of Φ_x and Φ_y via

$$\Phi = \left(\Phi_y V_{Ly} - \Phi_x \sqrt{\frac{m(\varphi_0)}{m_{ab}}} V_{Lx} \right) \frac{4\Gamma e \hbar}{b_{GL} \sigma_{ab}} \sqrt{\frac{|a_{GL}|}{2 m_{ab}}}. \tag{2.15}$$

Note that there is a relation connecting the components η_x and η_y:

$$\eta_y(s, u) = \eta_x \left(\frac{1}{s}, \frac{u}{\sqrt{s}} \right). \tag{2.16}$$

Equations (2.5), (2.7) and (2.8) can be written in a more compact form with the help of the dissipation function, $W_d[\psi, \Phi]$ [77]:

$$W_d[\psi, \Phi] = \nabla \Phi \hat{\sigma}_n \nabla \Phi + \frac{2\Gamma}{\hbar} \left| \hbar \frac{\partial \psi}{\partial t} - 2ie\Phi\psi \right|^2. \tag{2.17}$$

This function defines the dissipation rate in a unit volume. The viscosity tensor satisfies the relation

$$\mathbf{V}_L \hat{\eta} \mathbf{V}_L = \int_{z=0} W_d[\psi, \Phi] d^2\boldsymbol{\rho}, \tag{2.18}$$

The disipation function consists of two parts, yielding the viscosity components $\hat{\eta}_{p0}$ and $\hat{\eta}_{oh}$:

$$\mathbf{V}_L \hat{\eta}_{p0} \mathbf{V}_L = 2\Gamma\hbar \int_{z=0} \left(\frac{\partial |\psi|}{\partial t} \right)^2 d^2\boldsymbol{\rho}, \tag{2.19}$$

$$\mathbf{V}_L \hat{\eta}_{oh} \mathbf{V}_L = \int_{z=0} \left[\nabla \Phi \hat{\sigma_n} \nabla \Phi + \frac{2\Gamma}{\hbar} |\psi|^2 \left(\hbar \frac{\partial \theta_S}{\partial t} - 2e\Phi \right)^2 \right] d^2\boldsymbol{\rho}. \tag{2.20}$$

To avoid confusion, it should be noted that the component $\hat{\eta}_{oh}$, apart from the ohmic losses, contains a part of the relaxational losses, as can be seen from Eq. (2.20). Nevertheless, we will call $\hat{\eta}_{oh}$ the ohmic vortex viscosity (or Bardeen-Stephen contribution), following the terminology used in [35, 40, 77].

Now we will analyze two limiting cases.

2.3 Asymptotic expansions for the viscosity tensor

2.3.1 The limit $l_E \ll \xi$

Let us consider such materials where the electric field penetration depth is much smaller than the coherence length:

$$l_{Eab} \ll \xi_{ab}, \qquad l_{Ec} \ll \xi_c. \tag{2.21}$$

This limiting case is more close to gapless superconductors with a high concentration of magnetic impurities which are characterized by the ration $\xi / l_E = \sqrt{12}$. The conditions

(2.21) impose the following restrictions on the parameters s and u: $u \gg 1$, $s \ll u^2$. In this subsection we will analyze the case $s \lesssim 1$. The case $1 \ll s \ll u^2$ can be considered in a similar way by dividing Eqs. (2.12) and (2.13) by s. We shall search the asymptotics of the viscosity when $u \to \infty$ neglecting small terms of order higher than u^{-2}.

The approximation used here is based on the fact that the characteristic length scale for the functions Φ_x and Φ_y is u^{-1}. Hence, these functions reach their asymptotic behavior at distances $\rho_1 \ll 1$ from the vortex axis, where the order parameter profile $f(\rho_1)$ is well approximated by the first several terms of its Taylor series:

$$f^2(\rho) \approx f_2\rho_1^2 + f_4\rho_1^4 + f_6\rho_1^6.$$

We substitute this expansion into Eq. (2.12) and introduce the new variables $\tilde{\boldsymbol{\rho}} = \boldsymbol{\rho}_1\sqrt{u}$, $\tilde{\Phi}_x = \Phi_x u^{3/2}$:

$$\frac{\partial^2\tilde{\Phi}_x}{\partial\tilde{y}^2} + s\frac{\partial^2\tilde{\Phi}_x}{\partial\tilde{x}^2} = \left(f_2\tilde{\rho}^2 + f_4\frac{\tilde{\rho}^4}{u} + ...\right)\left(\tilde{\Phi}_x - \frac{\tilde{y}}{\tilde{\rho}^2}\right). \tag{2.22}$$

Further the tilde over $\tilde{x}$ and $\tilde{y}$ will be omitted. The solution of Eq. (2.22) can be expanded in the powers of u^{-1}:

$$\tilde{\Phi}_x = \Phi_x^{(0)} + u^{-1}\Phi_x^{(1)} + R_x, \tag{2.23}$$

where $\Phi_x^{(0)}$ and $\Phi_x^{(1)}$ satisfy the following relations:

$$\frac{\partial^2\Phi_x^{(0)}}{\partial y^2} + s\frac{\partial^2\Phi_x^{(0)}}{\partial x^2} = f_2\rho^2\Phi_x^{(0)} - f_2 y, \tag{2.24}$$

$$\frac{\partial^2\Phi_x^{(1)}}{\partial y^2} + s\frac{\partial^2\Phi_x^{(1)}}{\partial x^2} = f_2\rho^2\Phi_x^{(1)} + f_4\rho^4\left(\Phi_x^{(0)} - \frac{y}{\rho^2}\right), \tag{2.25}$$

and R_x is a remainder term. It is proved in Appendix C that an analogous expansion can be made in the integral in the right-hand side of Eq. (2.7):

$$\eta_x = -2n_0\Gamma\hbar\left[\frac{I_{1x}(s)}{u} + \frac{I_{2x}(s)}{u^2} + o(u^{-2})\right], \tag{2.26}$$

where

$$I_{1x}(s) = \int f_2 y\left(\Phi_x^{(0)} - \frac{y}{\rho^2}\right)dx\,dy, \tag{2.27}$$

$$I_{2x}(s) = \int \frac{y}{\rho^2}\left[f_4\rho^4\left(\Phi_x^{(0)} - \frac{y}{\rho^2}\right) + f_2\rho^2\Phi_x^{(1)}\right]dx\,dy. \tag{2.28}$$

The viscosity component η_y can be calculated similarly:

$$\eta_y = -2n_0\Gamma\hbar\left[\frac{I_{1y}(s)}{u} + \frac{I_{2y}(s)}{u^2} + o(u^{-2})\right]. \tag{2.29}$$

Using Eq. (2.16) we obtain

$$I_{1y}(s) = I_{1x}(s^{-1})\sqrt{s}, \qquad I_{2y}(s) = I_{2x}(s^{-1})s. \tag{2.30}$$

In principle, the functions $I_{1x}(s)$ and $I_{2x}(s)$ can be determined by numerical calculations, however, in Section 2.4 some analytical expressions for these functions are given.

In [40] the $u \gg 1$ limit was considered using the Bardeen-Stephen model. This approach is essentially based on the assumption about a step-like order parameter profile within the core and does not allow to obtain a leading term of the order of u^{-1} in the expansion (2.26).

The particular case $s = 1$ has been considered in a number of works mentioned above [33, 36, 37, 38]. It corresponds to isotropic superconductors, or anisotropic superconductors with no anisotropy mismatch: $(m_c\sigma_c)/(m_{ab}\sigma_{ab}) = 1$. If $s = 1$, Eqs. (2.24) and (2.25) can be solved exactly:

$$\Phi_x^{(0)} = \frac{1 - \exp(-\sqrt{f_2}\rho^2/2)}{\rho^2} y,$$

$$\Phi_x^{(1)} = \frac{f_4 y}{u f_2} \left(\frac{1}{4} + \frac{\sqrt{f_2}\rho^2}{8} \right) \exp(-\sqrt{f_2}\rho^2/2).$$

After some integration we obtain a simple relation for the viscous drag coefficients:

$$\eta_x = \eta_y = 2\pi n_0 \Gamma \hbar \alpha_2(u), \tag{2.31}$$

$$\alpha_2(u) \approx \frac{\sqrt{f_2}}{u} + \frac{f_4}{2 f_2 u^2} = \frac{0.583}{u} - \frac{1}{8u^2}. \tag{2.32}$$

Here the value $\sqrt{f_2} = 0.583$ was taken from [37], and the relation $f_4 = -f_2/4$ follows from Eq. (2.11).

It is appropriate to recall here the result obtained by Hu [37]:

$$\alpha_2 = \frac{\mathrm{K}_0(\delta u)}{\delta u \cdot \mathrm{K}_1(\delta u)}, \tag{2.33}$$

where K_0 and K_1 are the modified Bessel functions of an imaginary argument and δ is a fitting parameter. Eq. (2.33) was derived from the exact solution of Eq. (B12) with an approximate order parameter profile:

$$f(\rho) = \frac{\rho}{\sqrt{\delta^2 + \rho^2}}. \tag{2.34}$$

According to Schmid [33] and Hu, the optimal value of δ is $\sqrt{2}$ which follows from a variational principle. We can compare different values of $\alpha_2(u)$. When $u = \sqrt{12}$ Eq. (2.33) yields $\alpha_2 = 0.186$, Eq. (2.32) yields $\alpha_2 = 0.158$, while the numerical result is $\alpha_2 = 0.159$ [38]. Thus, the relation (2.32) gives an error less than 1%. If we keep only the term of order u^{-1} in Eq. (2.32), we will get a 6% error which increases with decreasing u.

2.3.2 The limit $s \gg u \gg 1$

Consider the range of parameters $s \gg u^2$ and $u \gtrsim 1$. In terms of l_E, ξ and φ_0 these conditions read

$$l_{Ec} \gg \xi_c, \qquad l_{Eab} \lesssim \xi_{ab}, \qquad \cos^2\varphi_0 \ll \frac{\sigma_c l_{Eab}^2}{\sigma_{ab}\xi_{ab}^2}.$$

Thus, the magnetic field must make a small angle with the ab-plane.

When $s \gg u^2$, the term $u^2\Phi_x$ in Eq. (2.12) is negligible compared to y_1/ρ_1^2 in the region $\rho \ll \sqrt{s}/u$, so we immediately obtain from Eq. (2.7)

$$\eta_x \sim \ln s/u^2.$$

More complicated calculations, which can be found in Appendix D, yield

$$\eta_x = 2\pi\hbar\Gamma n_0 \left(\ln \frac{\sqrt{s}}{u} - 1.475 \right), \tag{2.35}$$

$$\eta_y = 2\pi\hbar\Gamma n_0 \left(\ln \frac{\sqrt{s}}{u} - 0.475 \right). \tag{2.36}$$

Note that in Ref. [40] in the $u \ll 1$ limit similar expressions containing $\ln u^{-1}$ have been derived. This similarity is not accidental: the presence of the logarithm $\ln(l_E/\xi)$ is a characteristic feature of the $l_E \gg \xi$ limit.

2.4 A variational principle

In this subsection a simple variational procedure is suggested for the calculation of the viscous drag tensor in the general case.

The electric potential Φ is determined by Eq. (B12), which can be viewed as a condition of zero variational derivative of the functional

$$\int_{z=0} W_d[\Phi] d^2\boldsymbol{\rho}, \tag{2.37}$$

where the dissipation function W_d is given by Eq. (2.17). This observation together with Eq. (2.18) yield the variational formulation of our problem:

$$\mathbf{V}_L \hat{\eta} \mathbf{V}_L = \min_{\Phi} \int_{z=0} W_d[\Phi] d^2\boldsymbol{\rho}. \tag{2.38}$$

This relation and the symmetry condition $\eta_{xy} = \eta_{yx}$ completely define the viscous drag tensor. Note that Eq. (2.38) is in good agreement with the general principle of minimum entropy production in stationary processes [87].

Let us rewrite Eq. (2.38) in the rescaled coordinate frame separately for both components of the Bardeen-Stephen contribution:

$$\eta_x = \tilde{\eta}(s, 1, u), \qquad \eta_y = \tilde{\eta}(1, s, u), \tag{2.39}$$

where

$$\tilde{\eta}(s_x, s_y, u) = 2n_0\Gamma\hbar u^2 \cdot \min_{\phi} \int \left[s_x \left(\frac{\partial\phi}{\partial x} \right)^2 + s_y \left(\frac{\partial\phi}{\partial y} \right)^2 + \frac{f^2(\rho)}{u^2} \left(u^2\phi - \frac{y}{\rho^2} \right)^2 \right] dx\, dy. \tag{2.40}$$

We can obtain an upper estimate for the viscosity components if we substitute a trial function into Eq. (2.40). To find an appropriate trial function consider the exact equation for ϕ:

$$s_x \frac{\partial^2\phi}{\partial x^2} + s_y \frac{\partial^2\phi}{\partial y^2} = \left(u^2\phi - \frac{y}{\rho^2} \right) f^2(\rho). \tag{2.41}$$

The solution of this equation is an even function of x and an odd function of y, so its Fourier series has the form

$$\phi = \sum_{n=0}^{\infty} \phi_{2n+1}(\rho) \sin(2n+1)\varphi, \tag{2.42}$$

where φ is the polar angle in the xy plane. When ρ is sufficiently large, $\phi \approx y/(u^2\rho^2)$, which means that the series in Eq. (2.42) contains only the first term at $\rho \to \infty$. Thus, the trial function

$$\phi_t = \frac{4\tilde{\phi}(\rho)}{s_x + 3s_y} \sin\varphi \tag{2.43}$$

has the correct parity and the correct asymptotics. Let us substitute this function into Eq. (2.40):

$$\tilde{\eta} \approx 2n_0\Gamma\hbar\pi\tilde{u}^2 \min_{\tilde{\phi}} \int_0^{\infty} \rho \left[\left(\frac{d\tilde{\phi}}{d\rho} \right)^2 + \frac{\tilde{\phi}^2}{\rho^2} + \frac{f^2(\rho)}{\tilde{u}^2} \left(\tilde{u}^2\tilde{\phi} - \frac{1}{\rho} \right)^2 \right] d\rho, \tag{2.44}$$

where

$$\tilde{u} = u \left(\frac{s_x}{4} + \frac{3s_y}{4} \right)^{-1/2}.$$

The differential equation for $\tilde{\phi}$ is

$$-\frac{1}{\rho}\frac{d}{d\rho}\left(\rho \frac{d\tilde{\phi}}{d\rho} \right) + \frac{\tilde{\phi}}{\rho^2} + f^2(\rho) \left(\tilde{u}^2\tilde{\phi} - \frac{1}{\rho} \right) = 0. \tag{2.45}$$

Note that we obtain exactly the same equation if we substitute $\Phi_x = \tilde{\phi}(\rho)\sin\varphi$ into Eq. (2.12) when $s = 1$ and $u = \tilde{u}$. This means that the trial function (2.43) reduces our problem to an isotropic one. Unfortunately, an exact solution of Eq. (2.45) is unknown. However, Schmid [33] found a solution with an approximate order parameter profile [see Eq. (2.34)]:

$$\tilde{\phi} = \frac{\mathrm{K}_1(\tilde{u}\delta)\delta - \sqrt{\delta^2+\rho^2}\mathrm{K}_1(\tilde{u}\sqrt{\delta^2+\rho^2})}{\delta \mathrm{K}_1(\tilde{u}\delta)\tilde{u}^2\rho}.$$

Using this function and the expression (2.34) for f we can calculate the right-hand side of Eq.(2.44):

$$\tilde{\eta} \approx 2n_0\Gamma\hbar\pi \frac{\mathrm{K}_0(\delta\tilde{u})}{\delta\tilde{u}\mathrm{K}_1(\delta\tilde{u})}. \tag{2.46}$$

We take $\delta = f'(0)^{-1} = f_2^{-1/2}$ in order to obtain the correct asymptotics when $u \to \infty$, $s = 1$ (this asymptotics is determined by $f'(0)$, see subsection 2.3.1). Finally, combining (2.39) and (2.46) we get approximate relations for the components of $\hat{\eta}'$:

$$\eta_x \approx 2\pi n_0\Gamma\hbar \frac{f'(0)}{2u}\sqrt{s+3} \frac{\mathrm{K}_0\left(\frac{2u}{f'(0)\sqrt{s+3}}\right)}{\mathrm{K}_1\left(\frac{2u}{f'(0)\sqrt{s+3}}\right)}, \tag{2.47}$$

$$\eta_y \approx 2\pi n_0 \Gamma\hbar \frac{f'(0)}{2u}\sqrt{3s+1}\frac{\mathrm{K}_0\left(\frac{2u}{f'(0)\sqrt{3s+1}}\right)}{\mathrm{K}_1\left(\frac{2u}{f'(0)\sqrt{3s+1}}\right)}. \tag{2.48}$$

No restrictions on the parameters s and u are implied here.

Let us check if these relations are in accordance with the results from Section 2.3. Expanding η_x in the form (2.47) in the powers of u^{-1} when $u \gg 1$ and $s \lesssim 1$ we obtain the following expressions for the coefficients I_{1x} and I_{2x}, which were introduced in subsection 2.3.1 (see Eq. (2.26)):

$$I_{1x}(s) = -\frac{\pi\sqrt{f_2}\sqrt{s+3}}{2}, \qquad I_{2x}(s) = \frac{\pi f_2(s+3)}{8}. \tag{2.49}$$

When $s = 1$

$$\eta_x = \eta_y = 2\pi n_0 \Gamma\hbar \frac{f'(0)}{u} + O(u^{-2}),$$

which should be compared with Eq. (2.32). The perfect agreement between the exact and approximate result is not surprising, because the trial function (2.43) is the exact solution of our variational problem in the isotropic case.

The applicability of Eqs. (2.47) and (2.48) for $s \neq 1$ has been checked using numerical calculations. Equation (2.41) was solved in the region $x > 0$, $y > 0$ with the boundary conditions

$$\left.\frac{\partial\phi}{\partial x}\right|_{x=0} = 0, \qquad \left.\phi\right|_{y=0} = 0.$$

A sufficiently large 450×450 mesh with a 0.03×0.03 unit cell has been used. The numerical algorithm applied was the method of steepest descent. After the determination of the function $\phi(\boldsymbol{\rho})$ numerical integration has been performed.

When $s = 0$ Eqs. (2.49) and (2.30) give

$$\eta_x = 2n_0\Gamma\hbar\frac{1.59}{u} + O(u^{-2}),$$

$$\eta_y = 2n_0\Gamma\hbar\frac{0.92}{u} + O(u^{-2}).$$

These analytical expressions are in a good agreement with the asymptotics derived by numerical calculations:

$$\eta_x = 2n_0\Gamma\hbar\frac{1.58}{u} + O(u^{-2}),$$

$$\eta_y = 2n_0\Gamma\hbar\frac{0.86}{u} + O(u^{-2}).$$

When $s \gg u^2$ Eqs. (2.47) and (2.48) give

$$\eta_x \approx \eta_y \approx 2\pi\hbar\Gamma n_0 \ln\frac{\sqrt{s}}{u},$$

which coincides with the main logarithmic term in Eqs. (2.35) and (2.36).

One can see that the agreement between the exact and approximate asymptotics is quite well. This is a strong argument in favor of the applicability of Eqs. (2.47) and (2.48) for intermediate values of s and u.

In Fig. 2.2 we plot the analytical and numerical φ_0 dependencies of the diagonal components of the full viscous drag tensor ($\hat{\eta} = \hat{\eta}_{p0} + \hat{\eta}_{oh}$).

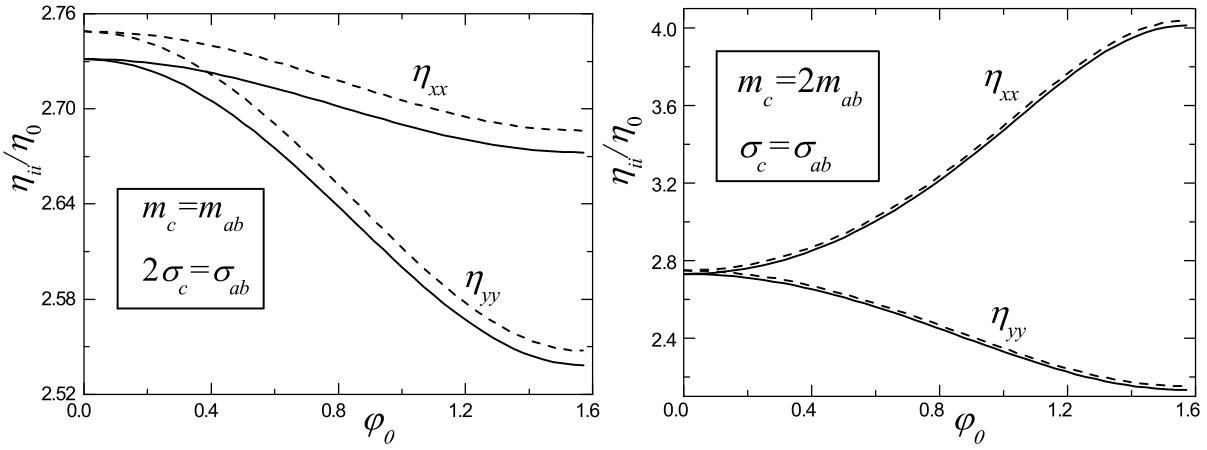

Figure 2.2: The φ_0 dependencies of the viscosity tensor components. Solid lines correspond to analytical results (Eqs. (2.47) and (2.48)), dashed lines show the results of numerical simulations. Here η_{xx} and η_{yy} are measured in the units $\eta_0 = \hbar\Gamma n_0$, $\xi_{ab}/l_{Eab} = \sqrt{12}$.

2.5 Temperature dependence of the vortex viscosity anisotropy

Within the framework of the TDGL equation (2.1) the viscosity anisotropy η_{xx}/η_{yy} does not depend on temperature. However, the region of applicability of Eq. (2.1) is limited by gapless superconductivity. In this section we consider a more general approach based on the generalized TDGL equations [88] (see also [35] for review):

$$2\hbar\Gamma\sqrt{1+q_{\rm ph}\left|\psi\right|^2/n_0}\frac{\partial\left|\psi\right|}{\partial t}=-\frac{\delta F}{\delta\left|\psi\right|}, \tag{2.50}$$

$$\frac{\Gamma\left|\psi\right|^2}{\sqrt{1+q_{\rm ph}\left|\psi\right|^2/n_0}}\left(\hbar\frac{\partial\theta_S}{\partial t}-2e\Phi\right)=\frac{\hbar^2}{2}\nabla\left(\left|\psi\right|^2\hat{m}^{-1}\nabla\theta_S\right), \tag{2.51}$$

$$q_{\rm ph}=\frac{32\pi^2\tau_{\rm ph}^2T_c(T_c-T)}{7\zeta(3)\,\hbar^2}.$$

Here $\tau_{\rm ph}$ is the electron-phonon mean free time. In the isotropic case Eqs. (2.50) and (2.51) are valid for dirty superconductors, when the temperature is close to T_c and variations of the order parameter in space and in time are sufficiently slow [35].

The main relations for the viscous drag tensor can be derived in same way as described in section 2.2 and in Appendix B. As a result, we find that the viscosity still comprises two terms representing two mechanisms of dissipation, but the viscosity components undergo some changes. For example, Eq. (2.5) is modified as follows:

$$(\eta'_{p0})_{ij}=2\pi\,\hbar\Gamma n_0\delta_{ij}\int_0^\infty\left(\frac{df}{d\rho}\right)^2\rho\sqrt{1+q_{\rm ph}f^2(\rho)}d\rho. \tag{2.52}$$

To obtain the counterparts of Eqs. (2.7), (2.8), (2.12) and (2.13) one should make the following substitutions in these equations:

$$\begin{aligned} u^2 \quad &\to \quad \frac{u^2}{\sqrt{1+q_{\rm ph}}}, \\ f^2 \quad &\to \quad \frac{\sqrt{1+q_{\rm ph}}f^2}{\sqrt{1+q_{\rm ph}f^2}}, \\ \eta_i \quad &\to \quad \eta_i\sqrt{1+q_{\rm ph}}, \qquad i=x,y. \end{aligned} \tag{2.53}$$

It can be seen from Eq. (2.51) that the electric field penetration depth is increased by a factor $(1+q_{\rm ph})^{1/4}$ as compared to Eq. (2.10). It may seem that at low temperatures we would reach the $l_E \gg \xi$ limit, which has been analyzed in [40]. However, this is not quite true because of the different relative impacts of the two mentioned mechanisms of dissipation in the simple and generalized TDGL models. Within the simple TDGL theory the Bardeen-Stephen contribution and the relaxational term are of the same order of magnitude in the $l_E \gg \xi$ limit. On the contrary, in the generalized model the viscosity is dominated by the relaxational term at low temperatures (see below).

It is obvious that all main relations from Sec. 2.3 can be derived again within the generalized TDGL theory, but they are slightly modified. For example, Eq. (2.31) now reads

$$\eta_x = \eta_y \approx 2\pi\,\hbar\Gamma n_0 \left[\frac{\sqrt{f_2}}{u} - \frac{1+2q_{\rm ph}}{8u^2}\right]. \tag{2.54}$$

Now consider the temperature dependence of the viscous drag tensor. The quantity $q_{\rm ph}$ depends on the temperature T: $(q_{\rm ph})'_T < 0$. Hence,

$$\frac{\partial}{\partial T}\frac{(\eta_{p0})_{xx}}{\eta_0} = \frac{\partial}{\partial T}\frac{(\eta_{p0})_{yy}}{\eta_0} < 0,$$

where $\eta_0 = \hbar\Gamma n_0$. On the other hand, the modified Eq. (2.40) can be written in the form

$$\begin{aligned} \tilde{\eta}(s_x, s_y, u) = 2n_0\Gamma\hbar u^2 \min_{\phi} \int \Bigg[s_x \left(\tfrac{\partial\phi}{\partial x}\right)^2 + s_y \left(\tfrac{\partial\phi}{\partial y}\right)^2 \\ + \tfrac{f^2(\rho)}{u^2\sqrt{1+q_{\rm ph}f^2(\rho)}} \left(u^2\phi - \tfrac{y}{\rho^2}\right)^2 \Bigg] dx\,dy, \end{aligned} \tag{2.55}$$

if we leave Eqs. (2.39) unchanged. Hence,

$$\frac{\partial}{\partial T}\frac{(\eta_{\rm oh})_{xx}}{\eta_0} > 0; \qquad \frac{\partial}{\partial T}\frac{(\eta_{\rm oh})_{yy}}{\eta_0} > 0.$$

At sufficiently low temperatures, when $q_{\rm ph} \gg 1$, $s \lesssim 1$ and $u \sim 1$, it may happen that

$$(\eta_{p0})_{xx} \gg (\eta_{\rm oh})_{xx}, \qquad (\eta_{p0})_{yy} \gg (\eta_{\rm oh})_{yy}.$$

Then the viscosity anisotropy is determined by the relaxational term:

$$\frac{\eta_{xx}}{\eta_{yy}} \approx \frac{(\eta_{p0})_{xx}}{(\eta_{p0})_{yy}} = \frac{1+\mu}{1+\mu\cos^2\varphi_0}.$$

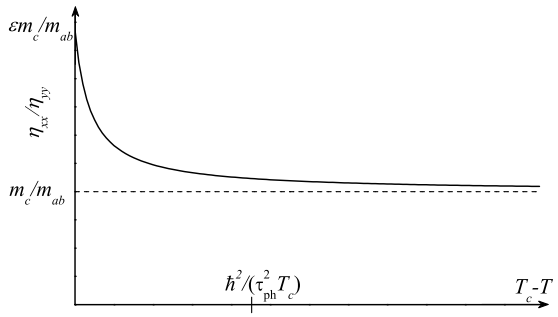

Figure 2.3: Schematic temperature dependence of the viscosity anisotropy for $\varphi_0 = \pi/2$. The parameter ϵ is of the order of unity.

Note that $\eta_x \neq \eta_y$ when $s \neq 1$, so

$$\frac{\eta_{xx}}{\eta_{yy}} \neq \frac{1+\mu}{1+\mu\cos^2\varphi_0}$$

when $q_{\rm ph} \lesssim 1$. We have proved that within the generalized TDGL theory the viscosity anisotropy and the flux-flow conductivity anisotropy do depend on temperature. The schematic T dependence of the ratio η_{xx}/η_{yy} is plotted in Fig. 2.3.

2.6 Summary

In the present Chapter the viscous flux-flow in anisotropic superconductors has been analyzed within the time-dependent Ginzburg-Landau theory. The Bardeen-Stephen contribution to the viscous drag tensor $\hat{\eta}$ has been calculated in the limits $l_E \ll \xi$ and $l_{Ec} \gg \xi_c$. Unlike in the preceding works, in these calculations no simplifying assumptions concerning the shape of the order parameter in a static vortex have been made. In addition, a variational procedure has been suggested, which allowed to derive the relations (2.47) and (2.48) suitable for arbitrary electric field penetration lengths (l_{Eab} and l_{Ec}), coherence lengths (ξ_{ab} and ξ_c) and orientation of the magnetic field. The mentioned approximate relations for $\hat{\eta}$ are in good agreement with numerical calculations.

The results obtained in this Chapter may be useful for interpretation of experimental data on the flux-flow conductivity in anisotropic superconductors in weak magnetic fields ($B \ll H_{c2}$).

Vortex motion has also been considered within a generalized TDGL theory. It has been found that the viscosity anisotropy may depend on temperature and, thus, the flux-flow conductivity anisotropy may be altered by heating or cooling the sample.

Chapter 3

Interaction between spin waves and vortices in superconductor-ferromagnet hybrids

3.1 Introduction

In magnetic materials the long-wavelength magnetization dynamics is well described by the simple phenomenological Landau-Lifshitz equation [3], or its generalization taking into account dissipation – the Landau-Lifshitz-Gilbert equation [72]:

$$\frac{\partial \mathbf{M}}{\partial t} = \gamma \left(\mathbf{M} \times \frac{\delta F}{\delta \mathbf{M}} \right) + \frac{\nu}{M^2} \left(\mathbf{M} \times \frac{\partial \mathbf{M}}{\partial t} \right). \tag{3.1}$$

Here, $\mathbf{M}$ is the local magnetization of the ferromagnet (or the sublattice magnetization in the case of a ferrimagnet), Γ is the gyromagnetic ratio, F is the free energy, and ν is a relaxation constant. Using Eq. (3.1) it is easy to obtain the classical spin-wave spectrum of a ferromagnet with an easy-axis type magnetocrystalline anisotropy [3]:

$$\omega(q) = \omega_F(1 + L^2 q^2), \tag{3.2}$$

Here, ω_F is the ferromagnetic resonance frequency, and L is a length of the order of the Bloch domain wall width. The antiferromagnetic counterpart of Eq. (3.2) is [3]

$$\omega(q) = \sqrt{\omega_{AF}^2 + s_{AF}^2 q^2}, \tag{3.3}$$

where ω_{AF} is the antiferromagnetic resonance frequency, and s_{AF} is the velocity of magnons with large wave numbers q. The spectra (3.2) and (3.3) do not account for the magnetostatic interaction. If it is taken into account, the dispersion relations become more complicated. For example, the ferromagnetic spectrum takes the form

$$\omega^2(q) = \omega_F^2 \left(1 + L^2 q^2 + \frac{B_0 - 4\pi M}{H_{\text{an}}} \right) \left(1 + L^2 q^2 + \frac{B_0 - 4\pi M}{H_{\text{an}}} + 4\pi - 4\pi \frac{(\mathbf{qe})^2}{q^2} \right). \tag{3.4}$$

Here, B_0 is the magnetic induction in the sample, $\mathbf{e}$ is a unit vector directed along the anisotropy axis, and H_{an} is the anisotropy field, defining the ferromagnetic resonance frequency: $\omega_F = \gamma H_{\text{an}}$.

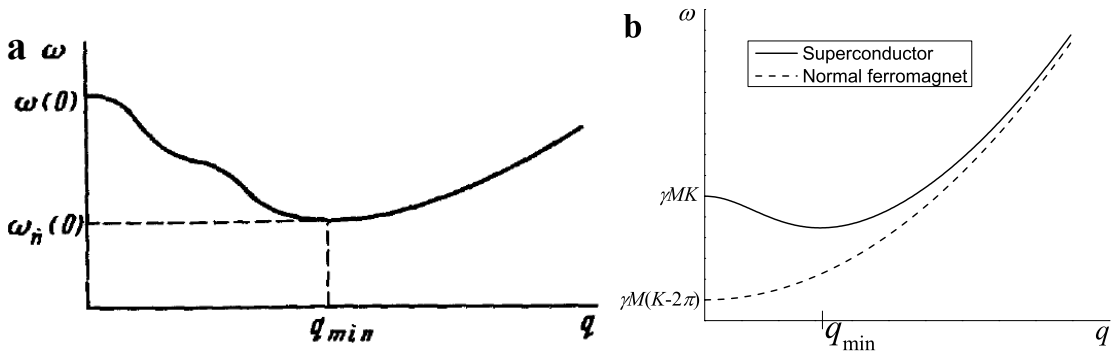

Figure 3.1: (a) The magnon spectrum in an antiferromagnetic superconductor at a fixed direction of the wave vector [61]. (b) The spectra of magnons propagating normal to the easy magnetization axis in a superconducting and ordinary ferromagnet. All graphs correspond to a vanishing internal magnetic induction B_0.

In magnetic superconductors the spin waves interact with the superconducting subsystem through the exchange and anisotropy fields, which leads to a further modification of the magnon spectrum. Buzdin [61] has shown that within the London approximation the antiferromagnetic spectrum becomes non-monotonic – see Fig. 3.1a. Later [62, 63], a similar result has been obtained for a ferromagnetic superconductor in the Meissner state – see Fig. 3.1b. The presence of a minimum on the $\omega(q)$ dependence is closely related to the appearance of a spiral magnetic order is some magnetic superconductors [51].

In later works the microwave surface impedance of a ferromagnetic superconductor has been studied in detail [89], and the spectra of 2-dimensional surface and domain wall magnons have been determined [90, 91]. In these papers it has been assumed that the superconductor is in the Meissner state, while experimental studies suggest that the ferromagnetic superconductors exhibit a spontaneous mixed state [55, 56, 57]. The spin-wave spectrum in the vortex phase has been previously considered only by Ng and Varma [62]. In this paper the coupled spin and vortex dynamics has been studied within the continuous medium approximation, which is applicable in the limit of long wavelengths λ_w: $\lambda_w \gg a_v$, where a_w is the intervortex distance.

In the papers [64, 65, 68, 69, 66] the reverse influence of magnons on vortex dynamics has been analyzed. Bulaevskii, Hruška and Maley showed [64] that vortex motion may be accompanied by Cherenkov generation of magnons. This new dissipation mechanism leads to the appearance of an additional damping force acting on vortices, which is reflected in the current-voltage characteristics of the sample. Thus, information about the spin-wave spectrum can be extracted from the I-V curve of a magnetic superconductor. In [65] an estimate of the magnetic contribution to the vortex viscosity in antiferromagnetic borocarbides is given. In [68] it is proposed study the magnon spectrum in magnetic superconductor by measuring the response of the material to a superposition of ac and dc currents. The nonlinear magnetization dynamics (corresponding to spin-waves with a large amplitude) was considered in [69]. The authors demonstrated numerically that vortices in magnetic superconductors may form clusters, and moving vortices may create domain walls, if the dissipation constant ν in Eq. (3.1) is sufficiently small.

In the papers [66, 70, 67, 71] vortex motion in systems with purely relaxational dy-

namics of the magnetization has been considered:

$$\tau_M \frac{\partial \mathbf{M}}{\partial t} = -\frac{1}{2}\frac{\delta F}{\delta \mathbf{M}}, \tag{3.5}$$

where τ_M — is the relaxation time. Obviously, such systems do not support oscillating magnon modes. In [66] a novel "polaronic" vortex pinning mechanism is proposed to explain the unusual magnetization curves of borocarbides. The new pinning mechanism appears due to the attraction of a vortex to magnetic moments which were polarized by the same vortex. The influence of this effect on the ac response of the material has been studied in [67]. In [70] it was proposed to improve the transport characteristics of superconductors with a small London penetration depth by creating superconductor-ferromagnet (SF) superlattices, where the "polaronic" pinning mechanism is realized.

In this Chapter of the thesis two problems are solved, concerning the interplay between Abrikosov vortices and spin waves in SF-hybrids: the calculation of the magnon spectrum in the presence of vortices, and the analysis of the ac and dc responses of vortices in the presence of magnetic moments. The initial equations for both problems are derived in Sec. 3.2. In Sec. 3.3 the spin wave spectrum in a ferromagnetic superconductor in the mixed state is studied. The results of the paper [62] are extended to the case of short wavelengths, $\lambda_w \lesssim a_v$, when Bragg scattering of magnons on the vortex lattice becomes important. Then the spin-wave spectrum acquires a Bloch-like band structure. In Sec. 3.4 the damping force, connected with magnon generation, acting on moving vortices in ferromagnetic superconductors and SF-superlattices is calculated. It is shown that the magnetic contribution to the vortex viscosity can be extracted from the surface impedance of a ferromagnetic superconductor.

3.2 Basic equations

Within the London approximation the free energy of a ferromagnetic superconductor can be written as

$$F = \int \left[\frac{1}{8\pi\lambda^2}\left(\mathbf{A} + \frac{\Phi_0}{2\pi}\nabla\theta_S\right)^2 + \frac{(\mathbf{B}-4\pi\mathbf{M})^2}{8\pi} + \frac{\alpha}{2}\left(\frac{\partial \mathbf{M}}{\partial x_i}\frac{\partial \mathbf{M}}{\partial x_i}\right) + \frac{K\mathbf{M}_\perp^2}{2} - \frac{\mathbf{B}\mathbf{H}_e}{4\pi}\right] d^3\mathbf{r}, \tag{3.6}$$

where α is an exchange constant, K is an anisotropy constant, $\mathbf{M}_\perp = \mathbf{M} - (\mathbf{M}\mathbf{e})\mathbf{e}$, and $\mathbf{H}_e$ is the external magnetic field. All terms in Eq. (3.6) are integrated over the whole space, except for the first term, which is integrated over the sample volume. We assume $\mathbf{M} = 0$ outside the sample, and $|\mathbf{M}| = \text{const}$ in the ferromagnetic superconductor.

Before considering the magnetization dynamics, we determine the equilibrium state by minimizing F with respect to $\mathbf{M}$, and then with respect to $\mathbf{A}$ and θ_S. The anisotropy field $H_{\text{an}} = KM$ in the U-based ferromagnetic superconductors is typically very large (see Table 3.1): it is comparable to or greater than the upper critical field. This means that the inequality $B \ll H_{\text{an}}$ holds for any internal field B that does not suppress superconductivity. Then the transverse component of the magnetization $\mathbf{M}_\perp$ can be estimated as $M_\perp \lesssim B/K \ll M$. Since $K \gg 1$, in a zero approximation with respect to K^{-1} we can neglect the transverse magnetization (even in the anisotropy energy, which

appears to be proportional to K^{-1}). Then

$$F(\mathbf{A},\theta_S) \approx \int \left[\frac{1}{8\pi\lambda^2} \left(\mathbf{A} + \frac{\Phi_0}{2\pi} \nabla\theta_S \right)^2 + \frac{B^2}{8\pi} - \mathbf{B}\mathbf{M}_0 - \frac{\mathbf{B}\mathbf{H}_e}{4\pi} + 2\pi M^2 \right] d^3\mathbf{r}, \qquad (3.7)$$

where $\mathbf{M}_0 = M\mathbf{e}$. For an arbitrary shaped sample further minimization can not be performed analytically. Here we assume the ferromagnetic superconductor to be an ellipsoid. The results derived below should be also valid in the extreme cases of slabs and long cylinders. It is reasonable to assume that the average internal magnetic field $\mathbf{B}_0$ in an ellipsoidal sample will be uniform (compare with a dielectric ellipsoid in a uniform external field – see [92]). Denoting the superconductor volume as V, we can rewrite the free energy as

$$F = V \left(f_S(B_0) - \mathbf{M}_0\mathbf{B}_0 - \frac{\mathbf{B}_0\mathbf{H}_e}{4\pi} \right) + \int_{\mathbf{r}\notin V} \left[\frac{B^2}{8\pi} - \frac{\mathbf{B}\mathbf{H}_e}{4\pi} \right] d^3\mathbf{r} + \text{const}, \qquad (3.8)$$

where the constant does not depend on the magnetic induction $\mathbf{B}$, and f_S is the free energy density of the vortex lattice:

$$f_S(B_0) = \left\langle \frac{1}{8\pi\lambda^2} \left(\mathbf{A} + \frac{\Phi_0}{2\pi} \nabla\theta_S \right)^2 + \frac{B^2}{8\pi} \right\rangle. \qquad (3.9)$$

Averaging is performed over a volume that is much larger than the inter-vortex distance. The function $f_S(B_0)$ can be determined explicitly by solving the London equation (3.14) with a given vortex lattice density, corresponding to the average field B_0. To transform the integral in Eq. (3.8) let us introduce several quantities: the self-field of the sample $\mathbf{B}_S = \mathbf{B} - \mathbf{H}_e$, the magnetization $\mathbf{M}_S$ due to supercurrents, the effective full magnetization $\mathbf{M}_{\text{eff}} = \mathbf{M}_0 + \mathbf{M}_S$, and the effective H-field $\mathbf{H}_{\text{eff}} = \mathbf{B}_S - 4\pi\mathbf{M}_{\text{eff}}$. Then the integral can be transformed as

$$\int_{\mathbf{r}\notin V} \left[\tfrac{B^2}{8\pi} - \tfrac{\mathbf{B}\mathbf{H}_e}{4\pi} \right] d^3\mathbf{r} = \int_{\mathbf{r}\notin V} \tfrac{B_S^2}{8\pi} d^3\mathbf{r} - \int_{\mathbf{r}\notin V} \tfrac{H_e^2}{8\pi} d^3\mathbf{r}$$
$$= \int \tfrac{\mathbf{H}_{\text{eff}}^2}{8\pi} d^3\mathbf{r} - \int_{\mathbf{r}\in V} \tfrac{\mathbf{H}_{\text{eff}}^2}{8\pi} d^3\mathbf{r} + \text{const} = \tfrac{V}{2} \mathbf{M}_{\text{eff}} \left(\hat{N} - \tfrac{\hat{N}^2}{4\pi} \right) \mathbf{M}_{\text{eff}} + \text{const}.$$

Here $\hat{N}$ is the demagnetizing tensor, connecting the effective magnetization and effective field inside the sample: $\mathbf{H}_{\text{eff}} = -\hat{N}\mathbf{M}_{\text{eff}}$. Analytical and numerical values of $\hat{N}$ can be found in Ref. [93]. Finally, if we eliminate $\mathbf{M}_{\text{eff}}$ using the relation

$$\mathbf{M}_{\text{eff}} = (4\pi - \hat{N})^{-1}(\mathbf{B}_0 - \mathbf{H}_e),$$

we obtain

$$\frac{F}{V} = f_S(B_0) - \mathbf{M}_0\mathbf{B}_0 - \frac{\mathbf{B}_0\mathbf{H}_e}{4\pi} + \frac{1}{8\pi}(\mathbf{B}_0 - \mathbf{H}_e)\hat{N}(4\pi - \hat{N})^{-1}(\mathbf{B}_0 - \mathbf{H}_e) + \text{const}. \qquad (3.10)$$

Here the only variable is the internal field $\mathbf{B}_0$, which should be determined from the equation

$$\frac{\partial F}{\partial \mathbf{B}_0} = 0. \qquad (3.11)$$

Compound	UGe_2	UCoGe	URhGe
T_c, K	0.7	0.8	0.25
Θ, K	50	3	9.5
λ, nm	1000	1200	900
$H_{\rm an}$, T	~ 100	~ 10	~ 10
M, Gs	150	9	70
μ_U	$1{,}4\mu_B$	$0{,}07\mu_B$	$0{,}3\mu_B$
ω_F, Hz	$\sim 10^{13}$	$\sim 10^{10}$	$\sim 10^{11}$
$V_{\rm th}$, cm/s	$\sim 10^7$	$\sim 10^5$	$\sim 10^7$
$K = H_{\rm an}/M$	$\sim 10^4$	$\sim 10^4$	$\sim 10^3 - 10^4$

Table 3.1: Parameters of U-based ferromagnetic superconductors. Θ is the Curie temperature, $H_{\rm an}$ is the anisotropy field, μ_U is the magnetic moment per U atom, μ_B is the Bohr magneton, ω_F is the ferromagnetic resonance frequency (the estimate $\omega_F \sim 2\mu_U H_{\rm an}/\hbar$ is used here), and $V_{\rm th}$ is the critical vortex velocity for magnon radiation (see Sec. 3.4). The data have been taken from [94, 55, 95, 96].

Equations (3.10) and (3.11) define the equilibrium state of the ferromagnetic superconductor.

Now we proceed from statics to coupled vortex and magnetization dynamics. Taking into account Eq. (3.6), we can rewrite the Landau-Lifshitz-Gilbert equation (3.1) as

$$\frac{\partial \mathbf{M}}{\partial t} = \gamma \left(\alpha \nabla^2 \mathbf{M} - K \mathbf{M}_\perp + \mathbf{B} \right) \times \mathbf{M} + \frac{\nu}{M^2} \left(\mathbf{M} \times \frac{\partial \mathbf{M}}{\partial t} \right). \tag{3.12}$$

Considering the high-anisotropy limit ($K \gg 1$), we assume the transverse magnetization $\mathbf{M}_\perp \equiv \mathbf{m}$ to be small: $|\mathbf{m}| \ll M$. Then Eq. (3.12) can be linearized with respect to $\mathbf{m}$:

$$\frac{\partial \mathbf{m}}{\partial t} = \gamma \left(\alpha \nabla^2 \mathbf{m} - K \mathbf{m} + \mathbf{B} \right) \times \mathbf{M}_0 + \gamma \mathbf{B} \times \mathbf{m} + \frac{\nu}{M^2} \mathbf{M}_0 \times \frac{\partial \mathbf{m}}{\partial t}. \tag{3.13}$$

The magnetic field $\mathbf{B}$ satisfies the London equation, which should account for the normal currents in the nonstationary case:

$$\operatorname{rot} \operatorname{rot} \mathbf{B} + \frac{\mathbf{B}}{\lambda^2} = \frac{\boldsymbol{\kappa}}{\lambda^2} + 4\pi \operatorname{rot} \operatorname{rot} \mathbf{m} - \frac{4\pi\sigma_n}{c^2} \frac{\partial \mathbf{B}}{\partial t}, \tag{3.14}$$

where σ_n is the normal conductivity outside the vortex core, and κ is the vorticity:

$$\boldsymbol{\kappa} = -\frac{\Phi_0}{2\pi} \operatorname{rot} \nabla \theta_S = \Phi_0 \sum_i \left(\mathbf{z}_0 + \frac{d\mathbf{R}_i}{dz} \right) \delta(\boldsymbol{\rho} - \mathbf{R}_i(z)). \tag{3.15}$$

Here the z axis is directed along the average field $\mathbf{B}_0$, and the function $\mathbf{R}_i(z)$ defines the shape of the i-th vortex. The vectors $\mathbf{R}_i$ and $\boldsymbol{\rho}$ lie in the xy plane. Vortex motion may be described phenomenologically by the relaxation equation [62]

$$\eta \frac{d\mathbf{R}_i(z)}{dt} = -\frac{\delta F}{\delta \mathbf{R}_i}, \tag{3.16}$$

where η is a viscosity coefficient connected with dissipative processes in the vortex core – see Chapter 2. Equations (3.13) - (3.16) comprise the basis for further analysis.

3.3 Band structure of magnetic excitations in the mixed state of a ferromagnetic superconductor

3.3.1 Equations for the magnetization Fourier components

In this section the magnon spectrum in a ferromagnetic superconductor in the presence of an ideal vortex lattice will be determined.

In the following we will neglect the contribution of the normal currents in Eq. (3.14), assuming that the inequality

$$\lambda^{-2} \gg \frac{4\pi}{c}\sigma_n\omega$$

holds. This condition can be satisfied at sufficiently low temperatures, when the normal conductivity is small.

For a start, let us determine the spectrum in the Meissner state. Then, we put $\boldsymbol{\kappa} = 0$, and

$$\mathbf{B}, \mathbf{m} \sim e^{-i\omega t + ik_z z + i\mathbf{qr}},$$

where $\mathbf{q} = (q_x, q_y, 0)$. In Eq. (3.13) the nonlinear term $\mathbf{B} \times \mathbf{m}$ should be dropped. Then, the solvability condition of the linear equations (3.13) (with $\nu = 0$) and (3.14) gives the magnon spectrum:

$$\omega = \omega_0(q) \equiv \gamma M\sqrt{K_1 K_2}, \tag{3.17}$$

$$K_1(q, k_z) = \tilde{K} + \alpha q^2 - \tfrac{4\pi k_z^2}{\lambda^{-2}+k_z^2+q^2}, \tag{3.18}$$

$$K_2(q, k_z) = \tilde{K} + \alpha q^2 - \tfrac{4\pi(k_z^2+q^2)}{\lambda^{-2}+k_z^2+q^2}, \tag{3.19}$$

where $\tilde{K} = K + \alpha k_z^2$. The high anisotropy of the U-based ferromagnetic superconductors allows to simplify the expression for the frequency by expanding the root in Eq. (3.17) in the powers of the small quantity $(K_1 - K_2)/K_1$:

$$\omega_0(q, k_z) \approx \gamma M \left[\tilde{K} + \alpha q^2 - \frac{2\pi(2k_z^2 + q^2)}{\lambda^{-2} + k_z^2 + q^2}\right]. \tag{3.20}$$

A characteristic feature of this spectrum is the presence of a minimum at

$$q = q_{min} = \sqrt{\sqrt{2\pi\frac{\lambda^{-2} - k_z^2}{\alpha}} - \lambda^{-2} - k_z^2} \tag{3.21}$$

for sufficiently small k_z (see Fig. 3.1b).

Now we turn to the more realistic case of a ferromagnetic superconductor in the mixed state. If the external magnetic field is absent or parallel to the easy axis, the Abrikosov vortices in equilibrium are directed along the magnetization vector. We assume the vortex lattice to be triangular with the positions of the vortices given by the vectors

$$\mathbf{R}_{i0} = a_v \mathbf{y}_0 p + a_v \left(\frac{\sqrt{3}}{2}\mathbf{x}_0 + \frac{1}{2}\mathbf{y}_0\right) n, \tag{3.22}$$

where p and n are integers. Then, the equilibrium vorticity $\boldsymbol{\kappa}_0$ and magnetic field $\mathbf{B}_v$ are

$$\boldsymbol{\kappa}_0 = \Phi_0 \mathbf{z}_0 \sum_i \delta^{(2)}(\boldsymbol{\rho} - \mathbf{R}_{i0}), \tag{3.23}$$

$$\mathbf{B}_v = \mathbf{z}_0 \sum_{G<\xi^{-1}} B_v(\mathbf{G}) e^{i\mathbf{G}\mathbf{r}}, \quad B_v(\mathbf{G}) = \frac{\Phi_0}{1+G^2\lambda^2} \cdot \frac{2}{\sqrt{3}a_v^2}, \tag{3.24}$$

where $\mathbf{G}$ are the vectors of the reciprocal lattice:

$$\mathbf{G} = p\mathbf{G}_1 + n\mathbf{G}_2, \quad \mathbf{G}_1 = \frac{4\pi}{\sqrt{3}a_v}\mathbf{x}_0, \quad \mathbf{G}_2 = \frac{2\pi}{\sqrt{3}a_v}\mathbf{x}_0 + \frac{2\pi}{a_v}\mathbf{y}_0. \tag{3.25}$$

The linearized equations (3.13) and (3.14) take the form

$$\frac{\partial \mathbf{m}}{\partial t} = \gamma M \left[\alpha \nabla^2 \mathbf{m} - \left(K + \frac{B_v(\mathbf{r})}{M}\right)\mathbf{m} + \mathbf{b}\right] \times \mathbf{z}_0 + \frac{\nu}{M}\mathbf{z}_0 \times \frac{\partial \mathbf{m}}{\partial t}, \tag{3.26}$$

$$-\nabla^2 \mathbf{b} + \frac{\mathbf{b}}{\lambda^2} = 4\pi \,\mathrm{rot}\,\mathrm{rot}\,\mathbf{m} + \frac{1}{\lambda^2}\boldsymbol{\kappa}_1, \tag{3.27}$$

where $\mathbf{b} = \mathbf{B} - \mathbf{B}_v$ and $\boldsymbol{\kappa}_1 = \boldsymbol{\kappa} - \boldsymbol{\kappa}_0$. At this point, we will drop the last term, which is responsible for dissipation, in Eq. (3.26). The linear correction to the equilibrium vorticity is

$$\boldsymbol{\kappa}_1 = \Phi_0 \sum_i \left\{ \delta(\boldsymbol{\rho} - \mathbf{R}_{i0}) \frac{d\Delta\mathbf{R}_i}{dz} - \mathbf{z}_0 [\Delta\mathbf{R}_i \cdot \nabla_{\boldsymbol{\rho}} \delta(\boldsymbol{\rho} - \mathbf{R}_i)] \right\}, \tag{3.28}$$

where $\Delta\mathbf{R}_i(z)$ is the local displacement of the i-th vortex with respect to the equilibrium state $\mathbf{R}_{i0}$. Equation (3.16) after the evaluation of the variational derivative takes the form

$$\begin{aligned} -\eta \tfrac{d}{dt}\Delta\mathbf{R}_i(z) = \tfrac{\Phi_0}{(2\pi)^{3/2}} \textstyle\int_{k<\xi^{-1}} \tfrac{-ik_z(\boldsymbol{\kappa}_{1k} - 4\pi\mathbf{m}_k) + i\mathbf{k}(\mathbf{z}_0\boldsymbol{\kappa}_{1k})}{4\pi(\lambda^2k^2+1)} \exp(i\mathbf{k}\mathbf{R}_i + ik_z z) d^3\mathbf{k} \\ - \textstyle\sum_{G<\xi^{-1}} \tfrac{B_0\Phi_0(\mathbf{G}\Delta\mathbf{R}_i)\mathbf{G}}{4\pi(\lambda^2G^2+1)}, \end{aligned} \tag{3.29}$$

where for any function $X(\mathbf{r})$ its Fourier transform X_k is defined as

$$X_k = \frac{1}{(2\pi)^{3/2}} \int X(\mathbf{r}) e^{-i\mathbf{k}\mathbf{r}} d^3\mathbf{r}.$$

We may rewrite Eqs. (3.26), (3.27) and (3.29) in the Fourier representation. If we do so, we will find that these equations connect the Fourier components of the functions $\mathbf{m}$, $\mathbf{b}$ and $\boldsymbol{\kappa}$ corresponding to wave-vectors satisfying the condition

$$\mathbf{k} = \mathbf{G} + \mathbf{k}_0, \tag{3.30}$$

where $\mathbf{k}_0$ is a fixed arbitrary vector, and the vector $\mathbf{G}$ runs over the whole reciprocal lattice (3.25). Hence, the general solution of Eqs. (3.26), (3.27) and (3.29) can be presented as a superposition of particular solutions having the form

$$\mathbf{m} = e^{-i\omega t + ik_z z + i\mathbf{q}\mathbf{r}} \textstyle\sum_{\mathbf{G}} \mathbf{m}(\mathbf{G}) e^{i\mathbf{G}\mathbf{r}}, \tag{3.31}$$

$$\mathbf{b} = e^{-i\omega t + ik_z z + i\mathbf{q}\mathbf{r}} \textstyle\sum_{\mathbf{G}} \mathbf{b}(\mathbf{G}) e^{i\mathbf{G}\mathbf{r}}, \tag{3.32}$$

$$\boldsymbol{\kappa}_1 = e^{-i\omega t + ik_z z + i\mathbf{q}\mathbf{r}} \textstyle\sum_{\mathbf{G}} \boldsymbol{\kappa}_1(\mathbf{G}) e^{i\mathbf{G}\mathbf{r}}, \tag{3.33}$$

where $\mathbf{q}$ is the quasi-wave vector in the xy-plane. The fact that the functions (3.31) - (3.33) satisfy our equations represents a simple generalization of the Bloch theorem. The condition (3.33) is equivalent to the following one:

$$\Delta\mathbf{R}_i(z) = \Delta\mathbf{R} e^{-i\omega t + ik_z z + i\mathbf{q}\mathbf{R}_i}. \tag{3.34}$$

If we substitute (3.31), (3.32) and (3.34) into Eqs. (3.26), (3.27) and (3.29), we obtain the system

$$\frac{i\omega\eta}{\Phi_0}\Delta\mathbf{R} = \sum_{G_i<\xi^{-1}} \frac{4\pi i k_z \mathbf{m}(\mathbf{G}_i) + B_0 k_z^2 \Delta\mathbf{R}}{4\pi\left[1+\lambda^2(k_z^2+q_i^2)\right]} + \sum_{G_i<\xi^{-1}} \frac{B_0}{4\pi}\left[\frac{\mathbf{q}_i(\mathbf{q}_i\Delta\mathbf{R})}{1+\lambda^2(q_i^2+k_z^2)} - \frac{\mathbf{G}_i(\mathbf{G}_i\Delta\mathbf{R})}{1+\lambda^2 G_i^2}\right], \tag{3.35}$$

$$-\tfrac{i\omega}{\gamma M}\mathbf{m}(\mathbf{G}_i) = \Big[-(\tilde{K}+\alpha q_i^2)\mathbf{m}(\mathbf{G}_i) + \tfrac{4\pi(k_z^2+q_i^2)\mathbf{m}(\mathbf{G}_i) - 4\pi\mathbf{q}_i(\mathbf{q}_i\mathbf{m}(\mathbf{G}_i)) + B_0\lambda^{-2}ik_z\Delta\mathbf{R}}{k_z^2+q_i^2+\lambda^{-2}}$$
$$-\tfrac{1}{M}\sum_{\mathbf{G}'\neq 0}\mathbf{m}(\mathbf{G}')B_v(\mathbf{G}_i-\mathbf{G}')\Big]\times\mathbf{z}_0, \tag{3.36}$$

where $\mathbf{q}_i = \mathbf{q} + \mathbf{G}_i$, and

$$\tilde{K} = K + B_0/M + \alpha k_z^2. \tag{3.37}$$

By solving Eqs. (3.35) and (3.36) the dispersion relation may be found.

First, we restrict ourselves to the case when the dissipation due to vortex motion is negligible, i. e., $\eta \to \infty$ and $\Delta\mathbf{R} = 0$. The role of thermal losses will be discussed in Sec. 3.3.4.

It has been mentioned that in the U-based compounds the magnetic anisotropy is rather large. Using this fact one can make an approximation which will considerably simplify the problem. Let the vectors $\mathbf{q}_i$ have the components $(q_i\cos\alpha_i, q_i\sin\alpha_i)$. For $q_i = 0$ the angle α_i is arbitrary. We introduce the new variables

$$m'_{ix} = [\cos\alpha_i m_x(\mathbf{G}_i) + \sin\alpha_i m_y(\mathbf{G}_i)]\sqrt[4]{\tfrac{K_1(q_i)}{K_2(q_i)}},$$
$$m'_{iy} = [\cos\alpha_i m_y(\mathbf{G}_i) - \sin\alpha_i m_x(\mathbf{G}_i)]\sqrt[4]{\tfrac{K_2(q_i)}{K_1(q_i)}},$$

where K_1 and K_2 are defined by Eqs. (3.18), (3.19) (and $\tilde{K}$ is given by (3.37)). Here and further we omit k_z in the list of arguments of K_1, K_2 and ω_0 for brevity. The quantities m'_{ix} and m'_{iy} satisfy the equations

$$-\tfrac{i\omega}{\gamma M}m'_{ix} = -\tfrac{\omega_0(q_i)}{\gamma M}m'_{iy} - \sum_{\mathbf{G}_j\neq 0} b_{ij}\Big[m'_{jy}\sqrt[4]{\tfrac{K_1(q_i)K_1(q_j)}{K_2(q_i)K_2(q_j)}}\cos(\alpha_i-\alpha_j)$$
$$-m'_{jx}\sqrt[4]{\tfrac{K_1(q_i)K_2(q_j)}{K_2(q_i)K_1(q_j)}}\sin(\alpha_i-\alpha_j)\Big], \tag{3.38}$$
$$-\tfrac{i\omega}{\gamma M}m'_{iy} = \tfrac{\omega_0(q_i)}{\gamma M}m'_{ix} + \sum_{\mathbf{G}_j\neq 0} b_{ij}\Big[m'_{jx}\sqrt[4]{\tfrac{K_2(q_i)K_2(q_j)}{K_1(q_i)K_1(q_j)}}\cos(\alpha_i-\alpha_j)$$
$$+m'_{jy}\sqrt[4]{\tfrac{K_2(q_i)K_1(q_j)}{K_1(q_i)K_2(q_j)}}\sin(\alpha_i-\alpha_j)\Big], \tag{3.39}$$

where $b_{ij} = B_v(\mathbf{G}_i - \mathbf{G}_j)/M$, and

$$\frac{\omega_0(q)}{\gamma M} \approx K + \alpha(q^2+k_z^2) + \frac{B_0}{M} - \frac{2\pi(2k_z^2+q^2)}{\lambda^{-2}+k_z^2+q^2}. \tag{3.40}$$

The main assumption of our approximation is that all fourth roots in Eqs. (3.38) and (3.39) can be replaced by unity. Indeed,

$$\sqrt[4]{\frac{K_1(q_i)K_1(q_j)}{K_2(q_i)K_2(q_j)}} - 1 \approx \frac{1}{4}\left[\frac{K_1(q_i) - K_2(q_i)}{K_2(q_i)} + \frac{K_1(q_j) - K_2(q_j)}{K_2(q_j)}\right] \ll 1.$$

It is convenient to introduce the variables $m_i^+ = (m'_{ix} - im'_{iy})e^{-i\alpha_i}$ and $m_i^- = (m'_{ix} + im'_{iy})e^{i\alpha_i}$. Equations (3.38) and (3.39) yield

$$\tfrac{\omega}{\gamma M} m_i^+ = \tfrac{\omega_0(q_i)}{\gamma M} m_i^+ + \sum_{\mathbf{G}_j \neq 0} b_{ij} m_j^+, \tag{3.41}$$

$$-\tfrac{\omega}{\gamma M} m_i^- = \tfrac{\omega_0(q_i)}{\gamma M} m_i^- + \sum_{\mathbf{G}_j \neq 0} b_{ij} m_j^-, \tag{3.42}$$

It can be seen that the solutions of Eq. (3.42) coincide with those of (3.41), but the frequencies have the opposite sign. A great advantage of Eq. (3.41) over Eq. (3.36) is that it represents an eigenvalue problem for a real symmetric matrix, so simple numerical and analytical procedures may be applied to solve it.

Equation (3.41) can be also derived if the uniaxial (z-axis) superconducting and exchange interaction anisotropy is taken into account. The only modification is that the Fourier components of the field and the unperturbed frequencies are given by

$$B_v(\mathbf{G}) = \frac{\Phi_0}{1 + G^2\lambda_\perp^2} \cdot \frac{2}{\sqrt{3}a_v^2}, \tag{3.43}$$

$$\frac{\omega_0(q)}{\gamma M} = K + \alpha_{||}k_z^2 + \alpha_\perp q^2 + \frac{B_0}{M} - \frac{2\pi k_z^2 \lambda_\perp^2}{1 + \lambda_\perp^2(k_z^2 + q^2)} - \frac{2\pi(k_z^2\lambda_\perp^2 + q^2\lambda_{||}^2)}{1 + k_z^2\lambda_\perp^2 + q^2\lambda_{||}^2}. \tag{3.44}$$

Here the quantities $\alpha_{||}$, $\lambda_{||}$ are related to the z axis, and $\alpha_\perp$, $\lambda_\perp$ are related to the perpendicular plane.

3.3.2 Calculations of the magnon spectra

To determine analytically the eigenvalues of the system (3.41) we may use a method, which is equivalent to the weak-binding approximation for electrons in a crystal. We will assume that several eigenvalues ω for a given vector $\mathbf{q}$ are close to $\omega_0(q)$, and the deviations $\omega - \omega_0(q)$ can be determined using the degenerate state perturbation theory.

Let us find the applicability conditions for this approximation. Consider the case when $\omega \approx \omega_0(q_i)$, $\left|m_i^+\right| \geq \left|m_j^+\right|$ and all the quantities $\omega_0(q_j)$ are not close to $\omega_0(q_i)$ for $j \neq i$. Then the perturbation theory in its simplest form can be applied. It follows from Eq. (3.41) that for $i \neq j$

$$m_j \approx \frac{b_{ij} m_i \gamma M}{\omega_0(q_i) - \omega_0(q_j)}.$$

Here and further the upper index "+" will be omitted for brevity. The correction to the unperturbed frequency $\omega_0(q_i)$ due to the fact that $m_j \neq 0$ equals

$$\delta\omega = \frac{b_{ij}^2 \gamma^2 M^2}{\omega_0(q_i) - \omega_0(q_j)}.$$

For the perturbation theory to be valid we have to demand at least $|\delta\omega| \ll |\omega_0(q_i) - \omega_0(q_j)|$, or

$$\left\{ \frac{b_{ij}}{(q_i - q_j)(q_i + q_j)\left[\alpha - \frac{2\pi\lambda^{-2}}{(\lambda^{-2}+q_i^2)(\lambda^{-2}+q_j^2)}\right]} \right\}^2 \ll 1 \tag{3.45}$$

for all $j \neq i$. Here we assumed $k_z = 0$ for simplicity.

If we apply the perturbation theory for a degenerate state, we can permit the condition (3.45) to be violated for $N_j > 1$ different indices j. The number N_j can be estimated as

$$N_j \sim S_q a_v^2, \tag{3.46}$$

where S_q is the area in the q-plane occupied by the vectors q_j for which the condition

$$\frac{b_{ij}}{|q_i - q_j|\,(q_i + q_j)\left|\alpha - \frac{2\pi\lambda^{-2}}{(\lambda^{-2}+q_i^2)(\lambda^{-2}+q_j^2)}\right|} \geq 1 \tag{3.47}$$

holds. To avoid solving secular equations for large matrices, we should demand $N_q \lesssim 1$. Hence, the area S_q should not be too large. Restrictions on S_q are the most strong in two cases: (i) q_i is close to the value corresponding to the minimum of $\omega_0(q_i)$ and (ii) q_i is sufficiently large. To estimate S_q in the first case, we take q_i equal to $q_{\min}$ (see Eq. (3.21)). Now the values of the exchange constant α are required. An estimate for this quantity can be obtained from the relation

$$\alpha \sim \Theta/d_a M^2, \tag{3.48}$$

where d_a is the interatomic distance. The relation (3.48) can be derived within the mean-field theory for localized spins [97].[1] Using the data from Table 3.1, assuming $d_a \sim 5$ Å, we obtain $\alpha \sim 10^{-10}$ cm^2 for UCoGe, and somewhat smaller values for URhGe and UGe_2. Thus, in the U-based ferromagnetic superconductors $\alpha \ll \lambda^2$, and $q_{\min} \gg \lambda^{-1}$. Note that in [A3] α has been estimated in a different way, and somewhat exaggerated numbers have been obtained due to the use of incorrect values of L.

Returning to the calculation of N_q, for $q_i = q_{\min}$ Eq. (3.47) gives

$$|q_j - q_{\min}|^2 \leq \frac{b_{ij}}{4\alpha},$$

where it has been assumed that $|q_j - q_{\min}| \ll q_{\min}$. Then

$$N_q \sim a_v^2 q_{\min}\sqrt{\frac{b_{ij}}{\alpha}} \sim \frac{a_v}{\sqrt{1 + G^2\lambda^2}}\sqrt{\frac{\Phi_0}{M\lambda\alpha^{3/2}}}.$$

The requirement $N_q \lesssim 1$ for all $G \neq 0$ leads to the condition

$$B_0 \gtrsim \frac{\Phi_0}{\lambda^2}\sqrt{\frac{\Phi_0\lambda}{M\alpha^{3/2}}}. \tag{3.49}$$

[1] Equation (3.48) does not account for the easy-axis magnetocrystalline anisotropy. Thus, it gives an upper estimate for α

One can easily show that in the limit $q_i \gg q_{\min}$ $N_q \lesssim 1$ when

$$B_0 \gtrsim \frac{\Phi_0}{\lambda^2}\frac{\Phi_0}{M\alpha}. \tag{3.50}$$

Thus, the inequalities (3.49) and (3.50) specify the weak-binding approximation applicability conditions in the corresponding limiting cases.

Similar to the electron spectrum in solid matter, the magnon spectrum in our system consists of bands separated by the gaps. Obviously, the gaps are the smallest on the lines of the $\mathbf{q}$ plane where adjacent bands would intersect if the matrix elements b_{ij} were negligible. On these lines $\omega \approx \omega_0(q_i) = \omega_0(q_j)$ for some different indices i and j. To find small corrections to the unperturbed frequency $\omega_0(q_i)$, within the weak-binding approximation one should solve the simple secular equation

$$\begin{vmatrix} \frac{\omega_0(q_i)-\omega}{\gamma M} & b_{ij} \\ b_{ij} & \frac{\omega_0(q_i)-\omega}{\gamma M} \end{vmatrix} = 0. \tag{3.51}$$

Then, the frequency gap Δ is

$$\Delta = 2\gamma B_v(\mathbf{G}_i - \mathbf{G}_j). \tag{3.52}$$

The spin wave spectrum was also analyzed numerically. The system (3.41) for 61 Fourier components m_i^+ has been solved (all other components were set equal to zero). The diagonalization of the 61×61 matrix has been performed using standard algorithms provided by the GNU C Library. As the parameters those of UCoGe were used: $\lambda = 1.2\mu$m, $\alpha = 10^{-10}$cm^2, $K = 10^4$, $M = 9$ emu/cm^3. In all calculations $k_z = 0$ was assumed, and the quasi-wave vector $\mathbf{q}$ ran over the first Brillouin zone of the vortex lattice – see Fig. 3.2.

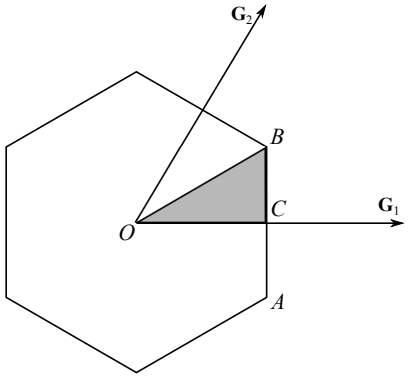

Figure 3.2: The first Brillouin zone for the vortex lattice. It is sufficient to calculate the spectrum in the shaded area to determine the spectrum in the whole zone using symmetry relations.

In Fig. 3.3a-c the magnon spectra in the lowest three bands for the average magnetic field equal to

$$B_p = \frac{\Phi_0\sqrt{3}}{2\pi^2}\left(\frac{2\pi}{\alpha} - \lambda^{-2}\right). \tag{3.53}$$

are depicted. At this field $\omega_0(0) = \omega_0(G_1/2)$. It may be seen that the spectra in the second and third bands have corners. These corners correspond to band intersection lines in zero order perturbation theory. In fact, the corners are smoothed out, but this may be visible only on a small-scale graph. In Fig. 3.3d,e two cross-sections of the 6 lowest bands are shown. The gaps between some bands are so small, that these bands are undistinguishable on the graphs, so they are represented by one curve. At the field $B_0 = B_p$ the numerical values of the gaps are well approximated by Eq. (3.52).

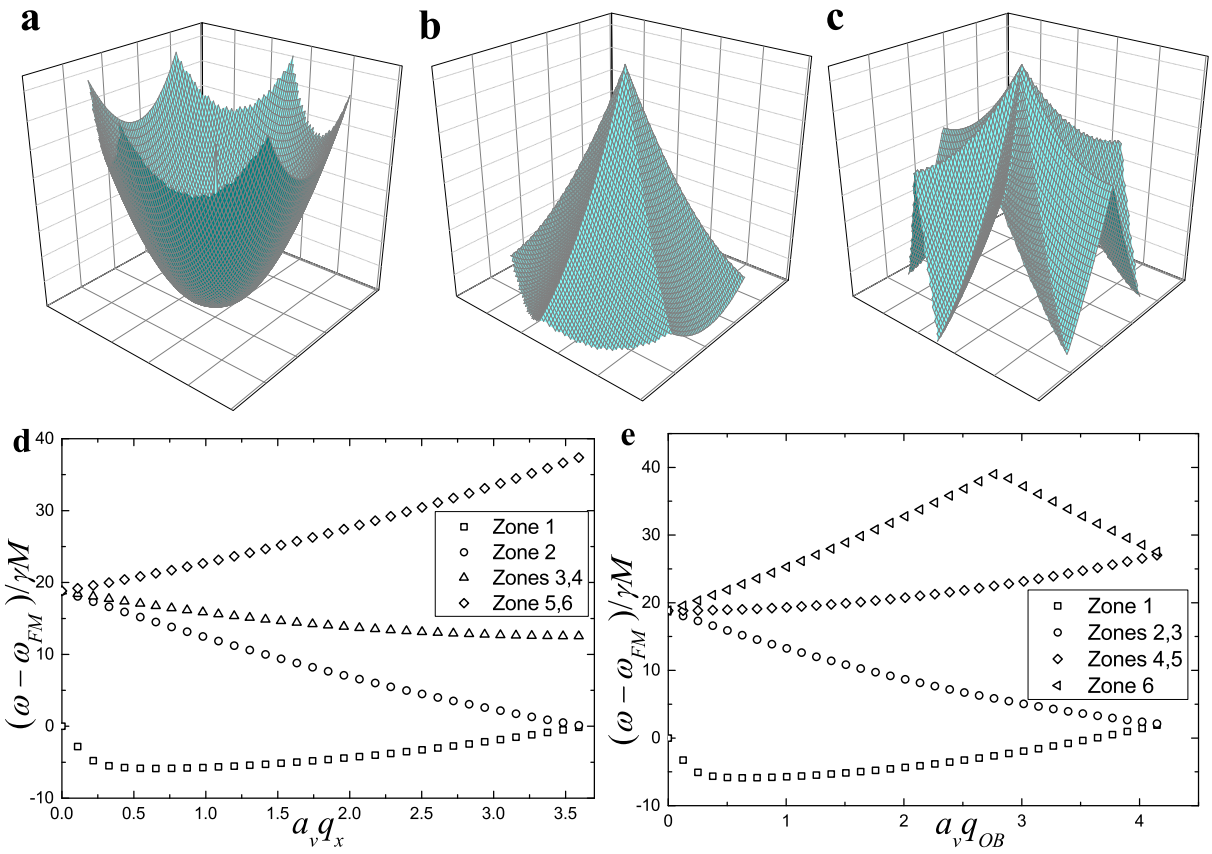

Figure 3.3: The magnon spectra in the first (a) second (b) and third (c) bands. $B_0 = B_p$. The cross-sections of the lowest 6 bands along the lines OC (d) and OB (e) of the Brillouin zone. $\omega_{FM} = \gamma(MK + B_0)$.

In Fig. 3.4 the same spectra for $B_0 = 0.1B_p$ are shown. As the field decreases, the shape of the band structure changes qualitatively: in the center of the Brillouin zone some complicated structure develops. This peculiar behavior is a consequence of the nonmonotonicity of the unperturbed spectrum (3.20) and is connected with a commensurability effect: the spectra are deformed when $\omega_0(0) > \omega_0(\mathbf{G}_1)$.

3.3.3 Symmetry considerations: intersections of bands

The calculations in the previous section were made assuming that the ferromagnet has isotropic superconducting properties, but the results derived there are also qualitatively valid for anisotropic (uniaxial and biaxial) superconductors. In this section we will an-

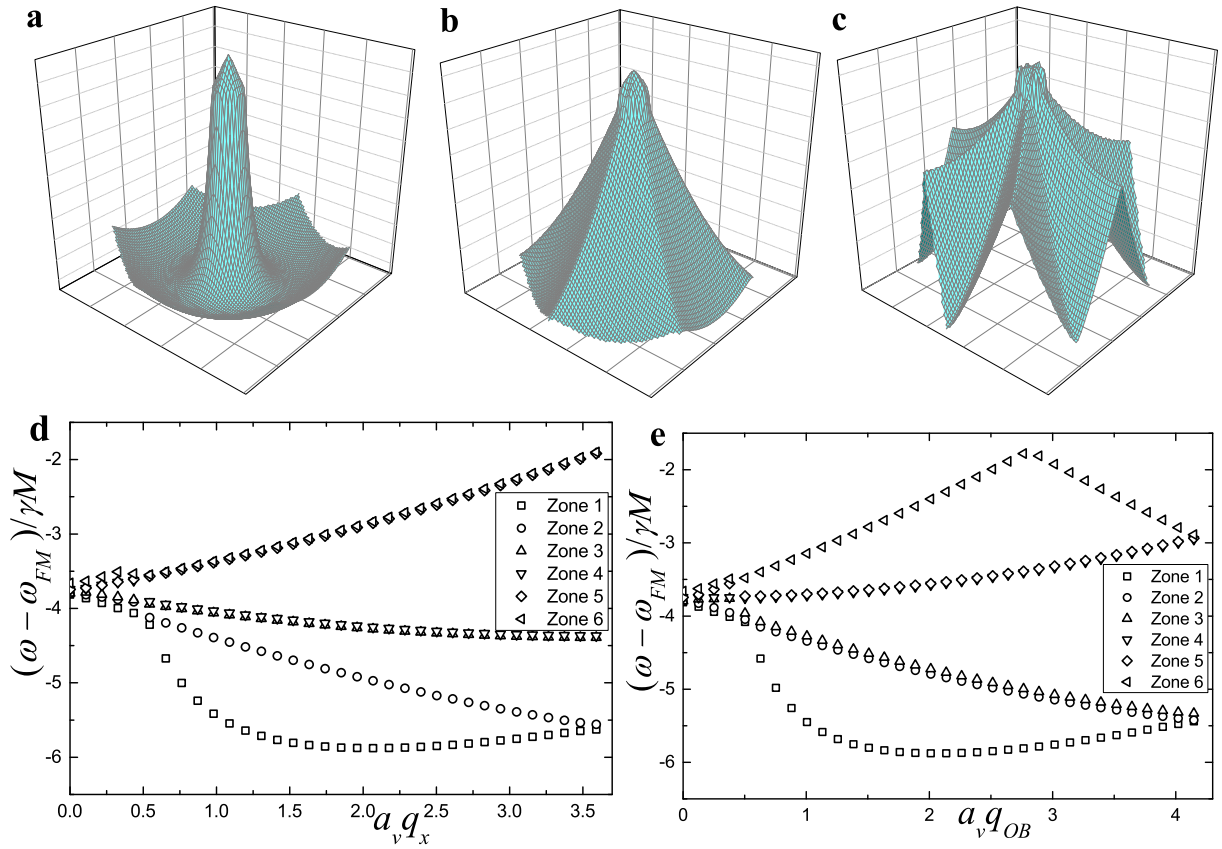

Figure 3.4: The magnon spectra in the first (a) second (b) and third (c) bands. $B_0 = 0.1B_p$. The cross-sections of the lowest 6 bands along the lines OC (d) and OB (e) of the Brillouin zone. $\omega_{FM} = \gamma(MK + B_0)$.

alyze the properties of the band structure which appear only in materials with uniaxial symmetry.

Let us consider the magnon spectrum in points of the Brillouin zone where the system (3.41) admits a nontrivial symmetry group. We restrict ourselves to the case of a relatively strong magnetic field, when $\omega_0(q_i) = \omega_0(q_j)$ implies $q_i = q_j$, so that the nonmonontonicity of the unperturbed spectrum (3.44) is irrelevant.

The point with the highest symmetry is the center of the Brillouin zone, where $\mathbf{q} = 0$. The corresponding symmetry group is

$$\mathcal{G}_0 = \{R^i, \sigma_i\}, \qquad i = 0..5, \tag{3.54}$$

which is isomorphic to the group C_{6v}. Here $\sigma_i = R^i\sigma_0$, and R and σ_0 are defined as follows:

$$\begin{aligned} R: &\qquad m_i = m(\mathbf{G}_i) \to m(\hat{T}\mathbf{G}_i), \\ &\hat{T} = \begin{pmatrix} \cos\frac{\pi}{3} & -\sin\frac{\pi}{3} \\ \sin\frac{\pi}{3} & \cos\frac{\pi}{3} \end{pmatrix}; \\ \sigma_0: &\qquad m_i = m(G_{ix}, G_{iy}) \to m(G_{ix}, -G_{iy}). \end{aligned} \tag{3.55}$$

The characters for the irreducible representations of the group $\mathcal{G}_0$ are listed in Table 3.2. Due to the presence of the two-dimensional representations B_1 and B_2 intersections of

	R^0	R, R^5	R^2, R^4	R^3	$\sigma_0, \sigma_2, \sigma_4$	$\sigma_1, \sigma_3, \sigma_5$
A_1	1	1	1	1	1	1
A_2	1	1	1	1	-1	-1
A_3	1	-1	1	-1	1	-1
A_4	1	-1	1	-1	-1	1
B_1	2	-1	-1	2	0	0
B_2	2	1	-1	-2	0	0

Table 3.2: Character table of the group $\mathcal{G}_0$.

Representation	Band numbers	Solutions $m(\hat{T}^k\mathbf{G}_1) = ...$	$\frac{\omega-\omega_0(\mathbf{G}_1)}{\gamma M}$
A_3	2	$(-1)^k m(\mathbf{G}_1)$	$-2b_{12} + 2b_{13} - b_{14}$
B_1	3,4	$e^{\pm 2ik\pi/3} m(\mathbf{G}_1)$	$-b_{12} - b_{13} + b_{14}$
B_2	5,6	$e^{\pm ik\pi/3} m(\mathbf{G}_1)$	$b_{12} - b_{13} - b_{14}$
A_1	7	$m(\mathbf{G}_1)$	$2b_{12} + 2b_{13} + b_{14}$

Table 3.3: The solutions of Eq.(3.41) with $q = 0$ in the first order perturbation theory.

two bands appear in the center of the Brillouin zone. Indeed, consider the bands with the numbers from 2 to 7. In the zero order perturbation theory $\omega(\mathbf{q} = 0) = \omega_0(\mathbf{G}_1)$ in all these bands. In the first order perturbation theory we have to take into account the six components $m(\hat{T}^i\mathbf{G}_1)$, $i = 0..5$, where the matrix $\hat{T}$ is defined by Eq. (3.55). The solutions of the sixth-order eigenvalue problem can be found in Table 3.3. Here $b_{12} = B_v(\mathbf{G}_1)/M$, $b_{13} = B_v(\mathbf{G}_1 + \mathbf{G}_2)/M$, $b_{14} = B_v(2\mathbf{G}_1)/M$. The pairs of bands 3,4 and 5,6 have a point of contact at $\mathbf{q} = 0$.

Another point of high symmetry is the B point (see Fig. 3.2), where $\mathbf{q} = \mathbf{q}_B = (\mathbf{G}_1 + \mathbf{G}_2)/3$. The corresponding symmetry group is

$$\mathcal{G}_B = \{R_B^i, \sigma_{Bi}\}, i = 0, 1, 2, \tag{3.56}$$

where

$$\begin{aligned} R_B: &\qquad m(\mathbf{G}_i) \to m(\hat{T}^2\mathbf{G}_i - \mathbf{G}_1), \\ \sigma_{B0}: &\qquad m(\mathbf{G}_i) \to m(\hat{\sigma}_{OB}\mathbf{G}_i), \\ &\sigma_{Bi} = R_B^i\sigma_{B0}, \end{aligned}$$

and $\hat{\sigma}_{OB}$ is the reflection operator with respect to the OB axis. The group $\mathcal{G}_B$ is isomorphic to the group C_{3v}. The characters of its irreducible representations are listed in Table 3.4. The intersection of bands in the B point occurs at frequencies close to $\omega_0(q_B)$. In the first order perturbation theory we have to take into account the elements $m(0)$, $m(-\mathbf{G}_1)$, and $m(-\mathbf{G}_2)$ in Eq. (3.41). The solutions of the eigenvalue problem are given in Table 3.5. At this time, the first and second band have a point of contact.

Finally, an important remark should be made here concerning the symmetry of the initial system (3.35) and (3.36). In Sec. 3.3.1 the approximate equation (3.41) has been derived using the fact that the quantity $\tilde{K}$ is typically very large. As a by-product of this simplification we gained the reflection symmetry operations σ_i and σ_{Bi}, which are not

	R_B^0	R_B, R_B^2	$\sigma_{Bi},\ i=0,1,2$
D_1	1	1	1
D_2	1	1	-1
E	2	-1	0

Table 3.4: Character table of the group $\mathcal{G}_B$.

Representation	Band numbers	Solutions	$\frac{\omega-\omega_0(\mathbf{q}_B)}{\gamma M}$
E	1,2	$m(-\mathbf{G}_1)=e^{\pm 2\pi i/3}m(0)$, $m(-\mathbf{G}_2)=e^{\mp 2\pi i/3}m(0)$	$-b_{12}$
D_1	3	$m(-\mathbf{G}_1)=m(-\mathbf{G}_2)=m(0)$	$2b_{12}$

Table 3.5: The solutions of Eq.(3.41) with $\mathbf{q}=\mathbf{q}_B$ in the first order perturbation theory.

present in the initial system (to be more accurate, the analogues of σ_i and σ_{Bi} involve complex conjugation, so these operations are not linear). The system (3.35) and (3.36) for $\mathbf{q}=0$ and $\mathbf{q}=\mathbf{q}_B$ admits symmetry groups which are isomorphic to the groups C_6 and C_3, respectively, which have only one-dimensional irreducible representations. As a result, a small gap exists between the the bands which had a point of contact within Eq. (3.41). However, this gap is negligible ($\Delta \sim \gamma M b_{ij}/\tilde{K}$) for materials with large magnetocrystalline anisotropy, or at large average magnetic fields B_0.

3.3.4 Influence of dissipation on the magnon spectrum

Now, let us discuss how the magnon spectrum is modified when dissipation is taken into account. First, we consider losses due to vortex motion. Generally, it is rather difficult to express the displacement amplitude $\Delta\mathbf{R}$ in terms of $\mathbf{m}(\mathbf{G}_i)$, using Eq. (3.35). However, a simplification is possible in the high-η limit, when all terms in the right-hand side of Eq. (3.35) containing $\Delta\mathbf{R}$ can be neglected as compared to the relaxational term in the left-hand side. For this approximation to be valid it is sufficient to demand

$$\frac{\omega\eta}{\Phi_0} \gg B_0\lambda^{-2}, H_{c1}k_z^2, H_{c1}k^2, \tag{3.57}$$

where H_{c1} is the lower critical field [see Eq. (2)]. The condition (3.57) can be satisfied in the clean limit, since the viscosity η grows with growing normal conductivity – see Chapter 2.

Within our approximation

$$\Delta\mathbf{R} = \sum_{G_i<\xi^{-1}} \frac{\Phi_0 k_z \mathbf{m}(\mathbf{G}_i)}{\omega\eta\left[1+\lambda^2(k_z^2+q_i^2)\right]} \tag{3.58}$$

After substituting this into Eq. (3.36) we can repeat the calculations from Sec. 3.3.1 and obtain the system (3.41) with

$$\omega_0(q,k_z) = \gamma M\left(\tilde{K}+\alpha q^2 - \frac{2\pi(2k_z^2+q^2)}{\lambda^{-2}+k_z^2+q^2} - \frac{iB_0\Phi_0 k_z^2}{\omega\eta(1+\lambda^2(k_z^2+q^2))^2}\right),$$

$$b_{ij} = \frac{B_v(\mathbf{G}_i - \mathbf{G}_j)}{M} - \frac{iB_0\Phi_0 k_z^2}{\omega\eta} \frac{1}{[1+\lambda^2(k_z^2+q_i^2)][1+\lambda^2(k_z^2+q_j^2)]}.$$

Now we have an eigenvalue problem for a symmetric non-Hermitian matrix. Due to dissipation the magnetic excitation levels are broadened, which can lead to the smearing of the gaps between the energy bands. To observe the effects conneted with the presence of the gap Δ for $q_i \approx q_j$ (within the applicability region of the weak-binding approximation) one should provide that

$$\frac{B_v(\mathbf{G}_i - \mathbf{G}_j)}{M} \gtrsim \frac{B_0\Phi_0 k_z^2}{\omega\eta(1+\lambda^2(k_z^2+q_i^2))^2}. \tag{3.59}$$

This means that the viscosity should be sufficienly large, or the longitudinal wave number k_z should be small so that vortex motion is not excited.

In metallic ferromagnets another important mechanism of dissipation exists, which is due to magnon-conduction electron scattering [60]. This kind of dissipation is qualitatively accounted for by the last term in Eq. (3.13). The constant ν defines the magnetization relaxation time $\tau_r = \omega^{-1}\nu/M$. Data on this time in the U-based ferromagnetic superconductors are not available yet. However, for rough estimates of the magnon spectrum broadening the typical values $\tau_r \sim 10^{-9} - 10^{-8}s$ for ordinary metallic ferromagnets may be used [60].

3.3.5 Proposal for experimental detection of the gaps in the magnon spectrum

In this section it will be demonstrated how the evidence of the gaps in the magnon spectrum can be found using microwave probing. Consider an electromagnetic TE wave with the wave vector $\mathbf{k}$ and amplitude $\mathbf{H}_0$ incident on a ferromagnetic superconductor occupying the half-space $x > 0$ (see Fig. 3.5). For simplicity, we assume $k_z = 0$. Note that in a TM wave the field $\mathbf{H}$ would oscillate along the direction of the uniform magnetization, hence, this wave does not excite magnons and is completely reflected. For this reason, we consider further a TE wave. Such a wave excites three magnon modes inside the ferromagnet: one propagating ($\mathbf{q}_1$) and two decaying modes ($\mathbf{q}_2$ and $\mathbf{q}_2'$). The wave vectors of these modes are determined from the two equations

$$\omega^2 = \omega_0^2(q) = \gamma^2 M^2 \left(K + \tfrac{B_0}{M} + \alpha q^2\right)\left(K + \tfrac{B_0}{M} + \alpha q^2 - \tfrac{4\pi q^2}{q^2+\lambda^{-2}}\right), \tag{3.60}$$

$$q_x^2 = q^2 - k_y^2. \tag{3.61}$$

The propagating mode can be reflected back to the surface of the ferromagnet due to Bragg scattering on vortices, if two conditions are fulfilled for some wave-vector $\mathbf{q}_3$:

$$\mathbf{q}_3 = \mathbf{q}_1 + \mathbf{G}, \tag{3.62}$$

$$\omega_0(q_3) \approx \omega_0(q_1), \tag{3.63}$$

where $\mathbf{G} = -G\mathbf{x}_0$ is a vector of the reciprocal lattice (3.25).

We will determine the amplitude $\mathbf{H}_1$ of the reflected electromagnetic wave. For the evaluation of this amplitude the equilibrium field distribution $\mathbf{B}_{\rm eq}(\mathbf{r})$ in the material is required:

$$\mathbf{B}_{\rm eq} = 4\pi M \mathbf{z}_0 e^{-x/\lambda} + \mathbf{B}_v(\mathbf{r} - x_v\mathbf{x}_0) + \mathbf{B}_0'(\mathbf{r}). \tag{3.64}$$

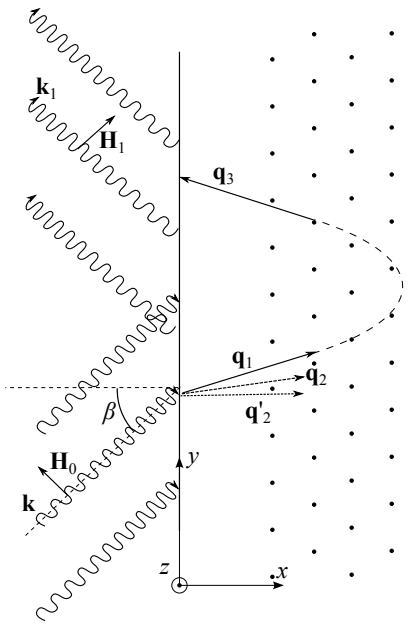

Figure 3.5: An electromagnetic wave ($\mathbf{k}$) incident on the flat surface of a ferromagnetic superconductor, is partially reflected back as a wave with the wave vector $\mathbf{k}_1$. Inside the material one propagating ($\mathbf{q}_1$) and two decaying magnon modes ($\mathbf{q}_2$ and $\mathbf{q}_2'$) are excited. The mode $\mathbf{q}_1$ undergoes Bragg reflection on the vortex lattice (represented by dots) and transforms into the mode $\mathbf{q}_3$ propagating towards the sample surface.

Here, the first term represents the screened intrinsic magnetic field (we will assume that there is no constant external field: $\mathbf{H}_e = 0$), $\mathbf{B}_v$ is the vortex field given by Eq. (3.24), x_v specifies the shift of the vortex lattice with respect to the surface, and the term $\mathbf{B}_0'(\mathbf{r})$ is responsible for the vortex lattice distortion in a surface layer with a thickness of the order of λ.

We will consider a dense vortex lattice, so that $\alpha/a_v^2 \gg 1$. To observe the effects connected with Bragg reflection of magnons we have to demand $q_1 \sim a_v^{-1}$, hence, $\alpha q_1^2 \gg 1$. The nonstationary component of the magnetization can be presented in the form

$$\mathbf{m} \approx \mathbf{m}_1(x)e^{i\mathbf{q}_1\mathbf{r}} + \mathbf{m}_2 e^{i\mathbf{q}_2\mathbf{r}} + \mathbf{m}_2' e^{i\mathbf{q}_2'\mathbf{r}} + \mathbf{m}_3(x)e^{i\mathbf{q}_3\mathbf{r}}, \tag{3.65}$$

where $\mathbf{m}_1(x)$ and $\mathbf{m}_3(x)$ vary slowly in space. In Appendix E, using a simple perturbation theory, it is demonstrated that the influence of the screened intrinsic field on the magnon modes is not essential. By similar reasons, the distortion field $\mathbf{B}_0'(\mathbf{r})$ also does not affect significantly the spin wave amplitudes. Hence, we can consider $\mathbf{m}_2$ and $\mathbf{m}_2'$ to be constant.

Now we determine the boundary conditions. Directly from Eq. (3.1) we obtain

$$\frac{\partial \mathbf{m}}{\partial x}(x = 0) = 0, \tag{3.66}$$

The continuity condition for the tangential component of the magnetic field $\mathbf{H}$ reads

$$(H_0 + H_1)\cos\beta = -4\pi \sum_i \frac{(\lambda^{-2} + k_y^2)m_{iy}(0) + k_y q_{ix} m_{ix}(0)}{q_i^2 + \lambda^{-2}}, \tag{3.67}$$

where summation is performed over all 4 modes, and β is the angle of incidence – see Fig. 3.5. The electric field inside the material is

$$\mathbf{E} = -4\pi k \sum_i \frac{\mathbf{q_i} \times \mathbf{m}_i}{q_i^2 + \lambda^{-2}} e^{i\mathbf{q}_i \mathbf{r}}. \tag{3.68}$$

The continuity condition for the electric field reads

$$H_1 - H_0 = 4\pi k \sum_i \frac{k_y m_{ix}(0) - q_{ix} m_{iy}(0)}{q_i^2 + \lambda^{-2}}, \tag{3.69}$$

The wave number q_2' has a large modulus ($q_2'^2 \approx -2\omega/\gamma M\alpha$) as compared to the other wave numbers, and the corresponding magnetization component, $\mathbf{m}_2'$, is small. It can be neglected in Eqs. (3.67) and (3.69). To exclude $\mathbf{m}_2'$ from Eq. (3.66), we note that $m_{2x}' \approx i m_{2y}'$, hence

$$\sum_{i=1}^{3} q_{ix}(m_{ix}(0) - i m_{iy}(0)) = 0,$$

or

$$\sum_{i=1}^{3} q_{ix} m_{iy}(0) = 0, \tag{3.70}$$

since $m_{ix} \approx -i m_{iy}$ for $i = 1, 2, 3$. Now we have to find a connection between $\mathbf{m}_1$ and the amplitude of the Bragg-reflected mode, $\mathbf{m}_3$. In these modes the magnetic field is small as compared to $\alpha\nabla^2\mathbf{m}$, so the linearized Landau-Lifshitz equation can be simplified as follows:

$$\frac{\omega}{\gamma M}\mathbf{m} = \tilde{K}\mathbf{m} - \alpha\nabla^2\mathbf{m} + \frac{1}{M} B_v(\mathbf{r} - x_v\mathbf{x}_0)\mathbf{m}. \tag{3.71}$$

To find a link between the mentioned modes it is sufficient to conserve only two terms in the Fourier series of the vortex field:

$$B_v(\mathbf{G})(e^{iG(x-x_v)} + e^{-iG(x-x_v)}),$$

where $\mathbf{G}$ is the reciprocal lattice vector defined by Eqs. (3.62) and (3.63). By substituting $\mathbf{m} = \mathbf{m}_1(x)e^{i\mathbf{q}_1\mathbf{r}} + \mathbf{m}_3(x)e^{i\mathbf{q}_3\mathbf{r}}$ into Eq. (3.71) and neglecting the second derivatives of $\mathbf{m}_1(x)$ and $\mathbf{m}_3(x)$, we obtain

$$i v_{gx} \frac{\partial \mathbf{m}_1}{\partial x} = \frac{\Delta}{2} e^{-i\varphi_v - i\delta x} \mathbf{m}_3(x), \tag{3.72}$$

$$i v_{gx} \frac{\partial \mathbf{m}_3}{\partial x} = -\frac{\Delta}{2} e^{i\varphi_v + i\delta x} \mathbf{m}_1(x), \tag{3.73}$$

where

$$v_{gx} = \frac{\partial \omega_0}{\partial q_x}(\mathbf{q}_1) = 2\gamma M \alpha q_{1x},$$

$\Delta = 2\gamma B_v(G)$ is the frequency gap [compare with Eq.(3.52)], $\varphi_v = G x_v$, and $\delta = 2q_{1x} - G$. The two linearly independent solutions of Eqs. (3.72) and (3.73) are

$$\mathbf{m}_1(x) = (\mathbf{x}_0 + i\mathbf{y}_0)e^{(\epsilon - i\delta/2)x},$$

$$\mathbf{m}_3(x) = \frac{2 i v_{gx} e^{i\varphi_v}}{\Delta} \left(\epsilon - i\frac{\delta}{2}\right)(\mathbf{x}_0 + i\mathbf{y}_0)e^{(\epsilon + i\delta/2)x},$$

$$\epsilon = \pm\frac{1}{2}\sqrt{\frac{\Delta^2}{v_{gx}^2} - \delta^2} \tag{3.74}$$

For $|\delta| < \Delta/v_{gx}$ we reject the growing solution, selecting the minus sign in Eq. (3.74). For $|\delta| > \Delta/v_{gx}$ we select the solution where $|\mathbf{m}_1| \gg |\mathbf{m}_3|$ when $|\delta| \gg \Delta/v_{gx}$:

$$\epsilon = \frac{i}{2}\sqrt{\delta^2 - \frac{\Delta^2}{v_{gx}^2}} \text{ for } \delta > 0, \qquad \epsilon = -\frac{i}{2}\sqrt{\delta^2 - \frac{\Delta^2}{v_{gx}^2}} \text{ for } \delta < 0. \tag{3.75}$$

This choice of the sign allows to reject the solution with the negative x-component of the group velocity. At $x = 0$ we have

$$\mathbf{m}_3(0) = A\mathbf{m}_1(0), \tag{3.76}$$

$$A = \frac{2iv_{gx}e^{i\varphi_v}}{\Delta}\left(\epsilon - i\frac{\delta}{2}\right) \tag{3.77}$$

Now we are ready to write the system of linear equations which will allow us to determine the amplitude of the reflected wave, H_1. Equations (3.67), (3.69), (3.70) and (3.76) yield

$$\tilde{q}_{1x}\tilde{m}_{1y} + q_{2x}m_{2y} = 0, \tag{3.78}$$

$$4\pi\frac{ik_y\tilde{q}_{1x} - \lambda^{-2} - k_y^2}{q_1^2 + \lambda^{-2}}\tilde{m}_{1y} + 4\pi\frac{ik_yq_{2x} - \lambda^{-2} - k_y^2}{q_2^2 + \lambda^{-2}}m_{2y} = (H_0 + H_1)\cos\beta, \tag{3.79}$$

$$-4\pi k\frac{ik_y + \tilde{q}_{1x}}{q_1^2 + \lambda^{-2}}\tilde{m}_{1y} - 4\pi k\frac{ik_y + q_{2x}}{q_2^2 + \lambda^{-2}}m_{2y} = H_1 - H_0, \tag{3.80}$$

where

$$\tilde{m}_{1y} = (A+1)m_{1y}(0), \qquad \tilde{q}_{1x} = \frac{1-A}{1+A}q_{1x}. \tag{3.81}$$

Note that the problem of electromagnetic wave reflection from a superconductor in the mixed state is formally equivalent to the same problem for a superconductor without vortices with the only difference that q_{1x} is replaced by $\tilde{q}_{1x}$. From the system (3.78) - (3.80) we find the reflection coefficient

$$R_H = \frac{H_1}{H_0} = \frac{\frac{\lambda^{-2}q_{2x}}{q_1^2+\lambda^{-2}} - \frac{\alpha(q_1^2+\lambda^{-2})}{2\pi}\tilde{q}_{1x} + e^{-i\beta}\left(kq_{2x}\frac{ik_y+\tilde{q}_{1x}}{q_1^2+\lambda^{-2}} - k\tilde{q}_{1x}\frac{(ik_y+q_{2x})\alpha(q_1^2+\lambda^{-2})}{2\pi\lambda^{-2}}\right)}{\frac{\lambda^{-2}q_{2x}}{q_1^2+\lambda^{-2}} - \frac{\alpha(q_1^2+\lambda^{-2})}{2\pi}\tilde{q}_{1x} - e^{i\beta}\left(kq_{2x}\frac{ik_y+\tilde{q}_{1x}}{q_1^2+\lambda^{-2}} - k\tilde{q}_{1x}\frac{(ik_y+q_{2x})\alpha(q_1^2+\lambda^{-2})}{2\pi\lambda^{-2}}\right)}. \tag{3.82}$$

Here, the relation

$$\alpha q_1^2 - \frac{2\pi q_1^2}{q_1^2 + \lambda^{-2}} = \alpha q_2^2 - \frac{2\pi q_2^2}{q_2^2 + \lambda^{-2}},$$

was used, which is valid in the large anisotropy limit. The expression for the reflectivity coefficient can be simplified, if we take into account that $q_1 \gg \lambda^{-1}$ and $q_{2x} \approx i\lambda^{-1}$:

$$R_H = \frac{1 + ik^2\lambda^2e^{-i\beta}\sin\beta + Q(i - k\lambda e^{-i\beta})}{1 - ik^2\lambda^2e^{i\beta}\sin\beta + Q(i + k\lambda e^{i\beta})}, \tag{3.83}$$

where

$$Q = \frac{\alpha\lambda^2q_1^4}{2\pi}q_{1x}\lambda\frac{1-A}{1+A}. \tag{3.84}$$

In Eq. (3.83) some small terms were dropped which have a negligible effect on the modulus of the reflectivity coefficient. Since the quantity A can take any value within the circle $|A| \leq 1$, so the only restriction on Q is $\Re(Q) \geq 0$.

When $|A| = 1$, Q is purely imaginary, and $|R| = 1$, i. e., the wave is completely reflected. This is explained by the fact that in this range of parameters the frequency ω is within the frequency gap, and magnons can not propagate in the sample.

Consider now frequencies far from the gap: $\delta \gg \Delta/v_{gx}$. In this case the magnons do not interact with the vortex lattice, and the quantity Q is real and large: $Q \gg 1$. From Eq. (3.83) we obtain

$$1 - |R_H|^2 = \frac{4k\lambda \cos\beta}{Q} \ll 1. \tag{3.85}$$

An interesting effect which follows from Eq. (3.83) is the complete transmission of the wave for a frequency close to the frequency gap. Let us put $R_H = 0$. Then,

$$Q \approx i + k\lambda e^{-i\beta}. \tag{3.86}$$

This is possible when $A \approx 1$ and $|A| < 1$, i. e., the detuning from the gap must be very small. For example, if $k\alpha\lambda^4 q_1^5 \gg 1$

$$\frac{|\delta|\, v_{gx}}{\Delta} - 1 \approx \frac{8\pi^2 k^2 \cos^2\beta}{\alpha^2 \lambda^4 q_1^{10}}. \tag{3.87}$$

Note, that for $A \approx 1$ $\mathbf{m}_1(0) \approx \mathbf{m}_3(0)$. The effect of complete transmission is related to a similar effect in a Fabri-Perrot resonator: in our system, the surface of the material and the vortex lattice play the roles of the first and second mirrors, respectively.

We need to stress that the system must be finely tuned to make the dip in the $R(\omega)$ dependence observable. Indeed, the parameter A must be equal to unity on the border of the gap, which imposes a constraint on the parameters G and x_v:

$$e^{iGx_v} = \pm 1. \tag{3.88}$$

This condition may be satisfied by applying an external magnetic field.

3.4 Magnon radiation by moving Abrikosov vortices

3.4.1 The magnetic moment induced force acting on vortices: general relations

In this section the response of vortices to an ac and dc current in ferromagnetic superconductors and SF-superlattices will be studied. Let the internal field $\mathbf{B}_0$ make an angle θ with the magnetization easy axis. The z axis is directed along the vortices, which are for simplicity assumed to be straight. Thus, the quantities $\mathbf{R}_i$ do not depend on z. The initial equations for the magnetization and field in a ferromagnetic superconductor were derived in Sec. 3.2. In SF-superlattices (see Fig. 3.6) the magnetic field satisfies the London equation (3.14) with $\mathbf{m} = 0$ in the superconducting layers. To obtain the

corresponding equation in the magnetic layers, one should simply put $\lambda = \infty$ in Eq. (3.14):

$$\frac{\partial^2 \mathbf{B}}{\partial z^2} + \nabla_{\boldsymbol{\rho}}^2 \mathbf{B} - \frac{4\pi\sigma_F}{c^2}\frac{\partial \mathbf{B}}{\partial t} + 4\pi \operatorname{rot}\operatorname{rot}\mathbf{m} = 0. \tag{3.89}$$

Here, σ_F is the conductivity of the ferromagnetic layers. In Eq. (3.89) the Josephson

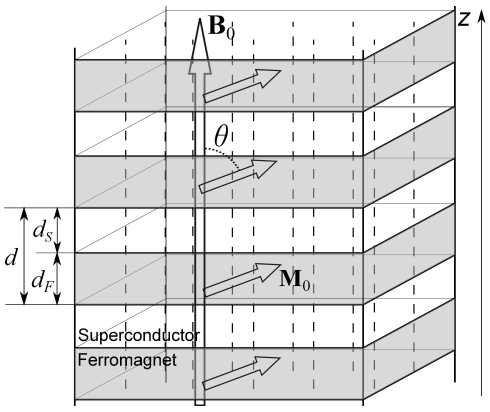

Figure 3.6: A scheme of the SF multilayer system. The dashed lines denote vortices.

current between neighboring superconducting layers has been neglected, which can be done in the case of a poorly transparent interface between layers, or when the magnetic layers are sufficiently thick [98].

On the SF interface the following boundary conditions should be imposed:

$$B_z\Big|_F = B_z\Big|_S, \qquad (\mathbf{B} - 4\pi\mathbf{M})_{x,y}\Big|_F = (\mathbf{B} - 4\pi\mathbf{M})_{x,y}\Big|_S \tag{3.90}$$

$$\frac{\partial \mathbf{m}}{\partial z}\Big|_F = 0. \tag{3.91}$$

Let us estimate the contribution of the normal currents flowing in the F-layers of the multilayer system to the magnetic field. In Eq. (3.89) we put

$$\frac{\partial \mathbf{B}}{\partial t} \approx -(\mathbf{V}_L \nabla_{\boldsymbol{\rho}})\mathbf{B},$$

where $\mathbf{V}_L$ is the flux velocity. One can see that the influence of the normal currents on the magnetic field is negligible, if the inequality

$$\frac{4\pi\sigma_F}{c^2} l V_L \ll 1$$

holds, where l is the characteristic in-plane length scale of the problem. Similar arguments can be applied to the S-layers. Then, the normal currents in the SF-superlattice have a negligible effect on the magnetic field when

$$V_L \ll \frac{c^2}{4\pi \max(\sigma_n, \sigma_F) l}, \tag{3.92}$$

where σ_n is the normal-state conductivity of the superconductor. In the case of a bulk ferromagnetic superconductor, the analogue of Eq. (3.92) reads

$$V_L \ll \frac{c^2}{4\pi\sigma_n l.} \tag{3.93}$$

As we will see, the main length scales of the problem are the inter-vortex distance a_v and the domain wall width $L = \sqrt{\alpha/K}$. Further on we will assume that Eqs. (3.92) and (3.93) with $l = \min(a_v, L)$ are satisfied. Then, we may not take into account the normal currents in Eqs. (3.14) and (3.89).

In Eqs. (3.14) and (3.89) it is convenient to present the magnetic field as the sum of the vortex field $\mathbf{h}$ and the magnetization field $\mathbf{b}_M$, satisfying the relations

$$-\nabla^2\mathbf{h} + \frac{\mathbf{h}}{\lambda^2} = \frac{\Phi_0}{\lambda^2}\mathbf{z}_0 \sum_i \delta^{(2)}(\boldsymbol{\rho} - \mathbf{R}_i), \tag{3.94}$$

$$-\nabla^2\mathbf{b}_M + \frac{\mathbf{b}_M}{\lambda^2} = 4\pi \operatorname{rot}\operatorname{rot}\mathbf{m} \tag{3.95}$$

inside the superconductor, and

$$\operatorname{rot}\mathbf{h} = 0, \qquad \operatorname{div}\mathbf{h} = 0, \tag{3.96}$$

$$\operatorname{rot}\mathbf{b}_M = 4\pi \operatorname{rot}\mathbf{m}, \qquad \operatorname{div}\mathbf{b}_M = 0 \tag{3.97}$$

in the ferromagnetic layers.

Now we proceed directly to the calculation of the magnetic moment induced force, acting on vortices. The total force per unit length of the i-th vortex is

$$\mathbf{f}_i = -\frac{1}{L_v}\frac{\partial F}{\partial \mathbf{R}_i}, \tag{3.98}$$

where L_v is the vortex length. Averaging $\mathbf{f}_i$ over all vortices, we obtain the average force

$$\mathbf{f} = -\frac{1}{L_v N_v}\sum_i \frac{\partial F}{\partial \mathbf{R}_i}, \tag{3.99}$$

where N_v is the number of vortices. The magnetic moments interact with vortices via the Zeeman-like term in the free energy:

$$F_Z = -\int \mathbf{M}\mathbf{h} d^3\mathbf{r}.$$

It can be shown (see Appendix F) that the part of the total force $\mathbf{f}$, connected with the magnetic moments, is

$$\mathbf{f}_M = -\frac{1}{L_v N_v}\int m_z \nabla h_z d^3\mathbf{r}. \tag{3.100}$$

For convenience, all further calculations in subsections 3.4.1 - 3.4.4 are carried out for a ferromagnetic superconductor. In Sec. 3.4.5 it will be discussed how the obtained results can be extended to the case of the multilayer system.

In the Fourier representation Eq. (3.100) reads

$$\mathbf{f}_M = \frac{4\pi^2}{N_v} i \int \mathbf{q} m_{qz} h^*_{qz} d^2\mathbf{q}, \tag{3.101}$$

where for any function $X(\boldsymbol{\rho})$ its Fourier transform is defined as

$$X_q = \frac{1}{(2\pi)^2} \int X(\boldsymbol{\rho}) e^{-i\mathbf{q}\boldsymbol{\rho}} d^2\boldsymbol{\rho}.$$

The quantity $\mathbf{m}_q$ should be determined from Eq. (3.13). As we have seen, the term $\gamma\mathbf{B}\times\mathbf{m}$ leads to the appearance of the band structure of the magnon spectrum. However, in the calculations of the force $\mathbf{f}_M$ the relatively small band effects are insignificant, since $\mathbf{f}_M$ is determined by the integral of $\mathbf{m}_q$. Moreover, in the highly anisotropic U-based superconductors (see Table 3.1) at $B_0 \ll H_{c2}$

$$|\gamma\mathbf{B}\times\mathbf{m}| \ll |\gamma K\mathbf{m}\times\mathbf{M}_0|.$$

For these reasons, the term $\gamma\mathbf{B}\times\mathbf{m}$ in Eq. (3.13) may be neglected.

By Fourier transforming Eqs. (3.13), (3.94), and (3.95) we obtain

$$\frac{\partial\mathbf{m}_q}{\partial t} = -\gamma\mathbf{M}_0 \times \left(-(K+\alpha q^2)\mathbf{m}_q + \mathbf{b}_{Mq} + \mathbf{h}_q\right) + \frac{\nu}{M^2}\mathbf{M}_0 \times \frac{\partial\mathbf{m}_q}{\partial t}. \tag{3.102}$$

$$h_{qz} = \frac{\Phi_0}{4\pi^2(1+\lambda^2 q^2)} \sum_i e^{-i\mathbf{q}\mathbf{R}_i(t)}. \tag{3.103}$$

$$\mathbf{b}_{Mq} = -4\pi \frac{\mathbf{q}\times(\mathbf{q}\times\mathbf{m}_q)}{q^2+\lambda^{-2}}. \tag{3.104}$$

It can be seen that the absolute value of the term $\mathbf{b}_{Mq}$ in Eq. (3.102) is much smaller than $|K\mathbf{m}_q|$. If ω is not very close to ω_F, this term may be dropped.

Equation (3.102) is an inhomogeneous linear differential equation with constant coefficients with respect to $\mathbf{m}_q$. It can be solved using standard methods. We are interested in the z-component of the magnetization, which equals

$$\begin{aligned} m_{qz} = \tfrac{\gamma M i}{2} \sin^2\theta \int_{-\infty}^{t} h_{qz}(t') \Big\{ \left(1 + i\tfrac{\nu}{M}\right)^{-1} \times \exp\left[-\left(1 + i\tfrac{\nu}{M}\right)^{-1} i\omega(q)(t-t') \right] \\ - \left(1 - i\tfrac{\nu}{M}\right)^{-1} \exp\left[\left(1 - i\tfrac{\nu}{M}\right)^{-1} i\omega(q)(t-t') \right] \Big\} dt', \end{aligned} \tag{3.105}$$

where $\omega(\mathbf{q})$ is given by Eq. (3.2). In the small dissipation limit, $\nu \ll M$, we have

$$\begin{aligned} m_{qz} = \tfrac{\gamma M i}{2} \sin^2\theta \int_{-\infty}^{t} h_{qz}(t') \left\{ \exp\left[\left(-i - \tfrac{\nu}{M}\right) \omega(q)(t-t') \right] \right. \\ \left. \times \left(1 - i\tfrac{\nu}{M}\right) - \exp\left[\left(i - \tfrac{\nu}{M}\right) \omega(q)(t-t') \right] \left(1 + i\tfrac{\nu}{M}\right) \right\} dt'. \end{aligned} \tag{3.106}$$

Then, the force $\mathbf{f}_M$ takes the form

$$\begin{aligned} \mathbf{f}_M = \tfrac{2\pi^2\gamma M}{N_v} \sin^2\theta \int d^2\mathbf{q} \int_{-\infty}^{t} h_{qz}(t') h^*_{qz}(t) \times \left\{ \exp\left[\left(i - \tfrac{\nu}{M}\right) \omega(q)(t-t') \right] \left(1 + i\tfrac{\nu}{M}\right) \right. \\ \left. - \exp\left[\left(-i - \tfrac{\nu}{M}\right) \omega(q)(t-t') \right] \left(1 - i\tfrac{\nu}{M}\right) \right\} \mathbf{q} dt'. \end{aligned} \tag{3.107}$$

3.4.2 Vortex motion under the action of a dc current

Let us consider the motion of vortices under the action of a constant external force (e. g., spatially uniform and time-independent transport current). Then the positions of individual vortices are given by

$$\mathbf{R}_i(t) = \mathbf{R}_{i0} + \mathbf{V}_L t + \Delta\mathbf{R}_i(t). \tag{3.108}$$

Here the vectors $\mathbf{R}_{i0}$ denote the vortex positions in a regular lattice, $\mathbf{V}_L$ is the average flux velocity, and $\Delta\mathbf{R}_i(t)$ is responsible for fluctuations of vortices due to interactions with pinning cites ($\langle\Delta\mathbf{R}_i(t)\rangle = 0$). It should be stressed that the influence of pinning on the flux velocity will be not taken into account here. The effect that will be important for us is the vortex lattice distortion caused by impurities, which strongly influences the efficiency of magnon generation.

The product of magnetic fields under the integral in Eq. (3.107) is

$$h_{qz}(t')h^*_{qz}(t) = \left(\frac{\Phi_0}{4\pi^2(1+\lambda^2q^2)}\right)^2 e^{i\mathbf{q}\mathbf{V}_L(t-t')}\mathcal{K}, \tag{3.109}$$

$$\mathcal{K} = \sum_{i,j} \exp\left[i\mathbf{q}(\mathbf{R}_{j0} - \mathbf{R}_{i0}) + i\mathbf{q}(\Delta\mathbf{R}_j(t) - \Delta\mathbf{R}_i(t'))\right].$$

We will analyze two cases when the sum in the right-hand side of the last relation can be calculated.

First, let us assume that the inhomogeneities of the material are insignificant, so that the vortex lattice is nearly perfect. We will put

$$\langle\exp\left[i\mathbf{q}(\Delta\mathbf{R}_j(t) - \Delta\mathbf{R}_i(t'))\right]\rangle \approx 1, \tag{3.110}$$

where the averaging is over i. This assumption is valid when

$$\Delta R_c q \ll 1, \tag{3.111}$$

where ΔR_c is the characteristic displacement of vortices from their positions in a perfect lattice. The inequality (3.111) must hold for all $\mathbf{q}$ giving a considerable contribution to the integral in Eq. (3.107). Below it will be shown that this leads to the condition

$$\Delta R_c \ll \min(L, a_v). \tag{3.112}$$

When this condition is satisfied, we may put

$$\mathcal{K} = \frac{4\pi^2 N_v B_0}{\Phi_0} \sum_{\mathbf{G}} \delta(\mathbf{q} - \mathbf{G}), \tag{3.113}$$

After integration over $\mathbf{q}$ and t' the magnetic force (3.107) takes the form

$$\mathbf{f}_M = \Phi_0 B_0 \gamma M \sin^2\theta \sum_{\mathbf{G}, G<\xi^{-1}} \frac{\mathbf{G}}{(1+\lambda^2G^2)^2} \frac{i\omega(G) + \frac{\nu}{M}\mathbf{G}\mathbf{V}_L}{\omega^2(G) - (\mathbf{V}_L\mathbf{G})^2 - 2i\frac{\nu}{M}\mathbf{V}_L\mathbf{G}\omega(G)}. \tag{3.114}$$

When the terms corresponding to $\mathbf{G}$ and $-\mathbf{G}$ are combined, this can be written as

$$\mathbf{f}_M = -\gamma\nu B_0\Phi_0 \sin^2\theta \sum_{\mathbf{G},G<\xi^{-1}} \frac{\mathbf{G}(\mathbf{G}\mathbf{V}_L)}{(1+\lambda^2G^2)^2} \frac{(\mathbf{G}\mathbf{V}_L)^2+\omega^2(G)}{[\omega^2(G)-(\mathbf{G}\mathbf{V}_L)^2]^2+4\frac{\nu^2}{M^2}(\mathbf{G}\mathbf{V}_L)^2\omega^2(G)}, \tag{3.115}$$

where small terms of the order of ν/M in the numerator have been dropped. From this it follows that the force has local maxima when for some $\mathbf{G}=\mathbf{G_0}$ the condition

$$\omega(G_0) \approx \mathbf{V}_L\mathbf{G_0} \tag{3.116}$$

is satisfied. This relation presents the well-known Cherenkov resonance condition. When Eq. (3.116) holds, magnons with the wave vector $\mathbf{G}_0$ are effectively generated. If the vortex velocity is close to a resonance value, in the sum in Eq. (3.115) we can drop all terms except the two resonant terms corresponding to $\mathbf{G}_0$ and $-\mathbf{G}_0$. Then

$$\mathbf{f}_M \approx -\gamma\nu B_0\Phi_0 \sin^2\theta \frac{\mathbf{G}_0}{(1+\lambda^2G_0^2)^2} \frac{\omega(G_0)}{(\omega(G_0)-\mathbf{V}_L\mathbf{G}_0)^2+\frac{\nu^2}{M^2}\omega^2(G_0).} \tag{3.117}$$

It can be seen that the $\mathbf{f}_M$ vs. V_L dependence for a given vortex velocity direction exhibits a Lorentzian-like peak with the width

$$\Delta V_L = \frac{\nu}{M}\omega(G_0)\frac{V_L}{\mathbf{G}_0\mathbf{V}_L}.$$

The maximum value of f_M is

$$|\mathbf{f}_M|_{\max} = \frac{\gamma M^2 B_0\Phi_0 G_0 \sin^2\theta}{(1+\lambda^2G_0^2)^2\nu\omega(G_0)}. \tag{3.118}$$

Another remarkable feature is that the force is directed at some angle to the velocity of the vortices: $\mathbf{f}_M$ is parallel to $\mathbf{G}_0$, and not $\mathbf{V}_L$. The angle between $\mathbf{f}_M$ and $\mathbf{V}_L$ may range from 0° to 90°. This effect also follows from Equation (3) in [66], though the authors did not mention it, because it has been assumed that $\mathbf{V}_L$ and $\mathbf{f}_M$ are always parallel.

Let us discuss how the Cherenkov resonances influence the current-voltage characteristics. Abrikosov vortex motion is governed by the equation

$$\frac{\Phi_0}{c}\mathbf{j}_{\rm tr}\times\mathbf{z}_0 - \eta\mathbf{V}_L + \mathbf{f}_M = 0. \tag{3.119}$$

Taking the cross product of this relation and $\mathbf{z}_0$, we obtain the expression for the current density

$$\mathbf{j}_{\rm tr} = -\frac{c\eta}{\Phi_0}\mathbf{V}_L\times\mathbf{z}_0 + \frac{c}{\Phi_0}\mathbf{f}_M(\mathbf{V}_L)\times\mathbf{z}_0. \tag{3.120}$$

The relation between $\mathbf{j}_{\rm tr}$ and $\mathbf{E}$ is established via Faraday's law (6). As follows from Eq. (3.120), the vortex-magnetic moment interaction leads to an increase $\Delta\mathbf{j}_{\rm tr}$ of the current density at a given electric field $\mathbf{E}$:

$$\Delta\mathbf{j}_{\rm tr} = \frac{c}{\Phi_0}\mathbf{f}_M\left(\frac{c}{B_0}\mathbf{E}\times\mathbf{z}_0\right)\times\mathbf{z}_0. \tag{3.121}$$

According to Eq. (3.117), near the Cherenkov resonance we have

$$\Delta\mathbf{j}_{\rm tr} = \gamma\nu B_0 c \sin^2\theta \frac{\mathbf{z}_0 \times \mathbf{G}_0}{(1+\lambda^2 G_0^2)^2} \frac{\omega(G_0)}{\left[\omega(G_0) - \frac{c}{B_0}(\mathbf{z}_0 \times \mathbf{G_0})\mathbf{E}\right]^2 + \frac{\nu^2}{M^2}\omega^2(\mathbf{G}_0)}. \qquad (3.122)$$

This relation indicates that the I-V curve exhibits a series of peaks corresponding to the resonance electric fields given by

$$\omega(G) - \frac{c}{B_0}(\mathbf{z}_0 \times \mathbf{G})\mathbf{E} \approx 0 \qquad (3.123)$$

Moreover, close to the resonance the additional current $\Delta\mathbf{j}_{\rm tr}$ is directed along the vector $\mathbf{z}_0 \times \mathbf{G}_0$ and not $\mathbf{E}$. As a result, locally the resistance is anisotropic. Here, it is important to take into account that generally the directions of the vectors $\mathbf{G}_0$ and $\mathbf{V}_L$ are not independent: it is known (for isotropic amorphous [99, 100] and polycrystalline [101] materials) that a moving vortex lattice tends to reorientate itself so that its shortest translation vector is either parallel or perpendicular to $\mathbf{V}_L$, depending on the the flux velocity and magnetic field. This effect is a consequence of vortex interaction with pinning centers or with the the quasiparticle tail of another vortex, as follows from theoretical considerations [102, 103] and numerical simulations [104, 105, 106, 107]. In our case the interaction of vortices with magnetic moments also should affect the vortex lattice orientation. As a result, in amorphous and polycrystalline superconductors the resistivity may remain isotropic even in the presence of magnetic moments. However, in monocrystalline materials there is a competing effect: here, in the static case the energetically favorable vortex nearest-neighbor directions are defined by the symmetry of the crystal [108]. When vortices move, the interplay of the two mentioned effects yields the stationary orientation of the vortex lattice. Then, the angle between $\mathbf{V}_L$ and $\mathbf{G}_0$ may be a complicated function of the current and magnetic field, and the anisotropy predicted by Eq. (3.122) is at least partially preserved.

Considering macroscopic ferromagnetic superconductors and multilayer systems, care should be taken when applying Eq. (3.122) to the whole sample: It is known that even a small concentration of pinning sites destroys the long-range order in the vortex lattice [109]. In fact, vortex lattice domains are formed in large superconducting samples; see [108, 110, 111, 112, 113]. In monocrystalline samples, as mentioned above, the symmetry of the crystal makes only few orientations of the vortex lattices energetically favorable. This fact allows us to put forward a qualitative argument. Let us denote as $\mathcal{G}$ the set of all reciprocal lattice vectors for all vortex lattice domains. Since there are only few possible orientations of the domains, the set $\mathcal{G}$ consists of isolated points. When the applied electric field satisfies Eq. (3.123) for some $\mathbf{G} \in \mathcal{G}$, the enhancement of the current should be observable. Hence, even if there are several vortex lattice domains, the peaks on the current-voltage characteristics are present. The measurement of the peak voltages at different applied magnetic fields makes it possible to probe the magnon spectrum $\omega(\mathbf{q})$.

Now we turn to the opposite limiting case, when there is considerable disorder in the vortex lattice. This situation may be realized in weak magnetic fields, $B_0 \lesssim \Phi_0/\lambda^2$ ($a_v \gtrsim \lambda$), when vortex-vortex interaction is weak and the lattice is easily destroyed by defects and thermal fluctuations. Assuming that the quantities $\mathbf{R}_j(t)$ and $\mathbf{R}_i(t')$ for $i \neq j$

are not correlated, we find that

$$\mathcal{K} = P\sum_{i\neq j} e^{i\mathbf{q}(\mathbf{R}_{i0}-\mathbf{R}_{j0})} + N_v\left\langle e^{i\mathbf{q}[\Delta\mathbf{R}_i(t)-\Delta\mathbf{R}_i(t')]}\right\rangle, \tag{3.124}$$

where

$$P = \left|\left\langle e^{i\mathbf{q}\Delta\mathbf{R}_i(t)}\right\rangle\right|^2,$$

and the averaging is over i. Next we assume that the vortex position fluctuations ΔR_i are sufficiently large, so that $P \ll 1$ for $q \gtrsim L^{-1}$. As we will see, the main contribution to $\mathbf{f}_M$ comes from $q \sim L^{-1}$, so the behavior of K at smaller q has a negligible effect on the result derived in this subsection. For an estimate of the required characteristic value of ΔR_i, we note that if the quantity $\mathbf{R}_i(t)$ has a Gaussian distribution function, then the condition $P \ll 1$ is satisfied for $\langle \Delta R_i^2\rangle \gg L^2$.

Concerning the second term in the right-hand side of Eq. (3.124), one can see that

$$\left\langle e^{i\mathbf{q}[\Delta\mathbf{R}_i(t)-\Delta\mathbf{R}_i(t')]}\right\rangle = 1,$$

when $t = t'$, and

$$\left\langle e^{i\mathbf{q}[\Delta\mathbf{R}_i(t)-\Delta\mathbf{R}_i(t')]}\right\rangle = P \ll 1,$$

when $|t - t'| \to \infty$. To proceed further, we put

$$\left\langle e^{i\mathbf{q}[\Delta\mathbf{R}_i(t)-\Delta\mathbf{R}_i(t')]}\right\rangle = e^{-|t-t'|/\tau(q)},$$

where the time $\tau(q)$ is chosen so that $\langle|\mathbf{q}[\Delta\mathbf{R}_i(t) - \Delta\mathbf{R}_i(t')]|\rangle \sim 1$ at $t - t' = \tau(q)$. The last assumption that will be used is that the vortex self-correlation time $\tau(q)$ is much larger than $\omega(q)^{-1}$ at $q \sim L^{-1}$. Then, due to the small factor P, the contribution to $\mathbf{f}_M$ of the first term in the right-hand side of Eq. (3.124) can be neglected, and we can put

$$\mathcal{K} = N_v e^{-|t-t'|/\tau(q)}. \tag{3.125}$$

After integration over t', Eq. (3.107) yields

$$\mathbf{f}_M = \frac{\gamma M\Phi_0^2\sin^2\theta}{4\pi^2}\int_{q<\xi^{-1}} \frac{\mathbf{q}d^2\mathbf{q}}{(1+\lambda^2q^2)^2}\frac{i\omega(q)}{[\omega^2(q)-(\mathbf{q}\mathbf{V}_L)^2-2i(\mathbf{q}\mathbf{V}_L)\tau_1^{-1}(q)]}, \tag{3.126}$$

where $\tau_1^{-1}(q) = \tau^{-1}(q) + \nu\omega(q)/M$, and in the numerator terms proportional to ν/M have been dropped. The main contribution to the integral comes from $\mathbf{q}$ lying in the vicinity of two circles in the $\mathbf{q}$-plane, given by $\omega(q) = \pm\mathbf{q}\mathbf{V}_L$ (this equation specifies the Cherenkov resonance condition). Near the circle $\omega(q) = \mathbf{q}\mathbf{V}_L$ we can make the following transformation:

$$\omega^2(q) - (\mathbf{q}\mathbf{V}_L)^2 - 2i(\mathbf{q}\mathbf{V}_L)\tau_1^{-1}(q) \approx 2\omega(q)[\omega(q) - \mathbf{q}\mathbf{V}_L - i\tau_1^{-1}(q)].$$

For the circle $\omega(q) = -\mathbf{q}\mathbf{V}_L$ the transformations are analogous. Then

$$\mathbf{f}_M \approx \frac{\gamma M\Phi_0^2\sin^2\theta}{4\pi^2}\int_{q<\xi^{-1}}\frac{\mathbf{q}d^2\mathbf{q}}{(1+\lambda^2q^2)^2}\Re\frac{i}{\omega(q)-\mathbf{q}\mathbf{V}_L-i\tau_1^{-1}(q)}. \tag{3.127}$$

The last fraction in the right-hand side resembles the expression

$$\Re \frac{i}{f(x) - i\epsilon},$$

which reduces to $-\pi\delta(f(x))$ when $\epsilon \to +0$. Hence, the last factor in Eq. (3.127) also can be replaced by a δ-function, when $\tau_1^{-1}(q)$ is sufficiently small. To derive the limitation on $\tau_1^{-1}(q)$ we direct the q_x-axis along $\mathbf{V}_L$ and rewrite the denominator of the large fraction in Eq. (3.127) as follows:

$$\omega_F(1 + L^2q^2) - q_xV_L - i\tau_1^{-1}(q) = \omega_F\left(1 - \frac{V_L^2}{V_{\rm th}^2}\right) - i\tau_1^{-1}(q) + \omega_F L^2\left[\left(q_x - \frac{V_L}{2L^2\omega_F}\right)^2 + q_y^2\right],$$

where $V_{\rm th} = 2\omega_F L$ is the magnon generation threshold velocity. Now it is evident that the δ-function can be introduced in Eq. (3.127) when

$$\tau_1^{-1}(q) \ll \omega_F \left|\frac{V_L^2}{V_{\rm th}^2} - 1\right|.$$

Then

$$\mathbf{f}_M \approx -\frac{\gamma M\Phi_0^2 \sin^2\theta}{4\pi}\int_{q<\xi^{-1}} \frac{\mathbf{q}d^2\mathbf{q}}{(1+\lambda^2q^2)^2}\delta(\omega(q) - \mathbf{q}\mathbf{V}_L). \tag{3.128}$$

Here, two points should be noted: (i) the expression for $\mathbf{f}_M$ does not depend on the dissipation rate and on the artificially introduced time $\tau(q)$; (ii) Equation (3.128) can be derived from Eq. (3.115) in the limit of an extremely sparse vortex lattice, when summation can be replaced by integration.

Technical details of integration in Eq. (3.128) are given in Appendix G. The final result is

$$\mathbf{f}_M = -\frac{\gamma M\Phi_0^2 \sin^2\theta}{8\lambda^4\omega_F^2}\left[1 + \left(\frac{V_L}{\lambda\omega_F}\right)^2\right]^{-3/2}\Theta(V_L - V_{\rm th})\mathbf{V}_L, \tag{3.129}$$

where Θ is the Heaviside function. Equation (3.129) is valid for $\lambda \gg L$ and

$$V_L < \max(V_{\rm th}, \omega_F\xi(1 + L^2\xi^{-2})$$

– see Appendix G. Thus, Eq. (3.129) is not applicable to the U-based ferromagnetic superconductors (see Table 3.1) at $V_L > V_{\rm th}$, since these materials have $L \ll \xi$. Still, Eq. (3.129) with appropriate modifications (see Sec. 3.4.5) may be applied to SF-superlattices with ferromagnetic layers having a sufficiently large value of L.

As follows from Eqs. (3.121) and (3.129), at the electric field $E = V_{\rm th}B_0/c$ the average current density should exhibit a stepwise increase by

$$\Delta j_{\rm tr} = \frac{c}{\Phi_0}f_M(V_{\rm th}) = \frac{\gamma M\Phi_0 c\sin^2\theta}{8\lambda^4\omega_F^2}V_{\rm th}.$$

The maximum enhancement of the current density due to vortex-magnetic moment interaction is reached at $E = \sqrt{2}\lambda\omega_F B_0/c$ and equals

$$\Delta j_{\rm max} = \frac{\Phi_0 c\gamma M\sin^2\theta}{8\sqrt{2}\lambda^3\omega_F 3^{3/2}}.$$

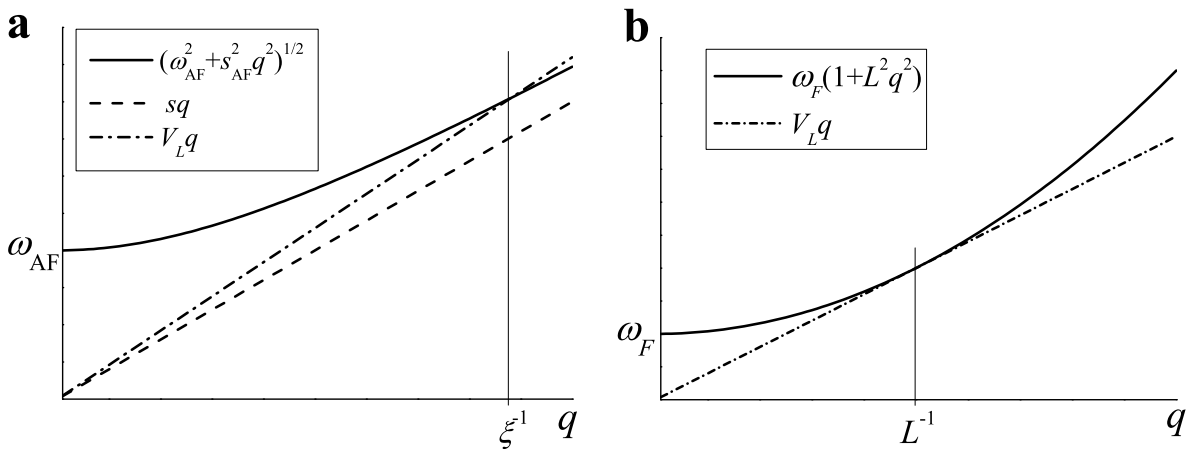

Figure 3.7: The magnon spectra in an (a) antiferromagnet and (b) ferromagnet. The dash-dotted line is given by $\omega = V_L q$, where V_L is the vortex velocity at which magnon generation becomes efficient ($V_L = V_c$ for antiferromagnetic superconductors and $V_L = V_{\rm th}$ for superconductor-ferromagnet hybrids).

In [65] it has been predicted that in antiferromagnetic superconductors in the sparse lattice limit the current enhancement $\Delta j_{\rm tr}$ is proportional to $\sqrt{V_L - V_c}$ (at $V_L > V_c$), where V_c is some critical velocity. This result is in contrast with the one obtained here: we found that $\Delta j_{\rm tr} \sim \Theta(V_L - V_{\rm th})$ near the magnon generation threshold. This difference is due to different magnon spectra in ferromagnets and antiferromagnets – see Fig. 3.7. In an antiferromagnet $\omega(q)$ is given by Eq. (3.3). As the vortex velocity is increased, the resonance condition $\omega(q) = \mathbf{V}_L\mathbf{q}$ is first satisfied at infinitely large q. However, at $q \gg \xi^{-1}$ the Fourier components h_{qz} are exponentially small. Magnon generation becomes efficient at $q \sim \xi^{-1}$, which is reached at a critical velocity that roughly equals $V_c = \sqrt{\omega_{AF}^2\xi^2 + s_{AF}^2}$. In short, the generation threshold in antiferromagnetic superconductors corresponds to an intersection of the curves $\omega = \omega(q)$ and $\omega = V_L q$ at $q \sim \xi^{-1}$ (see Fig. 3.7a), yielding a $\Delta j_{\rm tr} \sim \sqrt{V_L - V_c}$ dependence. On the contrary, in ferromagnet-superconductor hybrids at $V_L = V_{\rm th}$ the curves $\omega = \omega(q)$ and $\omega = V_L q$ touch each other (see Fig. 3.7b). This fact leads to a stepwise increase of the current at the threshold vortex velocity. Of course, the step-like feature on the I-V curve may be observed only in hybrid systems with $L \gtrsim \xi$.

Before proceeding to numeric estimates, a remark should be made concerning the condition (3.112), providing that the ideal lattice approximation can be used. It follows from Fig. 3.7b that near the generation threshold magnons with wave numbers $q \approx L^{-1}$ are generated. This means that for $V_L \gtrsim V_{\rm th}$ the main contribution to the integral in Eq. (3.107) comes from $q \sim L^{-1}$. Thus, the condition (3.112) should be imposed to ensure the applicability of the perfect lattice approximation.

Now, let us check whether it is possible to observe the features connected with the Cherenkov resonances on the current-voltage characteristics of ferromagnetic superconductors and SF multilayers. First, it is important to note that the real magnon generation threshold velocity $V'_{\rm th}$ in the U-based ferromagnetic superconductors is larger than $V_{\rm th}$ and is of the order of $\omega_F\xi$, since in these materials $\xi \gg L$. As a result, instead of a step-like increase of the current at a critical voltage we may expect a threshold behavior

similar to the one described in [65] for superconducting antiferromagnets. We will estimate the supercurrent density $j_{\rm th}$ which is sufficient to accelerate the vortices up to the velocity $V'_{\rm th}$. Equation (3.120) yields

$$j_{\rm th} \approx \frac{c\eta}{\Phi_0} V'_{\rm th} \tag{3.130}$$

For the viscosity η we use the Bardeen and Stephen expression [32] (which is a good estimate for relatively slow processes [114])

$$\eta = \Phi_0 H_{c2} \sigma_n / c^2, \tag{3.131}$$

For the normal state conductivity we may use Drude's estimate

$$\sigma_n \sim \frac{e^2 n \ell}{m V_F}.$$

Here n is the concentration of charge carriers, m is their mass, ℓ is the mean free path, and V_F is the Fermi velocity. Then

$$j_{\rm th} \sim \frac{e^2 n \ell H_{c2} V'_{\rm th}}{mcV_F}. \tag{3.132}$$

This value should be compared with the depairing current density which is given within the BCS theory by

$$j_{\rm cr} \sim en \frac{\Delta}{mV_F},$$

where Δ is the superconducting gap. We demand $j_{\rm th} \ll j_{\rm cr}$. Using the relation $\Delta \sim \hbar V_F/\xi$ (valid for clean superconductors) we can rewrite the inequality above as

$$V'_{\rm th} \ll \frac{\xi}{\ell} V_F, \tag{3.133}$$

or

$$\omega_F \ll \frac{V_F}{\ell}. \tag{3.134}$$

According to the estimates given in [55, 56, 57], in the U-based compounds ℓ is typically of the order of 50 nm. The Fermi velocities are of the order of $10^8 cm/s$ in UGe_2 and $10^5 cm/s$ in UCoGe and URhGe – see [115, 116, 117]. Thus, the inequality (3.133) is satisfied in neither of these compounds, and the model used here breaks down at vortex velocities below $V'_{\rm th}$. This is a consequence of the high magnetic anisotropy and large quasiparticle mass in the U-compounds.

The situation seems to be more optimistic in SF superlattices. Certainly, we should consider if Eq. (3.131) is valid for multilayers. A study of the vortex viscosity in superconductor/normal metal multilayers is presented in [118] and [119]. It has been shown that the Bardeen-Stephen viscosity (3.131) may be significantly modified for vortices inclined with respect to the z-axis, or for strongly conducting normal metal layers. Still, in our case Eq. (3.131) is a good order-of magnitude estimate for $d_S \sim d_F$ and $\sigma_F \lesssim \sigma_n$, where d_S and d_F are the thicknesses of the superconducting and ferromagnetic layers (see Fig. 3.6), respectively.

Recently, a number of experimental papers [120, 121, 122, 123, 124, 125, 126, 127, 128, 129] have reported successful fabrication of high-quality $YBa_2Cu_3O_7/La_{2/3}Ca_{1/3}MnO_3$ superlattices. In [130] the value $H_{\rm an} = 1200$ Oe for $La_{0.7}Ca_{0.3}MnO_3$ is given, though it is noted that the anisotropy is significantly influenced by strain. Strictly speaking, $La_{0.7}Ca_{0.3}MnO_3$ with $M = 530$ emu/cm^3 (see [130]) and $K \sim 2$ is not in the $K \gg 1$ limit, which means that the magnetostatic term $\mathbf{b}_{Mq}$ in Eq. (3.102) cannot be ignored. However, the order-of-magnitude estimate for $V_{\rm th}$ given here remains valid for ferromagnets with $K \sim 1$, and it can be applied to the mentioned compound.

The measured domain wall width in $La_{0.7}Ca_{0.3}MnO_3$, denoted as δ in [131], is 12 nm. Assuming $\gamma \sim \mu_B/\hbar$, where μ_B is the Bohr magneton, we obtain the following estimate for the vortex threshold velocity:

$$V_{\rm th} = 2\gamma H_{\rm an} L \sim 10^4 cm/s. \tag{3.135}$$

The Fermi velocity in $YBa_2Cu_3O_7$ is of the order of or greater than $10^7 cm/s$ [132]. Thus, the condition (3.133) (with $V_{\rm th}$ in place of $V'_{\rm th}$) can surely be satisfied in the cuprate/manganite superlattices.

Of course, the the Bardeen-Stephen estimate for the viscosity η may break down at transport currents that are considerably smaller than the depairing current. This may happen, for example, due to the Larkin-Ovchinnikov instability [133, 134] (in dirty samples at high temperatures), or due to the overheating instability. These effects lead to a dependence of η on $\mathbf{E}$, and thus to a non-linear current-voltage characteristic. Still, considering that vortex velocities 10^5 cm/s can be achieved in the linear flux-flow regime in both high-temperature [135, 136] and low-temperature [137] superconductors, one can expect the effects caused by the magnon radiation to be observable.

3.4.3 Vortex motion under the action of an ac current

As has been shown in Sec. 3.4.2, magnon generation in U-based ferromagnetic superconductors by a vortex array moving with constant velocity seems problematic due to the high required vortex velocities. In this subsection we will study a more feasible approach to magnon generation in magnetic superconductors, analyzing the case of a harmonic external current acting on the vortices. Experimentally, the oscillating current in the superconductor can be created using the microwave technique (for example, see [138]). Then, the surface impedance yields information about the high-frequency properties of the sample – see Sec. 3.4.4.

Before we calculate the force $\mathbf{f}_M$, we note that there is an obvious limitation on the frequency ω for the applicability of the London approach, namely $\hbar\omega < \Delta$. On the other hand, magnon radiation by vortices starts at $\omega > \omega_F$. Hence, it is required that $\hbar\omega_F < \Delta$ to make the resonant features described below observable.

Subjected to the action of a harmonic force, in the linear regime the vortices oscillate harmonically:

$$\mathbf{R}_i(t) = \mathbf{R}'_{i0} + \mathbf{R}e^{-i\omega t} + \mathbf{R}^* e^{-i\omega t}. \tag{3.136}$$

Here $\mathbf{R}'_{i0}$ are the equilibrium positions of the vortices, which are defined by vortex-vortex interaction as well as pinning. The vectors $\mathbf{R}'_{i0}$ do not necessarily form a regular lattice, unlike $\mathbf{R}_{i0}$. $\mathbf{R}$ is the amplitude of vortex oscillations. We will consider frequencies of

the order of the ferromagnetic resonance frequency in ferromagnetic superconductors, $\omega_F \sim 100$GHz. This frequency is several orders of magnitude larger than the typical depinning frequency [139]. This fact allows to neglect the influence of the pinning force on vortex motion and to assume that the oscillation amplitudes of all vortices are equal to $\mathbf{R}$.

The product of the magnetic fields in Eq. (3.107) equals

$$\begin{aligned} h_{qz}(t')h^*_{qz}(t) &= \left[\tfrac{\Phi_0}{4\pi^2(1+\lambda^2q^2)}\right]^2 \mathcal{K}' e^{i\mathbf{q}(\mathbf{R}_i(t)-\mathbf{R}_i(t'))} \\ &\approx \left[\tfrac{\Phi_0}{4\pi^2(1+\lambda^2q^2)}\right]^2 \mathcal{K}' \left\{1 + i\mathbf{q}[\mathbf{R}_i(t) - \mathbf{R}_i(t')]\right\}, \end{aligned} \tag{3.137}$$

where

$$\mathcal{K}' = \sum_{i,j} e^{-i\mathbf{q}\mathbf{R}'_{i0}+i\mathbf{q}\mathbf{R}'_{j0}} = N_v \left\langle \sum_j e^{-i\mathbf{q}\mathbf{R}'_{i0}+i\mathbf{q}\mathbf{R}'_{j0}} \right\rangle. \tag{3.138}$$

Here the averaging is over i. The linear with respect to $\mathbf{R}$ contribution to the force takes the form

$$\begin{aligned} \mathbf{f}_M &= \tfrac{\gamma M\Phi_0^2}{8\pi^2 N_v} \sin^2\theta \int_{q<\xi^{-1}} d^2\mathbf{q} \int_{-\infty}^{t} \tfrac{i\mathcal{K}'\mathbf{q}\mathbf{R}}{(1+\lambda^2q^2)^2}(e^{-i\omega t} - e^{-i\omega t'}) \\ &\times \left\{ e^{\left[i\omega(q)-\frac{\nu}{M}\omega(q)\right](t-t')} - e^{\left[-i\omega(q)-\frac{\nu}{M}\omega(q)\right](t-t')} \right\} \mathbf{q}dt' + c.c. \\ &\approx \tfrac{\gamma M\Phi_0^2}{4\pi^2 N_v} \sin^2\theta e^{-i\omega t} \int_{q<\xi^{-1}} d^2\mathbf{q} \tfrac{\mathcal{K}'(q)\mathbf{q}\mathbf{R}}{(1+\lambda^2q^2)^2} \left[\tfrac{\omega(q)}{\omega^2(q)-\omega^2-2i\frac{\nu}{M}\omega\omega(q)} - \omega^{-1}(q)\right] \mathbf{q} + c.c. \end{aligned} \tag{3.139}$$

Here $c.c.$ denotes the complex conjugate. Like before, small terms of the order of ν/M were dropped.

To proceed further, the explicit form of $\mathcal{K}'(q)$ is required. Again, we will consider the cases of a perfect vortex lattice and a disordered array.

First, let us assume that pinning is sufficiently weak, so that

$$q\Delta R_c \ll 1, \tag{3.140}$$

where $\Delta R_c \sim |\mathbf{R}'_{i0} - \mathbf{R}_{i0}|$ is the characteristic deviation of the vortices from their positions in a perfect lattice. The inequality (3.140) should hold for all $\mathbf{q}$ giving a considerable contribution to the integral in Eq. (3.139). The characteristic value of q will be estimated below.

For $q\Delta R_c \ll 1$ we have

$$\mathcal{K}' = \frac{4\pi^2 N_v B_0}{\Phi_0} \sum_{\mathbf{G}} \delta(\mathbf{q} - \mathbf{G}). \tag{3.141}$$

Substituting Eq. (3.141) into Eq. (3.139), assuming that the vortex lattice is either square or regular triangular, we obtain

$$\mathbf{f}_M = i\omega\eta_M \mathbf{R} e^{-i\omega t} + c.c., \tag{3.142}$$

$$\eta_M = -\frac{i\gamma M\Phi_0 B_0}{2\omega} \sin^2\theta \sum_{G<\xi^{-1}} \frac{G^2}{(1+\lambda^2G^2)^2} \left[\frac{\omega(G)}{\omega^2(G)-\omega^2-2i\frac{\nu}{M}\omega\omega(G)} - \omega^{-1}(G)\right]. \tag{3.143}$$

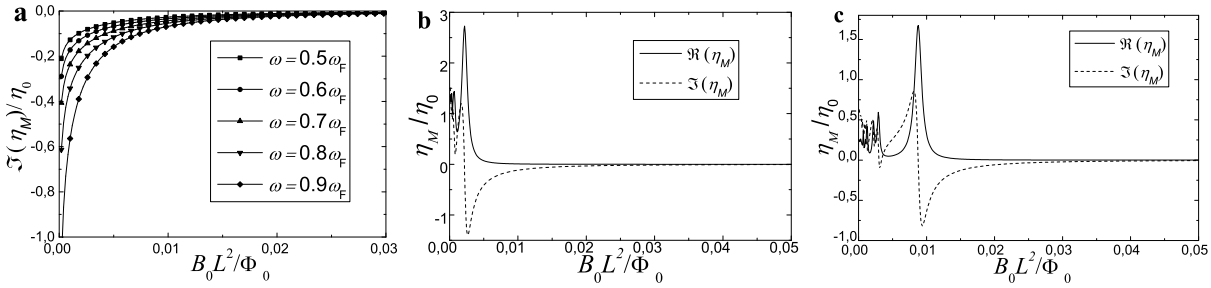

Figure 3.8: (a) The $\Im(\eta_M)$ vs. magnetic field dependence at frequencies below the ferromagnetic resonance frequency for an ideal triangular vortex lattice [see Eq. (3.144)]. $\eta_0 = \gamma M \Phi_0^2 \sin^2\theta/(2\lambda^4\omega_F^2)$. The η_M vs. B_0 dependencies at $\omega = 1.1\omega_F$ (b) and $\omega = 1.4\omega_F$ (c). $\nu/M = 0.02$.

Here, the complex quantity η_M has been introduced, playing the role of a generalized vortex viscosity. Indeed, when η_M is purely real, the magnetic force is simply $\mathbf{f}_M = -\eta_M d\mathbf{R}_i/dt$. In our system there is a phase shift between the vortex velocity and $\mathbf{f}_M$, and the more general expression (3.142) is valid. Further on η_M will be called the magnetic viscosity.

The ideal vortex lattice is likely to form when vortex-vortex interaction is sufficiently strong, which may happen when the inter-vortex distance is sufficiently small. Let this distance be much smaller than the London penetration depth, which means $B_0 \gg \Phi_0/\lambda^2$. Then $\lambda G \gg 1$ for all $\mathbf{G} \neq 0$, and

$$\eta_M \approx -\frac{i\gamma M \Phi_0 B_0 \omega}{2\lambda^4} \sin^2\theta \sum_{\mathbf{G}\neq 0, G<\xi^{-1}} G^{-2}\omega^{-1}(G)\left[\omega^2(G) - \omega^2 - 2i\frac{\nu}{M}\omega\omega(G)\right]^{-1}. \quad (3.144)$$

Now we will consider the behavior of η_M in different frequency ranges. First, let the frequency be below the ferromagnetic resonance frequency ($\omega < \omega_F$). Then magnon generation is inefficient. However, if we put $\nu = 0$, the force $\mathbf{f}_M$ will not vanish below the generation threshold, unlike in the case of constant vortex velocity. Instead, the magnetic viscosity will be purely imaginary, signifying that there are no magnetic losses. In Fig. 3.8a the imaginary part of η vs. magnetic field B_0 dependencies for different frequencies (below ω_F) and for a fixed angle θ are plotted.

At frequencies above the ferromagnetic resonance frequency magnetic dissipation can not be neglected, and the real part of η_M becomes significant. In Fig. 3.8b and c the η_M vs. B_0 dependencies for two frequencies and for a fixed angle θ and dissipation rate $\nu/M = 0.02$ are plotted. The graphs exhibit a sequence of Lorentzian-like ($\Re(\eta_M)$) and N-shaped ($\Im(\eta_M)$) features, located at some resonant field values, B_R, which are determined from the relation

$$\omega(G) = \omega. \quad (3.145)$$

For small fields these features may overlap, but the resonance corresponding to the highest field remains well distinguishable. For a triangular vortex lattice the largest resonance field equals

$$B_R = \frac{\sqrt{3}}{8\pi^2}\frac{\Phi_0}{L^2}\left(\frac{\omega}{\omega_F} - 1\right),$$

and for a square lattice

$$B_R = \frac{1}{4\pi^2}\frac{\Phi_0}{L^2}\left(\frac{\omega}{\omega_F} - 1\right).$$

Solving Eq. (3.145) with respect to G, we obtain

$$G = q_0 \equiv L^{-1}\sqrt{\frac{\omega - \omega_F}{\omega_F}}. \tag{3.146}$$

Hence, the peaks on the η_M vs. B_0 dependencies must be observable if the characteristic deviation ΔR_c of the vortices from their positions in an ideal lattice satisfies

$$\Delta R_c \ll \min(q_0^{-1}, a_v). \tag{3.147}$$

When $\omega < \omega_F$ one can see from Eq. (3.144) that the main contribution to η_M comes from the vectors $\mathbf{G}$ for which $\omega(G) - \omega$ is of the order of $\omega_F - \omega$, since the terms on the right-hand side of Eq. (3.144) are proportional to $[\omega(G) - \omega]^{-1}$ when $\nu \to 0$. Then, for an arbitrary frequency ω we obtain the following applicability condition for the ideal lattice approximation:

$$\Delta R_c \ll \min\left[a_v, L\sqrt{\frac{\omega_F}{|\omega - \omega_F|}}\right]. \tag{3.148}$$

Note that when the frequency is close to ω_F this condition is weaker than the one imposed by Eq. (3.112).

Let us compare the values of η_M and of the main contribution to the viscosity, which was denoted as η. When the resonance condition (3.145) is satisfied, we obtain from Eq. (3.144)

$$\eta_M \sim \frac{\gamma M \Phi_0 B_0}{\lambda^4 G^2 \omega^2}\frac{M}{\nu}.$$

Since $B_0 G^{-2} \sim \Phi_0$, and the lowest allowable value of ω is $\omega_F = \gamma M K$, we have

$$\eta_M \lesssim \frac{\Phi_0^2}{K\lambda^4\omega_F}\frac{M}{\nu}. \tag{3.149}$$

Then, according to Eq. (3.131), the ratio of η_M to η is

$$\eta_M/\eta \lesssim \frac{M}{\nu}\frac{\xi^2 c^2}{K\lambda^4\omega_F\sigma_n}. \tag{3.150}$$

For UCoGe, the U-superconductor with the lowest value of ω_F, in [57] we find the value $12\mu\Omega cm$ for the normal resistivity, and the maximal value 200Å for the coherence length. Using Table 3.1, we obtain

$$\eta_M/\eta \sim \frac{M}{\nu}3 \times 10^{-5}. \tag{3.151}$$

Data on the ratio M/ν are not available yet. The small factor 10^{-5} in Eq. (3.151) appears due to the large magnetocrystalline anisotropy of UCoGe: it can be seen from Eq. (3.150) that η_M/η is proportional to K^{-2}, since $\omega_F = \gamma M K$. Hence, to increase the ratio of η_M to η, compounds (or multilayer systems) with a lower anisotropy are preferable.

Now consider the situation when the vortex lattice is strongly distorted by pinning centers. To obtain a qualitative understanding of the behavior of η_M in this case, we will

calculate the magnetic viscosity under the assumption that the quantities R'_{i0} and R'_{j0} for $i \neq j$ are uncorrelated. In other words, there is even no short-range order in the vortex lattice, so that the average concentration of vortices at a distance R from a given vortex does not depend on R and equals B_0/Φ_0. Then

$$\mathcal{K}' = N_v + N_v \left\langle \sum_{j(j\neq i)} e^{-i\mathbf{q}\mathbf{R}'_{i0}+i\mathbf{q}\mathbf{R}'_{j0}} \right\rangle = N_v \left(\int \frac{B_0}{\Phi_0} e^{-i\mathbf{q}\mathbf{R}} d^2\mathbf{R} + 1 \right) = N_v \left[4\pi^2 \frac{B_0}{\Phi_0} \delta(\mathbf{q}) + 1 \right]. \tag{3.152}$$

It should be noted that the product $h_{qz}(t')h^*_{qz}(t)$ does not decay with increasing $t - t'$, unlike in the case of a constant driving force; see Eq. (3.125). This is explained by the fact that the vortices oscillate close to their equilibrium positions and do not travel from one pinning site to another. Thus, the positions $\mathbf{R}_i(t)$ and $\mathbf{R}_i(t')$ of a single vortex are always well correlated, corresponding to an infinite correlation time $\tau(q)$.

With $\mathcal{K}'$ given by Eq. (3.152) the magnetic viscosity takes the form

$$\eta_M = -\frac{i\gamma M \Phi_0^2}{4\pi\omega} \sin^2\theta \int_0^{\xi^{-1}} \frac{q^3 dq}{(1+q^2\lambda^2)^2} \left[\frac{\omega(q)}{\omega^2(q) - \omega^2 - i\epsilon} - \omega^{-1}(q) \right]. \tag{3.153}$$

Here, like in Sec. 3.4.2, we will assume that the imaginary term $-i\epsilon$ ($\epsilon > 0$) in the denominator is an infinitesimal. To simplify the expression in the right-hand side of Eq. (3.153), we note that the contribution to the integral from small q ($q \lesssim \lambda^{-1}$) can be neglected in the $\lambda \gg L$ limit. Then we can put $1 + \lambda^2 q^2 \approx \lambda^2 q^2$, and cut the integral off at $q = \lambda^{-1}$:

$$\eta_M = -\frac{i\gamma M \Phi_0^2}{4\pi\omega\lambda^4} \int_{\lambda^{-1}}^{\xi^{-1}} \frac{dq}{q} \left\{ \frac{\omega(q)}{[\omega + \omega(q)][\omega(q) - \omega - i\epsilon]} - \omega^{-1}(q) \right\}. \tag{3.154}$$

Further integration is straightforward:

$$\eta_M = \frac{\gamma M \Phi_0^2 \sin^2\theta}{16\lambda^4(\omega - \omega_F)} \left\{ \frac{1}{\omega} \Theta(\omega - \omega_F) \Theta \left[\omega_F \left(1 + \frac{L^2}{\xi^2} \right) - \omega \right] + i \frac{4\omega}{\pi\omega_F(\omega + \omega_F)} \ln\frac{\lambda}{\xi} \right\}, \tag{3.155}$$

when $L \ll \xi$. As above, at $\omega < \omega_F$ the magnetic viscosity is purely imaginary. However, unlike in the case of a perfect vortex lattice, now the viscosity does not depend on the magnetic field and has only one resonance at $\omega = \omega_F$. In the limit $B_0 \to 0$ Eq. (3.144) after summation transforms into (3.155), i.e., the cases of isolated vortices and chaotically placed vortices are equivalent, like in Sec. 3.4.2.

As we have seen, at $\omega < \omega_F$ the magnetic viscosity is purely imaginary. Moreover, at $\omega \ll \omega_F$ the viscosity is proportional to ω. This signifies that the vortex can be ascribed a mass per unit length, M_v, so that the equation of motion becomes

$$M_v \frac{d^2\mathbf{R}_i}{dt^2} = \mathbf{f}_{\text{ext}}, \tag{3.156}$$

where $\mathbf{f}_{\text{ext}}$ includes all forces, except for the force $\mathbf{f}_M$. The mass is defined by

$$M_v = \left. \frac{i\eta_M}{\omega} \right|_{\omega=0}. \tag{3.157}$$

Using Eq. (3.144), we find that the magnetic contribution to the vortex mass for a perfect lattice is

$$M_v = \frac{\gamma M \Phi_0 B_0}{2\lambda^4} \sin^2\theta \sum_{\mathbf{G}\neq 0} G^{-2}\omega^{-3}(G) \tag{3.158}$$

when $B_0 \gg \Phi_0/\lambda^2$. For a disordered array we may obtain from Eq. (3.153)

$$M_v = \frac{\gamma M \Phi_0^2}{4\pi\omega_F^3} \sin^2\theta \int_0^{\xi^{-1}} \frac{q^3 dq}{(1+q^2\lambda^2)^2(1+L^2q^2)^3} \approx \frac{\gamma M \Phi_0^2 \sin^2\theta}{4\pi\omega_F^3\lambda^4} \ln\frac{\lambda}{\xi} \qquad (\lambda \gg \xi \gg L). \tag{3.159}$$

Let us estimate the characteristic magnetic contribution M_v to the vortex mass and compare it with the electronic contribution (see, for example, [11]), which is present in any superconductor:

$$M_e = \frac{2}{\pi^3}\frac{m^2 V_F}{\hbar}. \tag{3.160}$$

For URhGe, the values of ω_F and λ can be found in Table 3.1. The electron mass and Fermi velocity for one of the Fermi surface pockets of URhGe have been measured in [117]. The values given there are $m = 22m_e$ and $V_F = 4.4 \times 10^5 cm/s$, where m_e is the free electron mass. Then

$$M_v \sim \frac{\gamma M \Phi_0^2}{4\pi\omega_F^3\lambda^4} \sim 10^{-24} g/cm, \qquad M_e \sim 10^{-20} g/cm.$$

It can be seen that the magnetic contribution to the vortex mass is negligible for URhGe. Estimates for UGe_2 and UCoGe yield the same result. This happens due to the very large ferromagnetic resonance frequency ω_F in these compounds: note that the right-hand side of Eq. (3.159) contains ω_F^{-3}. Thus, the magnetic mass M_v should be detectable in materials with a smaller ferromagnetic resonance frequency.

Finally, a remark should be made concerning the connection between the vortex mass enhancement in SF hybrids and the polaronic vortex pinning mechanism discussed in [66] and [67]. In the mentioned papers purely dissipative vortex dynamics has been considered, i. e., $\nu/M \gg 1$, which is in contrast to the case studied in the present Chapter. Thus, the polaronic pinning mechanism contributes rather to the real part of η_M than to its imaginary part, an it is not related to the vortex mass enhancement discussed here.

3.4.4 Connection between the vortex viscosity and the surface impedance of a ferromagnetic superconductor

A simple experimental method to study vortex dynamics in type-II superconductors is based on the measurement of the surface impedance. A possible geometry for such experiment is depicted in Fig. 3.9. We will analyze the simplest situation, when the vortices are perpendicular to the sample surface, and the probing electromagnetic wave with the amplitude $\mathbf{h}_e$ is normally incident on this surface (note the difference with Sec. 3.3.5, where a different geometry was considered). Then, for a non-magnetic superconductor ($\mathbf{M}_0 = 0$) theory [77, 140] predicts that in a wide range of parameters the surface impedance $Z(\omega)$ equals

$$Z(\omega) = \left(\frac{-i\omega\mu_s\rho_f}{4\pi}\right)^{1/2}, \tag{3.161}$$

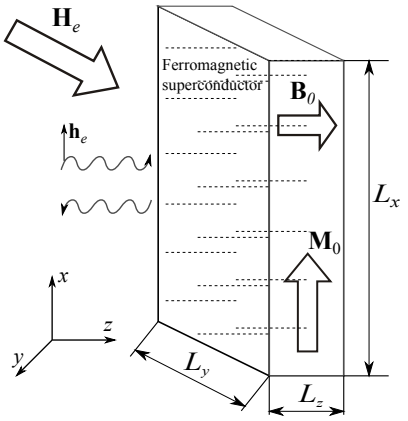

Figure 3.9: The geometry for the measurement of the vortex viscosity in a ferromagnetic superconductor. The dashed lines denote vortices.

where μ_s is the static differential magnetic permeability,

$$\mu_s = \frac{dB_{0z}}{dH_{ez}},$$

and ρ_f is the flux-flow resistance,

$$\rho_f = \frac{B\Phi_0}{c^2\eta}.$$

Thus, the experimental value of the surface impedance provides information about the viscosity coefficient η.

We will prove that for a ferromagnetic superconductor a range of parameters exists, where Eq. (3.161) can be applied, if the magnetic viscosity is taken into account: η should be replaced by $\eta + \eta_M$.

First, the applicability conditions of Eq. (3.161) for an ordinary superconductor should be outlined. Within the continuous medium approximation used in [140] an alternating external field $\mathbf{h}_e$ excites a long-wavelength and a short-wavelength mode in the superconductor. For convenience, we will call these modes type-1 and type-2, and denote the z-projections of their wave vectors as k_1 and k_2, respectively. These quantities are explicitly defined by Equation (24) in [140]. To use the simple expression (3.161) for the impedance, three conditions must be fulfilled: (i) $|k_1|\,\lambda \ll 1$, (ii) $|k_1| \ll |k_2|$, and (iii) $|k_2|\,L_z \gg 1$ (L_z is the sample thickness – see Fig. 3.9). According to [140], the conditions (i) and (ii) are satisfied, if

$$\omega \ll \omega_C \equiv \frac{\Phi_0 C_{44}^*}{B_0\lambda^2\eta}, \tag{3.162}$$

where C_{44}^* is an elastic modulus of the vortex lattice. This inequality presents a limitation on the frequency. In the limit $H_{c1} \ll B_0 \ll H_{c2}$ the condition (3.162) can be weakened, namely

$$\omega \ll \omega_B \equiv \frac{\Phi_0 B_0}{4\pi\lambda^2\eta} \qquad (\omega_B \gg \omega_C). \tag{3.163}$$

This follows directly from Equation (22) in [140].

Let us turn to the case of a ferromagnetic superconductor. We will assume the sample is a slab with dimensions L_x, L_y and L_z, where $L_z \ll L_x, L_y$ – see Fig. 3.9. The x-axis,

parallel to the large surface of the sample, is the magnetization easy-axis. In fact, the slab geometry is not a key point, but the equilibrium magnetization must be parallel to one of the sample surfaces. By applying an external field one can provide that the internal field $\mathbf{B}_0$ is parallel to the z-axis. In the slab geometry the components of the demagnetizing tensor are $N_{xx} \approx 0$, $N_{yy} \approx 0$, $N_{zz} \approx 4\pi$. Then, according to Eq. (3.10), if the external field is $\mathbf{H}_e = (-4\pi M, 0, H_{ez})$, the internal field is $\mathbf{B}_0 = (0, 0, H_{ez})$.

When considering the surface impedance of a ferromagnetic superconductor, an additional complication arises due to the presence of new degrees of freedom, which are absent in a conventional superconductor. These are the magnon modes, which can be directly excited by an electromagnetic wave even in the absence of vortices [63, 89] (see also Sec. 3.3.5). However, in the geometry shown in Fig. 3.9 the excitation of these modes can be avoided, as will be demonstrated below.

If the frequency is not too close to the ferromagnetic resonance frequency ($|\omega - \omega_F| / \omega_F \gg K^{-1}$) we can neglect the magnetostatic interaction in the Landau-Lifshitz equation when analyzing the additional magnon-like modes, as has been done in Sec. 3.4.1 (where the term $\mathbf{b}_{Mq}$ has been dropped). Then, in the limit of small dissipation, Eq. (3.13) takes the form

$$\frac{\partial \mathbf{m}}{\partial t} = -\gamma \mathbf{M}_0 \times \left(\alpha \frac{\partial^2 \mathbf{m}}{\partial z^2} - K \mathbf{m} \right). \tag{3.164}$$

Equation (3.164) yields two modes, which will be labeled as type-3 and 4:

$$\begin{gathered} \mathbf{m} = (\mathbf{z}_0 \mp i \mathbf{y}_0) m_{3,4} e^{i k_{3,4} z}, \\ k_3 = L^{-1} \sqrt{\tfrac{\omega}{\omega_F} - 1}, \qquad k_4 = i L^{-1} \sqrt{\tfrac{\omega}{\omega_F} + 1}, \end{gathered} \tag{3.165}$$

where m_3 and m_4 are scalar amplitudes. Note that the effects connected with the band structure of the magnon spectrum (see Sec. 3.3) do not affect the modes 3 and 4, since these magnetization waves propagate along the vortices and do not undergo Bragg scattering on the vortex lattice.

Now suppose that the magnetic field $\mathbf{h}_e$ in the probing electromagnetic wave oscillates along the x-axis, i. e., along the equilibrium magnetization (see Fig. 3.9). It is reasonable to assume that inside the sample the alternating magnetic induction $\langle \mathbf{b} \rangle$, averaged over the xy-plane, is also parallel to the x-axis. It will be shown that this statement is self-consistent. Indeed, for $\langle \mathbf{b} \rangle$ parallel to $\mathbf{M}_0$ we see from Eqs. (3.13) and (3.66) that $\partial \langle \mathbf{m} \rangle / \partial t = 0$. This means that the magnon-like type-3 and 4 modes are not excited. In the type-1 and 2 modes $\langle \mathbf{m} \rangle = 0$, but $\langle \mathbf{b} \rangle \neq 0$. Hence, these modes differ from their analogues in non-magnetic superconductors only by the presence of the magnetic contribution to the viscosity, η_M, which is due to the Fourier-components $\mathbf{m}_q$ with $\mathbf{q} \neq 0$. Then, according to [140], the internal field $\langle \mathbf{b} \rangle$ will be parallel to the probing field $\mathbf{h}_e$ (which follows from the London equation (3.14), if the deformation of the vortex lattice is taken into account). Thus, we have proved the validity of our assumption, having shown in addition that only the type-1 and 2 modes are excited.

Strictly speaking, the effective viscosity for the long-wavelength type-1 mode differs from $\eta + \eta_M$, because the vortices are not straight. However, since $|k_1| \ll \lambda^{-1}$, the radius of curvature of the vortices is sufficiently large to make this difference negligible.

3.4.5 Extension of the results to the case of SF superlattices

In the end of this Chapter let us consider how the results from Secs. 3.4.2 and 3.4.3 can be extended to the case of SF multilayers with vortices oriented perpendicular to the layers – see Fig. 3.6. Here, S and F are an ordinary type-II superconductor and ordinary ferromagnet, respectively. We will assume the period d of the structure to be sufficiently small (see below). Then, the generalization of the results from Secs. 3.4.2 and 3.4.3 is straightforward, if two points are taken into account:

(i) Since the magnetic moments now occupy only a fraction of the sample, the force $\mathbf{f}_M$ is reduced by a factor of d/d'_F, where $d'_F \leq d_F$ is the effective thickness of the ferromagnetic layer. Formally, all expressions for $\mathbf{f}_M$, starting with Eq. (3.101), should be multiplied by d'_F/d. The quantities d'_F and d_F coincide, if the mutual influence of the superconducting and magnetic orders is negligible. However, this is not the case for cuprate/manganite superlattices. Experimental papers report giant superconductivity induced modulation of the magnetization [125] and the suppression of magnetic order in the manganite layer close to the SF interface [126, 127, 128, 129]. In the latter case, $d'_F < d_F$, but both quantities are of the same order of magnitude.

(ii) Due to the fact that the structure is only partially superconducting, the in-plane London penetration depth now equals $\lambda_{\text{eff}} = \lambda(d/d_S)^{1/2}$ (see [141], for example). The expression for the single vortex field

$$h_{qz} \approx \frac{\Phi_0}{4\pi^2(1+q^2\lambda_{\text{eff}}^2)} \tag{3.166}$$

can be used if the period d of the structure is much smaller than the characteristic in-plane length scale of the problem. To apply the results obtained for the case of a constant driving force, we have to demand $d \ll \min(a_v, L)$, according to Sec. 3.4.2. The constraint is somewhat weaker in the case of the harmonic driving current. Indeed, as we have seen in Sec. 3.4.3, the main contribution to $\mathbf{f}_M$ comes from $q \sim L^{-1}\sqrt{|\omega/\omega_F - 1|}$, hence, the limitation on the period of the structure is

$$d \ll \min\left[a_v, L\sqrt{\frac{\omega_F}{|\omega-\omega_F|}}\right].$$

A study of the vortex viscosity in a SFS trilayer has been presented in [138]. In this paper the flux-flow resistivity in Nb/PdNi/Nb structure was measured. It was found that in the presence of the magnetic PdNi layer the flux-flow resistivity in Nb exceeds the Bardeen-Stephen estimate [32], as if the vortex viscosity is reduced by the interaction with magnetic moments. At first sight, this seems to contradict the prediction from the present Chapter. However, this experiment can not be interpreted in the framework of the model used here, since the ferromagnetic alloy PdNi does not possess a well-defined magnetic anisotropy, and the magnon modes can not be characterized by a wave vector $\mathbf{q}$ due to the lack of translational symmetry. Moreover, the dependence of the critical temperature of Nb on the PdNi layer thickness signifies strong influence of the magnetic order on superconductivity. The explanation of the viscosity reduction in the mentioned experiment requires a more complicated microscopic treatment.

3.5 Summary

In the present Chapter different aspects of the interplay between vortices and spin waves in superconductor-ferromagnet hybrids have been analyzed. It has been shown that the magnon spectrum in a ferromagnetic superconductor in the mixed state acquires a Bloch-like band structure. The spectrum has been calculated both analytically and numerically. The band structure changes qualitatively with varying applied field (see Figs. 3.3 and 3.4): as the field is lowered, a complicated structure develops in the center of the first Brillouin zone. This behavior is a consequence of the nonmonotonicity of the spectrum in the Meissner state.

Moving Abrikosov vortices in hybrid SF structures may radiate spin waves, which leads to the appearance of a magnetic contribution $\mathbf{f}_M$ to the damping force acting on the vortices. It has been demonstrated that when the vortices are set in motion by a dc current, either a series of resonances or a step should appear on the I-V curve: the type of the resonant feature depends on the degree of ordering of the vortex lattice. The mentioned effects should be observable in SF superlattices with a relatively low value of the magnon generation threshold velocity $V_{\rm th}$. For the case of a low-amplitude ac driving current, the magnetic contribution η_M to the vortex viscosity has been calculated. This quantity is purely imaginary at $\omega < \omega_F$, signifying that additional dissipation is negligible, but the vortex mass is increased. At $\omega > \omega_F$ magnons are generated, and η_M becomes complex.

Both the vortex-induced gaps in the magnon spectrum and the magnetic viscosity η_M affect the surface impedance Z and microwave reflectivity coefficient of the SF systems. The gaps in the magnon spectrum are best probed in the geometry with the vortices directed parallel to the sample surface – see Fig. 3.5. In this geometry dissipation connected with vortex motion is avoided. On the other hand, to measure the quantity η_M the perpendicular geometry may be used – see Fig. 3.9. Since η_M in the U-based ferromagnetic superconductors is much smaller than the Bardeen-Stephen contribution η, an experiment allowing to detect η_M should involve measurements of Z at different frequencies and applied magnetic fields. The resonant features connected with η_M should emerge on the $Z(\omega)$ or $Z(B_0)$ dependencies.

Generally, the influence of magnetic moments on vortex dynamics is stronger in structures with a lower value of the ferromagnetic resonance frequency. Thus, the mentioned effects may be best observed in SF superlattices with F layers having a small magnetic anisotropy.

Chapter 4

Nonlocal electrodynamics and vortex-vortex attraction in superconductor-ferromagnet hybrids

4.1 Introduction

As has been said in the introduction to the Thesis, the Ginzburg-Landau (GL) theory allows to classify all superconducting materials as either type-I or type-II superconductors, according to their value of their parameter κ. A remarkable feature of type-II compounds is that they support a vortex phase, which is stable due to the vortices always repelling each other. On the contrary, in bulk type-I superconductors vortices are attracted to each other, tending to merge into a single giant vortex. Thus, the GL theory states that in uniform bulk superconductors the vortex-vortex interaction is either purely repulsive (when $\kappa > 1/\sqrt{2}$) or purely attractive ($\kappa < 1/\sqrt{2}$). However, for more than 40 years it has been known that this simple picture is incomplete. It has been found that in materials with $1/\sqrt{2} < \kappa \lesssim 1$ (low-κ superconductors), such as pure Nb, at sufficiently low temperatures the vortex-vortex interaction potential may become attractive at long distances [142, 143, 144, 145] (note that this statement does not contradict the GL theory, which is valid only in the close vicinity of T_c). As a result, the magnetization curve of the superconductor acquires an unstable S-shape [146], and the transition from the Meissner state to the mixed state becomes a first-order phase transition: at the lower critical field vortices enter the superconductor at a finite concentration (see the experimental papers [147, 148] and references in [146, 149]). This phenomenon was coined "type-II/1 superconductivity" [148], as opposed to "type-II/2 superconductivity", which stands for ordinary type-II behavior. Later, analogous effects have been observed in the so-called type-1.5 multiband superconductors [150, 151], where the coherence lengths for Cooper pairs in different bands do not necessary coincide [152, 153].

In some cases the vortex-vortex interaction may be attractive also in high-κ superconductors. At low magnetic fields, $B \ll H_{c2}$, the electrodynamics of these materials, being essentially local, is well described within the London theory. Therefore, the reversal of the magnetic field of a single flux line is a sufficient condition for vortex-vortex attraction [154, 155, 156, 157]. The field reversal indeed occurs in anisotropic non-magnetic [154, 155, 156, 157] and magnetic [158] superconductors at certain orientations of the

vortices. Then, their interaction potential is strongly anisotropic, the vortices penetrate the sample in the form of separated chains [159], and the phase transition at H_{c1} is still of second order.

In the present Chapter a new mechanism of vortex-vortex attraction in SF hybrids is discussed. Here, the attractive interaction may arise due to the spatial dispersion of the magnetic susceptibility, which introduces a non-local relation between the current density $\mathbf{j}$ and the vector potential $\mathbf{A}$. The nonlocality scale here is the Bloch domain wall width L. The nonlocal effects become strongly pronounced when L is of the order of or larger than the London penetration depth λ. Then, the vortex-vortex interaction potential and the phase diagram of the SF system undergo dramatic changes. In particular, the phase transition from the Meissner state to the mixed state will be a first order phase transition.[1]

The Chapter is structured as follows. In Sec. 4.2 the field of an isolated vortex in a SF structure with large L is derived. In Sec. 4.3 the phase diagram of the SF system is discussed. In the final Section 4.4 a summary of the obtained results is given, and some systems suitable for the observation the new effects are proposed.

4.2 The vortex field and vortex-vortex interaction potential in SF hybrids with large L

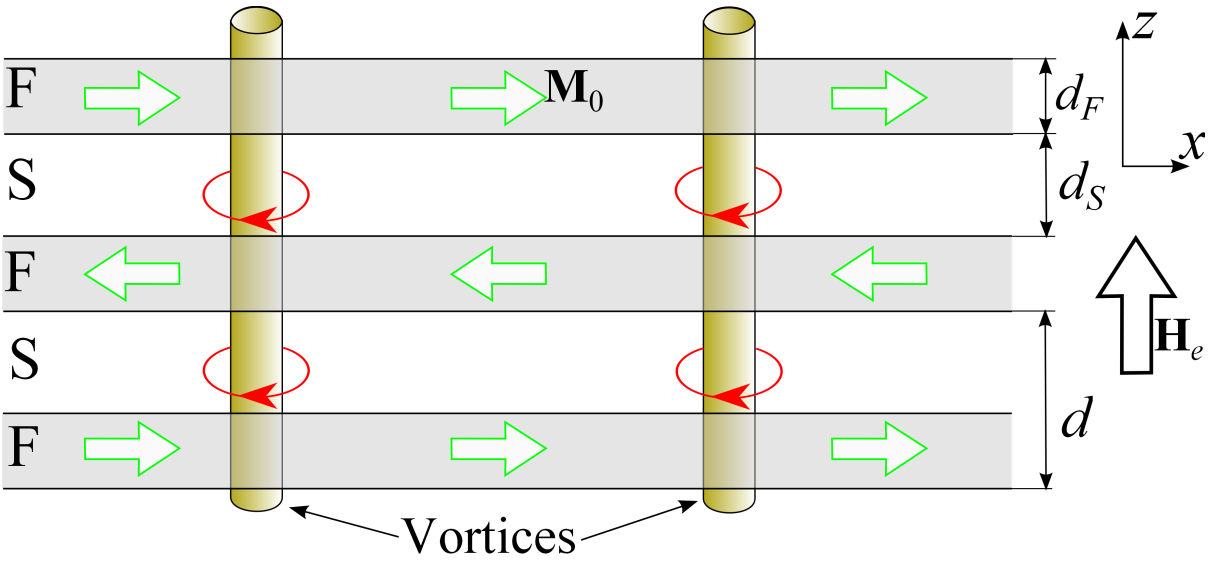

Figure 4.1: A schematic picture of the multilayer system.

First, we will consider an SF multilayer system – see Fig. 4.1. Let the magnetic layers have an easy x-axis magnetocrystalline anisotropy. Like in the previous Chapter, the Josephson current between neighboring S layers will be neglected, so that Josephson vortices do not appear. Such approximation is valid in the case of insulating or sufficiently

[1]The mentioned effects do not take place in the U-based ferromagnetic superconductors, studied in the previous Chapter. In these compounds $L \ll \lambda$, thus, the influence of spatial dispersion on the vortex lattice is negligible

thick F layers, or in the presence of thin oxide interlayers between adjacent S and F layers. Then, within the London approximation Eq. (3.6) may be used for the free energy of the system. Let us rewrite this equation as

$$F = \int \left[\frac{1}{8\pi\lambda_0^2} \left(\mathbf{A} + \frac{\Phi_0}{2\pi} \nabla\theta_S \right)^2 + \frac{(\mathbf{B} - 4\pi\mathbf{M})^2}{8\pi} + \frac{\alpha_0}{2} \left(\frac{\partial \mathbf{M}}{\partial x_i} \frac{\partial \mathbf{M}}{\partial x_i} \right) + \frac{K_0 \mathbf{M}_\perp^2}{2} - \frac{\mathbf{B}\mathbf{H}_e}{4\pi} \right] d^3\mathbf{r}. \tag{4.1}$$

Here and further in this Chapter we will use the notations λ_0, K_0 and α_0 to designate the characteristics of individual layers, while α, K and λ are reserved for averaged characteristics. Note that the superconducting and magnetic terms in Eq. (4.1) are integrated only over the corresponding layers.

In the absence of an external field we may expect that the magnetization vectors in neighboring F layers point in opposite directions, as shown in Fig. 4.1. This configuration minimizes the magnetostatic energy. Then, an external field directed along the z axis (normal to the layers) will induce Abrikosov vortices oriented also along the z-axis (see Fig. 4.1).

Let us make the following transformations:

$$\begin{aligned} \tfrac{(\mathbf{B}-4\pi\mathbf{M})^2}{8\pi} &= \tfrac{B_{M0}^2}{8\pi} + \tfrac{B_v^2}{8\pi} + \tfrac{\mathbf{B}_{M0}\mathbf{B}_v}{4\pi} - \mathbf{B}_v\mathbf{M}_0 - \mathbf{B}_{M0}\mathbf{M}_0 \\ &\quad -\mathbf{B}_{M0}(\mathbf{M}-\mathbf{M}_0) - \mathbf{B}_v(\mathbf{M}-\mathbf{M}_0) + 2\pi M^2, \end{aligned} \tag{4.2}$$

where $\mathbf{M}_0$ is the magnetization in the absence of vortices, $\mathbf{B}_{M0}$ is the magnetic field induced by $\mathbf{M}_0$, $\mathbf{B}_v$ is the magnetic field of the vortices (note that $\mathbf{B} = \mathbf{B}_{M0} + \mathbf{B}_v$). The magnetization modulus M is assumed constant, which is the case when $T \ll \Theta$. Now we will consider the thin-layer limit, when the period of the structure is much smaller than the size of the sample, the London penetration depth and all other in-plane length scales of the problem. Then, the field induced in a magnetic layer by all other layers averages to zero, and $\mathbf{B}_{M0} = 4\pi\mathbf{M}_0$. Like in Chapter 3, we will assume the perpendicular to the easy axis magnetization component $\mathbf{m}$ to be small: $m \ll M$. If we keep in the right-hand side of Eq. (4.2) all terms of the order of m^2 and neglect higher order small terms (e. g., m^4/M^2), bearing in mind that $\mathbf{B}_v$ and $\mathbf{m}$ are of the same order of magnitude we obtain

$$\begin{aligned} \tfrac{(\mathbf{B}-4\pi\mathbf{M})^2}{8\pi} &= \tfrac{(\mathbf{B}_{M0}-4\pi\mathbf{M}_0)^2}{8\pi} + \tfrac{B_v^2}{8\pi} - \mathbf{B}_{M0}(\mathbf{M}-\mathbf{M}_0) - \mathbf{B}_v\mathbf{m} \\ &\approx \tfrac{(\mathbf{B}_{M0}-4\pi\mathbf{M}_0)^2}{8\pi} + \tfrac{B_v^2}{8\pi} + 2\pi m^2 - \mathbf{B}_v\mathbf{m}, \end{aligned} \tag{4.3}$$

since $M_x - M_{0x} \approx -M_{0x}m^2/(2M)$.

In Eq. (4.1) the vector potential and the superconducting phase can be presented as $\mathbf{A} = \mathbf{A}_{M0} + \mathbf{a}$ and $\theta_S = \theta_{M0} + \theta'$, where $\mathbf{A}_{M0}$ and θ_{M0} are induced by $\mathbf{M}_0$, and $\mathbf{a}$ and θ' are connected with the vortices. The field $\mathbf{B}_{M0}$ penetrates the superconducting layers only on the sample edges and does not induce any supercurrents in the bulk, hence, we can put

$$\mathbf{A} + \frac{\Phi_0}{2\pi}\nabla\theta_S = \mathbf{a} + \frac{\Phi_0}{2\pi}\nabla\theta'.$$

Thus, the free energy takes the form

$$\begin{aligned} F = \int \Big[&\tfrac{1}{8\pi\lambda_0^2} \left(\mathbf{a} + \tfrac{\Phi_0}{2\pi}\nabla\theta' \right)^2 + \tfrac{\alpha_0}{2} \left(\tfrac{\partial \mathbf{m}}{\partial x_i} \tfrac{\partial \mathbf{m}}{\partial x_i} \right) + \tfrac{K_0 \mathbf{m}^2}{2} \\ &+ \tfrac{\mathbf{B}_v^2}{8\pi} + 2\pi m^2 - \mathbf{B}_v\mathbf{m} - \tfrac{\mathbf{H}_e\mathbf{B}_v}{4\pi} \Big] d^3\mathbf{r} + F_0, \end{aligned} \tag{4.4}$$

where

$$F_0 = \int \frac{(\mathbf{B}_{M0} - 4\pi\mathbf{M}_0)^2}{8\pi} d^3\mathbf{r} = \text{const}$$

does not depend on the external field and the concentration of vortices.

In the thin layer limit we may rewrite the free energy within the continuous medium approximation. To do this we should multiply the superconducting and magnetic terms by the corresponding filling factors d_S/d and d_F/d, where d_S and d_F are the thicknesses of the superconducting and magnetic layers:

$$F = \int \left[\frac{d_S}{8\pi\lambda_0^2 d} \left(\mathbf{a} + \frac{\Phi_0}{2\pi} \nabla\theta' \right)^2 + \frac{\alpha_0 d_F}{2d} \left(\frac{\partial \mathbf{m}}{\partial x_i} \frac{\partial \mathbf{m}}{\partial x_i} \right) + (K_0 + 4\pi) \frac{d_F \mathbf{m}^2}{2d} + \frac{\mathbf{B}_v^2}{8\pi} - \frac{d_F}{d} \mathbf{B}_v \mathbf{m} - \frac{\mathbf{H}_e \mathbf{B}_v}{4\pi} \right] d^3\mathbf{r} + \text{const}. \tag{4.5}$$

Here, unlike in Eq. (4.4), all terms are integrated over the whole sample. Now if we minimize F with respect to $\mathbf{m}$ we obtain

$$\mathbf{m} = (K_0 + 4\pi - \alpha_0 \nabla^2)^{-1} \mathbf{B}_v, \qquad \text{and}$$

$$F = \int \left[\frac{1}{8\pi\lambda^2} \left(\mathbf{a} + \frac{\Phi_0}{2\pi} \nabla\theta' \right)^2 + \frac{\mathbf{B}_v \hat{\mu}_{zz}^{-1} \mathbf{B}_v}{8\pi} - \frac{\mathbf{B}_v \mathbf{H}_{ec}}{4\pi} \right] d^3\mathbf{r} + \text{const}, \tag{4.6}$$

where $\hat{\mu}_{zz}$ is the permeability operator, given by

$$\hat{\mu}_{zz} = 1 + 4\pi (K - 4\pi - \alpha \nabla^2)^{-1}, \tag{4.7}$$

and

$$\lambda = \lambda_0 \sqrt{d/d_S}, \qquad \alpha = \alpha_0 d/d_F, \qquad K = (K_0 + 4\pi) d/d_F. \tag{4.8}$$

The same expression (4.6) can be derived for a bulk ferromagnetic superconductor. Indeed, in this case the free energy (3.6) can be transformed as follows:

$$F = \int \left[\frac{1}{8\pi\lambda^2} \left(\mathbf{A} + \frac{\Phi_0}{2\pi} \nabla\theta_S \right)^2 + \frac{B^2}{8\pi} - B_x (M_x - M) - B_y m_y - B_z m_z + \frac{\alpha}{2} \left(\frac{\partial \mathbf{m}}{\partial x_i} \frac{\partial \mathbf{m}}{\partial x_i} \right) + \frac{K \mathbf{m}^2}{2} - \frac{\mathbf{B}(\mathbf{H}_e + 4\pi\mathbf{M}_0)}{4\pi} \right] d^3\mathbf{r} + \text{const}. \tag{4.9}$$

It can be seen that the magnetization $\mathbf{M}_0$ (which is now directed in the $+x$ direction in the whole sample) acts as an external field, which leads to the emergence of a spontaneous mixed state in ferromagnetic superconductors with the vortices directed along $\mathbf{M}_0$. This situation is not very interesting, since the spatial dispersion does not matter when the magnetic field is parallel to $\mathbf{M}_0$. The influence of the spontaneous magnetization can be compensated by an external field directed in the $-x$ direction. If the sample has a vanishing demagnetizing factor N_{xx}, the compensating field $\mathbf{H}_{ec}$ simply equals $-4\pi\mathbf{M}_0$. Let us substitute $\mathbf{H}_e = \mathbf{H}_{ec} + \mathbf{H}'_e$ into Eq. (4.9), where $\mathbf{H}'_e$ is directed along the z-axis:

$$F = \int \left[\frac{1}{8\pi\lambda^2} \left(\mathbf{A} + \frac{\Phi_0}{2\pi} \nabla\theta_S \right)^2 + \frac{B^2}{8\pi} + \frac{B_x m^2}{2M} - B_y m_y - B_z m_z + \frac{\alpha}{2} \left(\frac{\partial \mathbf{m}}{\partial x_i} \frac{\partial \mathbf{m}}{\partial x_i} \right) + \frac{K \mathbf{m}^2}{2} - \frac{\mathbf{B}\mathbf{H}'_e}{4\pi} \right] d^3\mathbf{r} + \text{const}. \tag{4.10}$$

From this relation it follows that in equilibrium the component B_x is of the order of or smaller than m^2/M, hence, the term containing $B_x m^2$ is much smaller than m^2, and it can be neglected. After the minimization of F with respect to $\mathbf{m}$ we arrive at Eqs. (4.6) and (4.7) with $\mathbf{H}'_e$ in place of $\mathbf{H}_e$. Thus, we may analyze FS superlattices with thin layers and ferromagnetic superconductors on a common basis.

It should be noted that when $K < 4\pi$ the state with $\mathbf{M} = M\mathbf{x}_0$ in a ferromagnetic superconductor becomes unstable: the compensating external field flips the magnetization vector. In a SF superlattice with K given by Eq. (4.8) the situation $K < 4\pi$ is formally impossible. Further we will assume that $K > 4\pi$.

Let us determine the magnetic field of a single vortex, directed along the z-axis. The minimization of F with respect to $\mathbf{a}$ gives the London equation,

$$i\mathbf{q} \times \mathbf{B}_{vq} = -\mathbf{q} \times (\mathbf{q} \times \mathbf{a}_q) = -\frac{1}{\lambda^2}\mu_{zz}(q)\left[\mathbf{a}_q + \frac{\Phi_0}{2\pi}\nabla\theta'_q\right], \tag{4.11}$$

where $\mathbf{B}_{vq}$, $\mathbf{a}_q$ and $\nabla\theta'_q$ are the 2D Fourier transforms of $\mathbf{B}_v$, $\mathbf{a}$ and $\nabla\theta'$, and

$$\mu_{zz}(q) = 1 + \frac{4\pi}{K - 4\pi + \alpha q^2}. \tag{4.12}$$

The second term in the right-hand side is responsible for the nonlocal electrodynamics generated by the magnetic subsystem (note that this term formally reminds the kernel proposed by Dichtel [160] for low-κ superconductors). Using Eqs. (4.11) and (4.12) it is easy to determine Fourier-transformed magnetic induction B_{qz} of an isolated vortes, which can be presented in the form

$$B_{qz} = \frac{\Phi_0}{4\pi^2\lambda^2 L^2(q_2^2 - q_1^2)}\left[\frac{1 - L^2q_1^2}{q^2 + q_1^2} - \frac{1 - L^2q_2^2}{q^2 + q_2^2}\right], \tag{4.13}$$

where

$$q_{1,2}^2 = \frac{\alpha + \lambda^2 K - 4\pi\lambda^2 \pm \sqrt{(\alpha + \lambda^2 K - 4\pi\lambda^2)^2 - 4K\lambda^2\alpha}}{2\lambda^2\alpha}, \tag{4.14}$$

and $L = \sqrt{\alpha/K}$, which coincides with the Bloch domain wall width in the case of a ferromagnetic superconductor. If we recall that in an ordinary vortex

$$B_{qz} = \frac{\Phi_0}{4\pi^2(1 + \lambda^2 q^2)}, \qquad B_z = \frac{\Phi_0}{2\pi\lambda^2}\mathrm{K}_0\left(\frac{\rho}{\lambda}\right),$$

we can easily perform the inverse Fourier transform of Eq. (4.13):

$$B_z = \frac{\Phi_0}{2\pi\lambda^2 L^2(q_2^2 - q_1^2)}\left[(1 - L^2q_1^2)\mathrm{K}_0(q_1\rho) - (1 - L^2q_2^2)\mathrm{K}_0(q_2\rho)\right]. \tag{4.15}$$

The field $\mathbf{H} \equiv \hat{\mu}^{-1}\mathbf{B}$ can be calculated in a similar way:

$$H_z = \frac{\Phi_0}{2\pi\lambda^2 L^2(q_2^2 - q_1^2)}\left[(1 - 4\pi K^{-1} - L^2q_1^2)\mathrm{K}_0(q_1\rho) - (1 - 4\pi K^{-1} - L^2q_2^2)\mathrm{K}_0(q_2\rho)\right]. \tag{4.16}$$

An interesting fact is that the quantities q_1 and q_2 become complex when $L_{\min} < L < L_{\max}$, where

$$L_{\min,\max} = \lambda[1 \mp \sqrt{4\pi K^{-1}}]. \tag{4.17}$$

Then, both B_z and H_z exhibit damped spatial oscillations. The situation resembles the behavior predicted by Eilenberger [161] and Dichtel [160] for low-κ superconductors. However, at $L > L_{\max}$ the oscillations disappear: the fields change their sign once, remaining negative at $\rho \to \infty$. Some graphs of $B_z(\rho)$ and $H_z(\rho)$ are shown in Fig. 4.2.

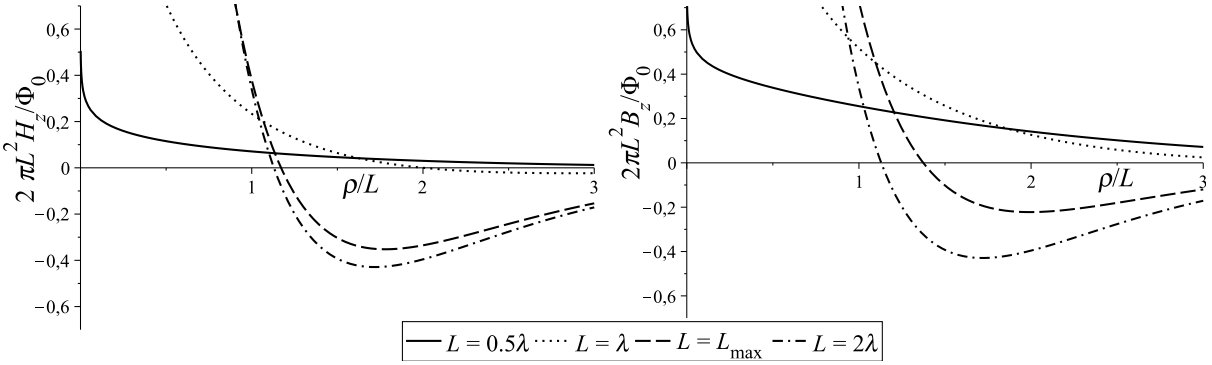

Figure 4.2: The H-field and magnetic induction profiles of a single vortex at different temperatures T, corresponding to different values of the ratio $L/\lambda(T)$. $\mu_{zz}(0) = 5$. In linear scale graphs only one oscillation of the vortex fields can be seen because the oscillation amplitude decays very rapidly with ρ.

Using Eq. (4.8), the vortex field sign revesal condition for a SF superlattice can be written as

$$L_0 > \lambda_0 \sqrt{\frac{d}{d_S}} \left[\sqrt{1 + \frac{4\pi}{K_0}} - \sqrt{\frac{4\pi d_F}{dK_0}} \right], \tag{4.18}$$

where $L_0 = \sqrt{\alpha_0/K_0}$.

4.3 The mixed state

Let us consider the case of a finite concentration of vortices. If the sample has a vanishing demagnetizing factor N_{zz}, the free energy of the system at $\mathbf{H}_e = 0$ ($\mathbf{H}'_e = 0$ in the case of a ferromagnetic superconductor) is

$$F = \int \frac{\boldsymbol{\kappa}\mathbf{H}_v}{8\pi} d^3\mathbf{r} + \text{const}, \tag{4.19}$$

where $\boldsymbol{\kappa} = -\Phi_0 \operatorname{rot} \nabla\theta_S/(2\pi)$ is the vorticity, and $\mathbf{H}_v \equiv \mu_{zz}^{-1}\mathbf{B}_v$. The relation (4.19) can be derived from Eq. (4.6) and the London equation, written in the form

$$\operatorname{rot} \mathbf{H}_v = -\lambda^{-2} \left(\mathbf{a} + \frac{\Phi_0}{2\pi} \nabla\theta' \right).$$

It follows from Eq. (4.19) that the vortex-vortex interaction potential is proportional to the H-field of an isolated vortex. Thus, the sign change of $H_z(\rho)$ in Eq. (4.16) (or, more

precisely, the sign change of its derivative) leads to the attraction of vortices. In our case the unusual behavior of the vortex field is a consequence of the strong spatial dispersion of $\hat{\mu}_{zz}$, unlike in [154, 155, 156, 157, 158], where the sign reversal appeared due to the anisotropy. In [69] it has been erroneously claimed that a large value of μ_{zz} is sufficient for the attraction of vortices, so that the dispersion is not required. Indeed, if we put $\alpha = 0$ in Eq. (4.12), we obtain a simple renormalization of λ, which is a well-known fact [51] and does not lead to any field reversal. Still, the numerical simulations presented in [69] revealed the clusterization of vortices, apparently connected with the dispersion of the permeability, which has been actually included in the model. This fact is in good accordance with the analysis given in the present Chapter.

To determine the equilibrium state of a system containing many vortices, some numerical simulations were performed. The relaxation to equilibrium of 800 vortices, confined in a box with rigid walls, was modeled. The relaxation process was governed by the equations

$$\eta \frac{d\mathbf{R}_i}{dt} = -\frac{\partial F}{\partial \mathbf{R}_i}, \tag{4.20}$$

where $\mathbf{R}_i$ is the position of the i-th vortex, and η is an arbitrary positive viscosity coefficient. This algorithm allows to find a local minimum of the free energy. The relaxation was stopped when all derivatives $d\mathbf{R}_i/dt$ became sufficiently small. Some final vortex configurations are shown in Fig. 4.3. The parameters K, L and λ were chosen so that the vortex field oscillations were present. In this respect the calculations presented here differ from those given in [162, 163, 164, 165, 166], where a non-oscillating attractive potential was used to study the vortex structures in multiband superconductors. However, the obtained pictures are similar to those given in the mentioned papers. Generally, we can observe either a uniform hexagonal vortex state with several defects (Fig. 4.3a and b) or vortex clusters with a regular internal hexagonal structure (Fig. 4.3c-f). No traces of square configurations have been found, even when other parameters were used. Relying on this observation, the magnetization curves of the SF system with $N_{zz} = 0$ were calculated, assuming that the vortex lattice is triangular. The internal field component B_{0z} satisfies the relation

$$H_{ez} = 4\pi V^{-1} \partial F / \partial B_{0z}, \tag{4.21}$$

Several B_{0z} vs. H_{ez} curves for different temperatures T are shown in Fig. 4.4a. For $L > L_{\min}$ the curves are S-shaped, having an unstable part at low B_0 (note the similarity with Klein's result [146] for low-κ superconductors). This means that the phase transition at H_{c1} is of first order. The jump of B_0 at H_{c1} is obtained by means of a Maxwell construction. We can also extract the metastable regions from the magnetization curves. In particular, the vortex state may exist at fields down to the overcooling field H_{c1m}, corresponding to a minimum of $H_{ez}(B_0)$ — see Fig. 4.4a. If the surface barrier for the vortices is absent, the overheating field for the Meissner state is $H_{c10} = H_{ez}(0) = 4\pi f_v/\Phi_0$, where f_v is the energy per unit length of an isolated vortex. The low-field phase diagram is shown in Fig. 4.4b. Here, it is assumed that $H_{c10} \sim \lambda^{-2}(T)$, and T_c is well below the Curie temperature, so that L and K are constants. The $\lambda(T)$ dependence has been taken from a textbook [6]. The first order phase transition appears below some critical temperature $T_{\rm cr}$, which is determined from the condition $L = L_{\min}(T_{\rm cr})$. Thus, by changing the temperature we can switch between type II/2 and type II/1 behavior.

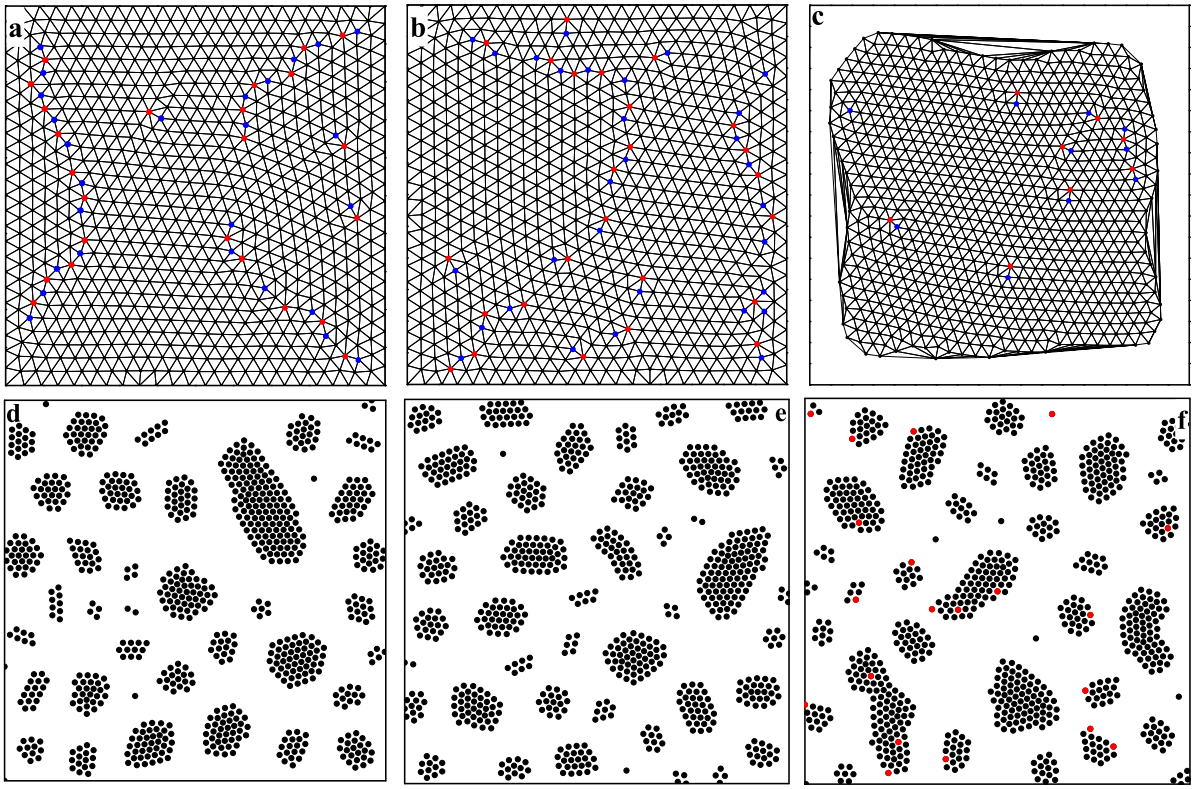

Figure 4.3: (a)-(c) Delaunay triangulations of vortex configurations in a ferromagnetic superconductors with $\mu_{zz}(0) = K/(K - 4\pi) \gg 1$ and $L\mu_{zz}(0)/\lambda = 2$. The size of the box is (a) $50\lambda' \times 50\lambda'$, (b) $60\lambda' \times 60\lambda'$, and (c) $90\lambda' \times 90\lambda'$, where $\lambda' = \sqrt{L\lambda}$. The fivefold- and sevenfold-coordinated vortices, forming lattice dislocations, are marked as blue and red points, respectively. (d),(e) Two realizations of a metastable state with different (random) initial conditions. The dots denote vortices. Note that the configurations with many clusters do not correspond to the absolute minimum of the free energy. (f) Metastable configuration with 20 pinned (fixed) vortices, marked as red dots. In (d)-(f) the size of the box is $150\lambda' \times 150\lambda'$.

Experimentally vortex structures are usually observed in films with the external field applied perpendicular to the film. In this geometry $N_{zz} \approx 4\pi$, and $B_{0z} \approx H_{ez}$, so that the average vortex density is fixed. In a film of a ferromagnetic superconductor with a thickness $l_z \gg \lambda$ the vortex-vortex interaction remains attractive at intermediate distances, acquiring a long-range repulsive tail due to the unscreened magnetostatic interaction through the free space. Then, an intermediate mixed state with coexisting vortex and Meissner phase domains should occur [149]. The equilibrium magnetic field in the vortex phase domains equals $B_{0z}(H_{c1})$, which is obtained by minimizing the free energy per vortex. Hence, the fraction of the sample volume occupied by the mixed state is $H_{ez}/B_{0z}(H_{c1})$.

Generally, in the intermediate mixed state a superconductor may exhibit rather diverse domain structures, depending on the experimental conditions [149]. To estimate the characteristic size D of the vortex domains we will assume that the pattern has a stripe structure, as shown in Fig. 4.5. Let us consider the free energy F_a per unit area of the film

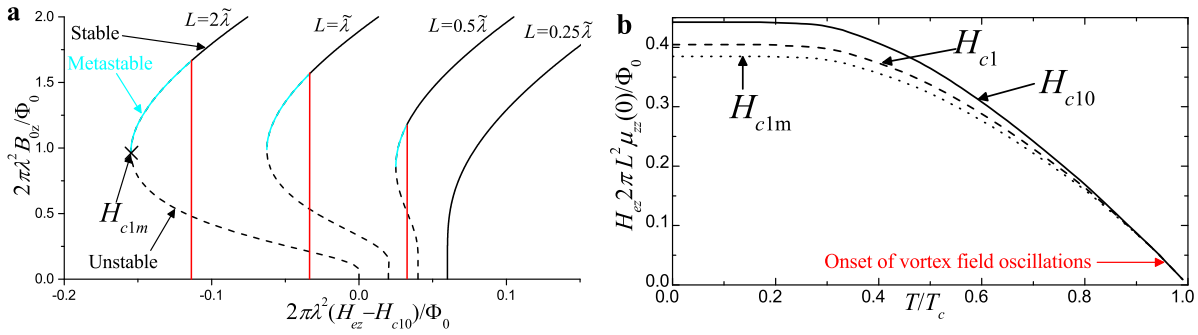

Figure 4.4: (a) The B_{0z} vs. H_{ez} dependencies [Eq. (4.21)] at low fields ($H_{ez} \ll H_{c2}$) and $\mu_{zz}(0) = 4$ ($L_{\min} = 0.268\tilde{\lambda}$, where $\tilde{\lambda} = \lambda\mu_{zz}(0)^{-1/2}$ is the renormalized London penetration depth [51]). The curves are indented for better visual separation. The jump of B_{0z} at H_{c1} is marked as a red line. (b) The low-field phase diagram of a ferromagnetic superconductor, or SF superlattice with $\mu_{zz}(0) = 10$ and $\tilde{\lambda}(T = 0) = L$.

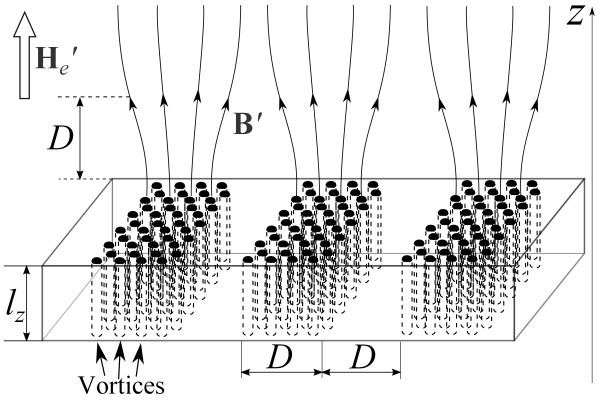

Figure 4.5: A schematic picture of the stripe domain structure in the intermediate mixed state of a SF hybrid system at $H_{ez} \approx B_{0z}(H_{c1})/2$. The field lines for $\mathbf{B}' = \mathbf{B} - \mathbf{H}_{ec}$ are shown.

at $H_{ez} \approx B_{0z}(H_{c1})/2$, when a half of the sample is in the mixed state. The contribution to F_a from the mixed / Meissner state interfaces equals $\sigma_s l_z/D$, where σ_s is the surface tension energy per unit area of the interface. Another contribution to F_a originates from the magnetostatic energy concentrated in the regions with a thickness of the order of D above and below the film, where the magnetic field is considerably inhomogeneous – see Fig. 4.5. Hence,

$$F_a = \tilde{C}(D)B_{0z}^2(H_{c1})D + \sigma_s l_z/D + \text{const}, \tag{4.22}$$

where $\tilde{C}(D)$ is a function of the order of unity, weakly depending on D. The minimization of F_a with respect to D yields $D \propto \sqrt{l_z}$, which resembles the behavior of the magnetic domains size in a ferromagnetic slab [92]. This estimate is valid when D is much larger than the inter-vortex distance: $D \gg \sqrt{\Phi_0/B_{0z}(H_{c1})}$.

4.4 Summary and proposals for experiments

In this Chapter, using the London theory, it has been demonstrated that in a high-κ SF systems with a large domain wall width L the superconducting electrodynamics becomes strongly nonlocal. Then, the magnetic field of a single vortex may change its sign, and even exhibit spatial oscillations. These peculiarities of the vortex field may be detected using muon spin rotation [167]. The sign reversal of the vortex field leads to mutual attraction of vortices at certain distances. As a result, the transition from the Meissner state to the mixed state becomes a first order phase transition. Such unusual type-II/1 behavior should appear at sufficiently low temperatures, when $L \lesssim \lambda$, while in the vicinity of T_c (when $\lambda \gg L$) ordinary type-II/2 behavior is expected (see the phase diagram in Fig. 4.4b). In a sample in the form of a slab, if the vortex-vortex attraction condition $L > L_{\min}$ is satisfied, an intermediate mixed state should emerge. This state may be visualized using the Bitter decoration technique [149]. The described effects are quite unexpected in high-κ materials.

Let us discuss particular systems, where the predicted effects may take place. The U-based ferromagnetic superconductors [55, 56, 57] possess a rather strong magnetocrystalline anisotropy, and their domain wall thickness is very small, so the vortex attraction condition, $L > L_{\min}$, can not be satisfied. Reliable data on the anisotropy of $EuFe_2As_2$ [59] are not available to date. The usage of SF superlattices provides much more freedom in manipulating the parameters, as we can select from a larger set of materials and choose appropriate thicknesses d_S and d_F. To satisfy Eq. (4.18), a ferromagnet with a large value of L_0 is required, such as yttrium iron garnet [168] or permalloy [169], both having $L_0 \gtrsim 100$ nm. As the superconducting material, niobium may be used ($\lambda_0 \lesssim 100$ nm), which typically has a large parameter κ due to impurities, when prepared as a thin film [170].

Conclusion

The Thesis has been aimed at the solution of several theoretical problems concerning vortex matter in superconducting systems. These problems include the calculation of the dynamic response of vortices in magnetic and nonmagnetic superconductors, the determination of the vortex pinning potential, and the study of the vortex-vortex interaction in superconductor-ferromagnet hybrids. Though considerations in this Thesis were based on phenomenological theories (London, Ginzburg-Landau (GL) and Landau-Lifshitz-Gilbert equations), both qualitative and quantitative predictions given here may be checked experimentally. The main obtained results are summarized below:

- Within the GL theory, a new approach for the calculation of the vortex pinning potential on a small cylindrical insulating defect has been developed. It has been shown that the shape of the potential well for a single vortex can be determined by solving a linear problem (Eqs. (1.27) and (1.28)) instead of the complicated GL equation. The exact pinning potential for a defect with an elliptic cross-section has been determined. It appears that the width of the potential well, even in the case of a very small defect, is of the order of the coherence length ξ. Due to this, at low currents a bound state should exist, where the vortex center is located outside the defect, but the vortex remains pinned. This state may be detected using scanning tunneling microscopy or a nano-SQUID [79].

- Using the exact order parameter profile of a vortex, the vortex viscosity tensor $\hat{\eta}$ has been calculated both numerically and analytically for a superconductor with a Cooper pair mass-normal conductivity anisotropy mismatch ($m_c\sigma_c/m_{ab}\sigma_{ab} \neq 1$). It has been predicted that the flux-flow conductivity anisotropy may depend considerably on temperature even in the close vicinity of T_c. These results may be useful for the interpretation of experimental data on the resistivity of the strongly anisotropic Fe-based and cuprate superconductors.

- It has been demonstrated that the magnon spectrum of a ferromagnetic superconductor in the mixed state has a Bloch-like band structure. The specrum was calculated analytically and numerically. The gaps in the magnon spectrum can be probed by measuring the surface impedance of the sample.

- In Sec. 3.4, the magnetic moment induced force $\mathbf{f}_M$, acting on moving vortices in hybrid SF structures has been calculated in the cases of a dc and ac driving force, and for both a perfect and disordered vortex lattice. When vortices radiate magnons, the force $\mathbf{f}_M$ is enhanced. As a result, certain resonant features should appear on the I-V curve of the sample and on the surface impedance vs. frequency and magnetic field dependencies.

- It has been shown that in SF systems with a large domain wall width $L \gtrsim \lambda$ the magnetic structure of vortices is significantly modified. In particular, the field of a single vortex may change its sign, which may be confirmed experimentally using the muon spin rotation technique [167]. The sign reversal of the vortex field results in attractive interaction between vortices and a first order phase transition from the Meissner to the mixed state. A consequence of this is the formation of an intermediate mixed state in a slab (see Fig. 4.5). Then, the vortex phase domains may be visualized using Bitter decoration.

Still, many questions remain open for future work. For example, it would be interesting to develop a method for the vortex viscosity calculation at lower temperatures, where the time dependent Ginzburg-Landau theory is not applicable. A microscopic calculation of the vortex pinning potential on a columnar defect would be also very useful. Concerning the interaction between vortices and magnetic moments in SF structures, there is much room for the improvement of the model. In ferromagnetic superconductors, the influence of the alternating exchange field on the superconducting properties may be taken into account. In addition, some limitations in Chapters 3 and 4 may be lifted by using the Ginzburg-Landau theory (or a more complicated microscopic approach), allowing to obtain a correct description on length scales of the order of ξ. Hopefully, for such future research the present Thesis will serve as a source of objectives and a comparative example.

Appendix A

An estimate of the contribution of $\psi_1^{(i)}$ to the integral in Eq. (1.21)

In this appendix we will demonstrate that the contribution from the function $\psi_1^{(i)}$ (see (1.24)) to the pinning force is negligible. It is sufficient to prove that the absolute value of the integral

$$I = \int_{\partial S} \left(\psi_1^{(i)} \nabla \psi_d^*(0) + \psi_1^{(i)*} \nabla \psi_d(0) \right) \mathbf{n} d\ell$$

is much smaller than $n_0 D^2/\xi^3$.

The function $\psi_1^{(i)}$ has the following properties:

$$\nabla \psi_1^{(i)} \mathbf{n} \Big|_{\partial S} \approx 0, \qquad \nabla^2 \psi_1^{(i)} = 0, \quad \text{when} \quad \rho < \rho_0, \tag{A1}$$

where ρ_0 is a quantity of the order of the coherence length. Let us introduce an auxiliary function v defined by the relations

$$\nabla^2 v = 0, \qquad \mathbf{n} \nabla v \Big|_{\partial S} = \xi \mathbf{n} \nabla \psi_d^*(0), \qquad v \Big|_{\rho \to \infty} = 0.$$

The properties of this function are identical to those of $\psi_1^{(d)}$: it is of the order of $\sqrt{n_0} D \xi^{-1}$ at the defect border and decays like ρ^{-1} at infinity. For a smooth defect $v \sim \sqrt{n_0} D^2/(\xi\rho)$. Now we make some simple calculations:

$$0 = \int_{\rho \notin S,\, \rho < \rho_0} \left(\psi_1^{(\mathrm{i})} \nabla^2 v - v \nabla^2 \psi_1^{(\mathrm{i})} \right) d^2 \boldsymbol{\rho} = - \int_{\partial S} \psi_1^{(\mathrm{i})} \nabla v \, \mathbf{n} d\ell + \int_{\rho = \rho_0} \left(\psi_1^{(\mathrm{i})} \frac{\partial v}{\partial \rho} - v \frac{\partial \psi_1^{(\mathrm{i})}}{\partial \rho} \right) d\ell.$$

Since $\psi_1^{(\mathrm{i})} \approx \psi_1$ when $\rho \sim \rho_0$,

$$I = \xi^{-1} \int_{\rho = \rho_0} \left(\psi_1 \frac{\partial v}{\partial \rho} - v \frac{\partial \psi_1}{\partial \rho} \right) d\ell + c.c., \tag{A2}$$

where *c.c.* denotes the complex conjugate. According to statement (B) from Sec. 1.2.1, when $\rho = \rho_0$, $|\psi_1| \ll \sqrt{n_0}$, and $|\partial \psi_1/\partial \rho| \ll \sqrt{n_0}/\xi$, since the characteristic length scale is ξ. Then it follows immediately from Eq. (A2) that $|I| \ll n_0 D^2/\xi^3$.

Appendix B

Derivation of the force balance equation (5) and of some general expressions for the viscosity tensor

In this appendix the relations (2.7), (2.8), (2.12) and (2.13) are derived. In Eqs. (2.1) and (2.2) it is convenient to make a scaling of the variables: $x' = x(m(\varphi_0)/m_{ab})^{1/2}$, $y' = y$, $z' = z$, where $m(\varphi_0)$ is given by Eq. (2.6). We rewrite Eq. (2.1) in the form

$$\Gamma\,\hbar\frac{\partial\,|\psi|}{\partial t} = \frac{\hbar^2}{2m_{ab}}\left[\nabla'^2\,|\psi| - |\psi|\,(\nabla'\theta_S)^2\right] - a_{GL}\,|\psi| - b_{GL}\,|\psi|^3\,, \tag{B1}$$

$$\Gamma\,|\psi|^2\left(\hbar\frac{\partial\theta_S}{\partial t} - 2e\Phi\right) = \frac{\hbar^2}{2m_{ab}}\nabla'(|\psi|^2\,\nabla'\theta). \tag{B2}$$

According to Eq. (2.3), the two-dimensional current $\mathbf{j}' = (j_x[m(\varphi_0)/m_{ab}]^{1/2}, j_y)$ satisfies the relation

$$\mathrm{div}'\mathbf{j}' = 0. \tag{B3}$$

Here we left only the linear with respect to $\mathbf{V}_L$ term. The derivative $\partial\rho_e/\partial t$ is proportional to V_L^2, since in a static vortex $\rho_e = 0$. It follows from Eqs. (B2) and (B3) that

$$\Gamma\,|\psi|^2\left(\hbar\frac{\partial\theta_S}{\partial t} - 2e\Phi\right) = -\frac{\hbar}{4e}\nabla'\left(\tilde{\sigma}_n\nabla'\Phi\right), \tag{B4}$$

where we introduced the tensor $\tilde{\sigma}_n$ with components

$$\tilde{\sigma}_{nx'x'} = s(\varphi_0)\sigma_{ab}, \quad \tilde{\sigma}_{ny'y'} = \sigma_{ab},$$
$$\tilde{\sigma}_{nx'y'} = \tilde{\sigma}_{ny'x'} = 0. \tag{B5}$$

The parameter $s(\varphi_0)$ is given by Eq. (2.14). For a moving vortex one should search the solution of Eqs. (B1), (B2) and (B3) in the form $\psi = \psi(\boldsymbol{\rho'} - \tilde{\mathbf{V}}_L t)$, $\Phi = \Phi(\boldsymbol{\rho'} - \tilde{\mathbf{V}}_L t)$, where $\tilde{\mathbf{V}}_\mathbf{L} = (V_{Lx}[m(\varphi_0)/m_{ab}]^{1/2},\ V_{Ly})$ and $\boldsymbol{\rho'} = (x', y')$. We expand $|\psi|$ and θ_S in powers of V_L up to the first order term, assuming the vortex velocity to be sufficiently small:

$$|\psi| \approx \Psi_0(\boldsymbol{\rho'} - \tilde{\mathbf{V}}_L t) + \Psi_1(\boldsymbol{\rho'} - \tilde{\mathbf{V}}_L t), \tag{B6}$$

$$\theta_S \approx \theta_0(\boldsymbol{\rho'} - \tilde{\mathbf{V}}_L t) + \theta_1(\boldsymbol{\rho'} - \tilde{\mathbf{V}}_L t). \tag{B7}$$

Here $\Psi_0(\boldsymbol{\rho'})$ and $\theta_0(\boldsymbol{\rho'})$ correspond to a static vortex. The functions Ψ_1, θ_1 and Φ are of the order V_L. We substitute (B6) and (B7) into Eqs. (B1), (B3) and (B4):

$$-\,a_{GL}\Psi_0 - b_{GL}\Psi_0^3 + \frac{\hbar^2}{2m_{ab}}\left[\nabla'^2\Psi_0 - \Psi_0(\nabla'\theta_0)^2\right] = 0, \tag{B8}$$

$$\frac{\hbar^2}{2m_{ab}}\left[\nabla'^2\Psi_1-\Psi_1(\nabla'\theta_0)^2-2\Psi_0\nabla'\theta_0\cdot\nabla'\theta_1\right]-a_{GL}\Psi_1-3b_{GL}\Psi_0^2\Psi_1=-\Gamma\hbar(\tilde{\mathbf{V}}_L\nabla')\Psi_0 \tag{B9}$$

$$\mathrm{div}'\mathbf{j}_0'=0,\qquad \mathbf{j}_0'=-\frac{2e\,\hbar\Psi_0^2}{m_{ab}}\nabla'\theta_0, \tag{B10}$$

$$\begin{gathered}\mathrm{div}'\mathbf{j}_1'=0,\\ \mathbf{j}_1'=-\tfrac{2e\,\hbar}{m_{ab}}\left(2\Psi_0\Psi_1\nabla'\theta_0+\Psi_0^2\nabla'\theta_1\right)-\tilde{\sigma}_n\nabla'\Phi,\end{gathered} \tag{B11}$$

$$\frac{\hbar\sigma_{ab}}{4e}\left[s(\varphi_0)\frac{\partial^2\Phi}{\partial x'^2}+\frac{\partial^2\Phi}{\partial y'^2}\right]=\Gamma\Psi_0^2\left(2e\Phi+\hbar\tilde{\mathbf{V}}_{\mathbf{L}}\cdot\nabla'\theta_0\right). \tag{B12}$$

Now we introduce some new notations: $\Psi_d=(\mathbf{d}\nabla')\Psi_0$, $\theta_d=(\mathbf{d}\nabla')\theta_0$, $\mathbf{j}_d'=(\mathbf{d}\nabla')\mathbf{j}_0'$, where $\mathbf{d}$ is an arbitrary vector. A simple equation connecting Ψ_d and θ_d can be obtained by applying the operator $\mathbf{d}\nabla'$ to Eq. (B8):

$$\frac{\hbar^2}{2m_{ab}}\left[\nabla'^2\Psi_d-\Psi_d(\nabla'\theta_0)^2-2\Psi_0\nabla'\theta_0\cdot\nabla'\theta_d\right]-a_{GL}\Psi_d-3b_{GL}\Psi_0^2\Psi_d=0. \tag{B13}$$

The vector $\mathbf{j}_d'$ satisfies the obvious relation $\mathrm{div}'\mathbf{j}_d'=0$. Let us multiply Eq. (B9) by Ψ_d, subtract Eq. (B13) multiplied by ψ_1 and integrate the resulting equation over a large volume containing the whole vortex. After some simple algebra and integration by parts we obtain

$$\begin{aligned}-\Gamma\hbar\textstyle\int(\tilde{\mathbf{V}}_L\nabla')\Psi_0\Psi_d d^3\mathbf{r}' &= -\tfrac{\hbar}{4e}\textstyle\int\left[(\mathbf{j}_1'+\tilde{\sigma}_n\nabla'\Phi)\nabla'\theta_d-\mathbf{j}_d'\nabla'\theta_1\right]d^3\mathbf{r}'\\ &= -\tfrac{\hbar}{4e}\textstyle\int(\tilde{\sigma}_n\nabla'\Phi)\nabla'\theta_d d^3\mathbf{r}'-\tfrac{\hbar}{4e}\int_S(\mathbf{j}_1'\theta_d-\mathbf{j}_d'\theta_1)d\mathbf{S}.\end{aligned} \tag{B14}$$

Here S is a surface far from the vortex axis. At large distances $\rho'\gg\xi_{ab}$ we have

$$\mathbf{j}_1'\approx-\frac{2e\hbar\,|a_{GL}|}{b_{GL}m_{ab}}\nabla'\theta_1=\mathbf{j}_{\mathrm{tr}}',\quad \theta_1=-\frac{b_{GL}m_{ab}}{2e\hbar\,|a_{GL}|}(\mathbf{j}_{\mathrm{tr}}'\cdot\boldsymbol{\rho}')+\mathrm{const},$$

where $\mathbf{j}_{\mathrm{tr}}'$ is the transport current density which is constant. If we calculate the surface integral in Eq. (B14) and make some simple transformations, we obtain the force balance equation [40]

$$\frac{\pi\hbar}{e}\mathbf{d}(\mathbf{j}_{\mathrm{tr}}'\times\mathbf{z}_0)=2\pi\Gamma\hbar(\mathbf{d}\tilde{\mathbf{V}}_L)\int_0^\infty\left(\frac{d\Psi_0}{d\rho}\right)^2\rho\,d\rho+\frac{\hbar\sigma_{ab}}{2e}\int\left[s(\varphi_0)\frac{\partial^2\Phi}{\partial x'^2}+\frac{\partial^2\Phi}{\partial y'^2}\right](\mathbf{d}\nabla'\theta_0)d^2\boldsymbol{\rho}'. \tag{B15}$$

If we compare Eqs. (5) and (B15), we can see that the viscous drag tensor in the frame (x',y',z') should be defined as follows:

$$\mathbf{d}\cdot\hat{\eta}'\tilde{\mathbf{V}}_L=2\pi\Gamma\,\hbar(\mathbf{d}\tilde{\mathbf{V}}_L)\frac{|a_{GL}|}{b_{GL}}\int_0^\infty\left(\frac{df}{d\rho}\right)^2\rho d\rho+\frac{\hbar\sigma_{ab}}{2e}\int\left[s(\varphi_0)\frac{\partial^2\Phi}{\partial x'^2}+\frac{\partial^2\Phi}{\partial y'^2}\right](\mathbf{d}\nabla'\theta_0)d^2\boldsymbol{\rho}', \tag{B16}$$

where

$$f(\rho)\equiv\Psi_0(\rho\xi_{ab})\sqrt{\frac{b_{GL}}{|a_{GL}|}}. \tag{B17}$$

The components of the tensor $\hat{\eta}$ in the frame (x, y, z) are given by

$$\eta_{xx} = [m(\varphi_0)/m_{ab}]^{1/2}\eta'_{x'x'}, \quad \eta_{yy} = [m_{ab}/m(\varphi_0)]^{1/2}\eta'_{y'y'} \tag{B18}$$

The right-hand side of Eq. (B16) contains two terms, representing two mechanisms of dissipation. The viscous drag tensor due to relaxation of the order parameter is [36, 37, 40, 38]:

$$(\eta'_{p0})_{ij} = 2\pi\hbar\Gamma\frac{|a_{GL}|}{b_{GL}}\alpha_1\delta_{ij}, \tag{B19}$$

$$\alpha_1 = \int_0^\infty \left(\frac{df}{d\rho}\right)^2 \rho d\rho = 0.279. \tag{B20}$$

The second term in the right-hand side of Eq. (B16) defines the ohmic viscosity tensor $\hat{\eta}'_{\rm oh}$, which is evaluated in Chapter 2:

$$\mathbf{d}\cdot\hat{\eta}'_{\rm oh}\tilde{\mathbf{V}}_L = \frac{\hbar\sigma_{ab}}{2e}\int\left[s(\varphi_0)\frac{\partial^2\Phi}{\partial x'^2} + \frac{\partial^2\Phi}{\partial y'^2}\right](\mathbf{d}\nabla'\theta_0)d^2\boldsymbol{\rho}'. \tag{B21}$$

Now, if we substitute Φ in the form (2.15) into Eqs. (B12) and (B21) and switch to the coordinates (x_1, y_1) (see Eq. (2.9)) we obtain Eqs. (2.7), (2.8), (2.12) and (2.13).

Appendix C

Expansion of the vortex viscosity in the limit $u \gg 1$

In this Appendix Eq. (2.26) will be derived. First, we divide the integral in Eq. (2.7) into two parts:

$$\eta_x = \eta_{x1} + \eta_{x2}, \tag{C1}$$

$$\eta_{x1} = -2n_0\Gamma\hbar \int_{\rho_1<\rho_0/\sqrt{u}} f^2(\rho_1)\frac{y_1}{\rho_1^2}\left(u^2\Phi_x - \frac{y_1}{\rho_1^2}\right) dx_1 dy_1, \tag{C2}$$

$$\eta_{x2} = -2n_0\Gamma\hbar \int_{\rho_1>\rho_0/\sqrt{u}} f^2(\rho_1)\frac{y_1}{\rho_1^2}\left(u^2\Phi_x - \frac{y_1}{\rho_1^2}\right) dx_1 dy_1, \tag{C3}$$

where $\rho_0 = u^{1/6+\delta}$, $\delta \ll 1/6$. Note that the left-hand side of Eq. (2.12) is small when $\rho_1 > \rho_0/\sqrt{u} \gg u^{-1/2}$, so it can be accounted for by perturbation theory:

$$\Phi_x = \frac{y_1}{u^2\rho_1^2} + \Phi_{x1} + \Phi_{x2} + ..., \tag{C4}$$

$$\Phi_{x1} = \frac{1}{u^4 f^2(\rho_1)}\left(\frac{\partial^2}{\partial y_1^2} + s\frac{\partial^2}{\partial x_1^2}\right)\frac{y_1}{\rho_1^2}, \qquad \Phi_{x2} = \frac{1}{u^6}\left[\frac{1}{f^2(\rho_1)}\left(\frac{\partial^2}{\partial y_1^2} + s\frac{\partial^2}{\partial x_1^2}\right)\right]^2\frac{y_1}{\rho_1^2}.$$

The main contribution to the integral in Eq. (C3) is determined by small ρ_1. The integral of Φ_{x2} is of the order of $(u\rho_0^6)^{-1} \ll u^{-2}$, the integrals of higher-order terms are also negligibly small, hence

$$\eta_{x2} \approx -2n_0\Gamma\hbar\frac{I'_{0x}}{u}, \qquad I'_{0x} = \int_{\rho>\rho_0}\frac{y}{\rho^2}\left(\frac{\partial^2}{\partial y^2} + s\frac{\partial^2}{\partial x^2}\right)\frac{y}{\rho^2}\,dx\,dy. \tag{C5}$$

Let us consider the component η_{x1}. In the new variables introduced in subsection 2.3.1 Eq. (C2) reads

$$\eta_{x1} = -2n_0\Gamma\hbar \int_{\rho<\rho_0} f^2\left(\frac{\rho}{\sqrt{u}}\right)\frac{y}{\rho^2}\left(\tilde{\Phi}_x - \frac{y}{\rho^2}\right) dx\,dy. \tag{C6}$$

Now we estimate the term R_x introduced in Eq. (2.23). It satisfies the following relation:

$$\begin{aligned}\tfrac{\partial^2 R_x}{\partial y^2} + s\tfrac{\partial^2 R_x}{\partial x^2} - uf^2\left(\tfrac{\rho}{\sqrt{u}}\right)R_x = \left[uf^2\left(\tfrac{\rho}{\sqrt{u}}\right) - f_2\rho^2 - \tfrac{f_4\rho^4}{u}\right]\left(\Phi_x^{(0)} - \tfrac{y}{\rho^2}\right)\\ + \left[uf^2\left(\tfrac{\rho}{\sqrt{u}}\right) - f_2\rho^2\right]\tfrac{\Phi_x^{(1)}}{u}.\end{aligned} \tag{C7}$$

Note that when $\rho \ll \sqrt{u}$ the source in the right-hand side of (C7) can be presented as $S(x,y)u^{-2}$, where $S(x,y)$ is some function independent of u. Since Eq. (C7) is a screening equation, the function $R_x(x,y,u)$ for small ρ does not depend on the behavior of the source in the area of big ρ and can be presented as $R_x = \tilde{R}_x(x,y)u^{-2}$. On the other hand, when $\rho \gg 1$ the derivatives in the left-hand side of Eq. (C7) are small, hence in the area $1 \ll \rho \ll \sqrt{u}$

$$R_x \approx \frac{1}{u^2}\left[-\frac{f_6\rho^4}{f_2}\left(\Phi_x^{(0)} - \frac{y}{\rho^2}\right) - \frac{f_4\rho^2}{f_2}\Phi_x^{(1)}\right], \text{ and} \qquad |R_x| \le \frac{\text{const}}{\rho u^2}. \tag{C8}$$

Now we substitute $\tilde{\Phi}_x$ in the form (2.23) into (C6):

$$\eta_{x1} = -2n_0\Gamma\hbar\left(\frac{I'_{1x}}{u} + \frac{I'_{2x}}{u^2} + I_{3x}\right), \tag{C9}$$

where

$$I'_{1x} = \int_{\rho<\rho_0} f_2 y\left(\Phi_x^{(0)} - \frac{y}{\rho^2}\right) dx\, dy, \tag{C10}$$

$$I'_{2x} = \int_{\rho<\rho_0} \frac{y}{\rho^2}\left[f_4\rho^4\left(\Phi_x^{(0)} - \frac{y}{\rho^2}\right) + f_2\rho^2\Phi_x^{(1)}\right] dx\, dy, \tag{C11}$$

$$\begin{aligned} I_{3x} = {} & \textstyle\int_{\rho<\rho_0}\left[f^2\left(\frac{\rho}{\sqrt{u}}\right) - \frac{f_2\rho^2}{u} - \frac{f_4\rho^4}{u^2}\right]\left(\Phi_x^{(0)} - \frac{y}{\rho^2}\right)\frac{y}{\rho^2}dx\, dy \\ & + \textstyle\int_{\rho<\rho_0}\left[f^2\left(\frac{\rho}{\sqrt{u}}\right) - \frac{f_2\rho^2}{u}\right]\frac{\Phi_x^{(1)}}{u}\frac{y}{\rho^2}dx\, dy + \int_{\rho<\rho_0} f^2\left(\frac{\rho}{\sqrt{u}}\right) R_x\frac{y}{\rho^2}dx\, dy. \end{aligned} \tag{C12}$$

One can easily prove that

$$\Phi_x^{(0)} = \frac{y}{\rho^2} + \frac{1}{f_2\rho^2}\left(\frac{\partial^2}{\partial y^2} + s\frac{\partial^2}{\partial x^2}\right)\frac{y}{\rho^2} + O(\rho^{-9}), \tag{C13}$$

$$\Phi_x^{(1)} = O(\rho^{-3}). \tag{C14}$$

From Eqs. (C13), (C14) and (C8) we can see that all integrals in Eq. (C12) are of the order ρ_0^2/u^3. Thus $|I_{3x}| \ll u^{-2}$, so it can be neglected. Also we can integrate in Eqs. (C10) and (C11) over the whole xy plane: using Eqs. (2.27), (C5), (C10), (C13) and (C11) one can prove that

$$|I'_{0x} + I'_{1x} - I_{1x}(s)| \ll u^{-1}, \tag{C15}$$

$$|I'_{2x} - I_{2x}(s)| \ll 1, \tag{C16}$$

Finally, taking into account Eqs. (C1), (C5) and (C9) we obtain Eq. (2.26).

Appendix D

Calculation of the vortex viscosity in the limit $s \gg u \gtrsim 1$

In this Appendix Eqs. (2.35) and (2.36) will be derived. Here the calculations for the η_y component are presented, since the calculations for the η_x component are less complicated. First, we rewrite Eq. (2.13) in the form

$$s\frac{\partial^2\Phi_y}{\partial x^2} - u^2\Phi_y + \frac{x}{\rho^2}f^2(\rho) = -\frac{\partial^2\Phi_y}{\partial y^2} - u^2\Phi_y\left(1 - f^2(\rho)\right). \tag{D1}$$

The index "1" is omitted. It will be proved below that the terms in the right-hand side of Eq. (D1) give a small contribution to the viscosity, so they can be neglected. Then the solution of Eq. (D1) has the form

$$\Phi_y \approx \Phi_{y0} = \int_{-\infty}^{+\infty} \frac{x' f^2(\rho')}{x'^2 + y^2} \frac{\exp(-u\,|x - x'|\,/\sqrt{s})}{2u\sqrt{s}} dx', \tag{D2}$$

where $\rho' = \sqrt{x'^2 + y^2}$. Consider a quantity y_0 in the range $1 \ll y_0 \ll \sqrt{s}/u$ (for example, $y_0 = s^{1/4}/u^{1/2}$). We divide the integral in Eq. (2.8) into three parts:

$$\begin{aligned}\eta_y = -2n_0\Gamma\hbar \left[\int_{|y|<y_0} f^2(\rho)\tfrac{x}{\rho^2}u^2\Phi_y\,dx\,dy - \int_{|y|<y_0} f^2(\rho)\tfrac{x^2}{\rho^4}\,dx\,dy\right] \\ -4n_0\Gamma\hbar\int_{y>y_0} f^2(\rho)\tfrac{x}{\rho^2}\left(u^2\Phi_y - \tfrac{x}{\rho^2}\right)dx\,dy,\end{aligned} \tag{D3}$$

Using the inequality

$$f^2(\rho) < \frac{\rho^2}{A_1 + \rho^2}, \tag{D4}$$

where A_1 is some constant, we can estimate the first integral:

$$\begin{aligned}\left|\int_{|y|<y_0} f^2(\rho)\tfrac{x}{\rho^2}u^2\Phi_y\,dxdy\right| < \tfrac{y_0 u}{\sqrt{s}}\int \tfrac{|x||x'|\exp(-u|x-x'|/\sqrt{s})dx\,dx'}{(x^2+A_1)(x'^2+A_1)} \\ < \text{const}\tfrac{y_0 u}{\sqrt{s}}\left(\ln\tfrac{\sqrt{s}}{u}\right)^2 \ll 1.\end{aligned} \tag{D5}$$

Here and further "const" denotes a constant independent of any parameters. The second term in Eq. (D3) has the following asymptotics when $y_0 \gg 1$:

$$\int_{|y|<y_0} f^2(\rho)\frac{x^2}{\rho^4}\,dx\,dy \approx \pi\ln y_0 + C_y. \tag{D6}$$

The constant C_y will be evaluated below. The third integral in Eq. (D3) can be simplified if we take into account that $\rho > y_0$, $\rho' > y_0$ and $y_0 \gg 1$, so we can substitute unity instead of f^2:

$$\begin{aligned}\int_{y>y_0} f^2(\rho)\tfrac{x}{\rho^2}\left(u^2\Phi_y - \tfrac{x}{\rho^2}\right) dx\,dy &\approx \int_{y_0}^{\infty}\left(\tfrac{\pi u}{\sqrt{s}}\int_{-\infty}^{+\infty}\tfrac{y\exp\left(-\frac{u|x|}{\sqrt{s}}\right)}{x^2+4y^2}dx - \tfrac{\pi}{2y}\right)dy \\ = \tfrac{\pi}{2}\int_0^{\infty}dx\int_{y_0}^{\infty}dy\left(\tfrac{4y}{sx^2/u^2+4y^2} - \tfrac{1}{y}\right)e^{-x} &\approx -\tfrac{\pi}{4}\int_0^{\infty}\ln\tfrac{sx^2}{4y_0^2u^2}e^{-x}dx \\ = \tfrac{\pi}{2}\ln y_0 - \tfrac{\pi}{4}\ln\tfrac{s}{4u^2} + \tfrac{\pi}{2}\mathcal{C}, &\end{aligned} \tag{D7}$$

where $\mathcal{C}$ is the Euler constant:

$$\mathcal{C} = -\int_0^{\infty}\ln x\cdot e^{-x}dx \approx 0.577.$$

Using (D3) - (D7) we obtain

$$\eta_y = 2\pi\hbar\Gamma n_0\left(\frac{1}{2}\ln\frac{s}{4u^2} + \frac{C_y}{\pi} - \mathcal{C}\right). \tag{D8}$$

The component η_x can be calculated in a similar way:

$$\eta_x = 2\pi\hbar\Gamma n_0\left(\frac{1}{2}\ln\frac{s}{4u^2} + \frac{C_x}{\pi} - \mathcal{C}\right), \tag{D9}$$

$$C_x = \lim_{y_0\to\infty}\left(\int_{|y|<y_0} f^2(\rho)\frac{y^2}{\rho^4}\,dxdy - \pi\ln y_0\right). \tag{D10}$$

Now we evaluate C_x and C_y. Here the constant g_4' from [37] will be useful:

$$g_4' = \int_0^{\infty}\left[f^2(\rho) - \frac{\rho^2}{1+\rho^2}\right]\rho^{-1}d\rho = -0.3982. \tag{D11}$$

It is easy to check that

$$C_x = \pi g_4' + \lim_{y_0\to\infty}\int_{|y|<y_0,\rho>y_0} y^2\rho^{-4}\,dx\,dy = \pi\left(g_4' + \ln 2 - \frac{1}{2}\right).$$

Similarly,

$$C_y = \pi\left(g_4' + \ln 2 + \frac{1}{2}\right).$$

Finally, the components of the viscous drag tensor take the form

$$\eta_x = 2\pi\hbar\Gamma n_0\left(\ln\frac{\sqrt{s}}{u} + g_4' - \mathcal{C} - \frac{1}{2}\right), \tag{D12}$$

$$\eta_y = 2\pi\hbar\Gamma n_0\left(\ln\frac{\sqrt{s}}{u} + g_4' - \mathcal{C} + \frac{1}{2}\right). \tag{D13}$$

If we substitute $\mathcal{C}$ and g_4' with their numerical values, we obtain Eqs. (2.35) and (2.36).

Now it is necessary to prove our assumption concerning the right-hand side of Eq. (D1). Consider it as a perturbation. The first order correction to the approximate solution Φ_{y0} has the form

$$\Phi_{y1} = R_y^{(1)} + R_y^{(2)},$$

$$R_y^{(1)} = \int_{-\infty}^{+\infty} \frac{u\Phi_{y0}(x', y)[1 - f^2(\rho')]}{2\sqrt{s}} \exp\left(-\frac{u\,|x - x'|}{\sqrt{s}}\right) dx', \tag{D14}$$

$$R_y^{(2)} = \frac{1}{2u\sqrt{s}} \int_{-\infty}^{+\infty} \frac{\partial^2 \Phi_{y0}}{\partial y^2}(x', y) \exp\left(-\frac{u\,|x - x'|}{\sqrt{s}}\right) dx'. \tag{D15}$$

The contribution of Φ_{y1} to η_y is equal to

$$\Delta\eta_y = -2n_0\Gamma\hbar(I_y^{(1)} + I_y^{(2)}),$$

where

$$I_y^{(1)} = \int f^2(\rho)\frac{x}{\rho^2}u^2 R_y^{(1)} dx\, dy, \tag{D16}$$

$$I_y^{(2)} = \int f^2(\rho)\frac{x}{\rho^2}u^2 R_y^{(2)} dx\, dy. \tag{D17}$$

It will be shown that $\left|I_y^{(1)}\right| \ll 1$ and $\left|I_y^{(2)}\right| \ll 1$ when $s \gg u^2$.

A simple estimate for $|\Phi_{y0}|$ can be obtained with the help of (D4):

$$|\Phi_{y0}| \leq \text{const}\frac{\ln\frac{\sqrt{s}}{u}}{u\sqrt{s}}. \tag{D18}$$

Using the inequality

$$1 - f^2(\rho) < \frac{A_2}{A_2 + \rho^2},$$

with $A_2 = \text{const}$ and Eq. (D18) we can estimate $I_y^{(1)}$:

$$\left|I_y^{(1)}\right| \leq \text{const}\frac{u}{\sqrt{s}} \ln\frac{\sqrt{s}}{u} \ll 1.$$

For all x' and y we can write

$$\left|\frac{\partial^2}{\partial y^2}\left(\frac{1}{x'^2 + y^2} f^2(\rho')\right)\right| \leq \frac{\text{const}}{(A_3 + x'^2 + y^2)^2}, \qquad (A_3 = \text{const})$$

whence

$$\left|I_y^{(2)}\right| \leq \frac{\text{const}}{s} \int \frac{|x| \exp\left(-\frac{u|x-x'|}{\sqrt{s}}\right) \exp\left(-\frac{u|x''-x'|}{\sqrt{s}}\right)}{(A_3+x''^2)(A_1+x^2)} dx' dx'' dx$$

$$\leq \frac{\text{const}}{s} \ln\frac{\sqrt{s}}{u} \int \frac{\exp\left(-\frac{u|x''-x'|}{\sqrt{s}}\right)}{x''^2+A_3} dx' dx'' \leq \frac{\text{const}}{\sqrt{s}u} \ln\frac{\sqrt{s}}{u} \ll 1$$

when $u \gtrsim 1$.

Appendix E

Estimate of the distortion of the decaying magnon modes

In this Appendix we will consider the modification of the mode with the wave-vector $\mathbf{q}_2$ in the vicinity of the surface. This consideration can be simply generalized for all other modes.

First, we note that $q_2^2 \approx -\lambda^{-2}$ and $q_{2x} \approx i\lambda^{-1}$, since $|k_y| \ll \lambda^{-1}$ (this inequality holds for frequencies, which are much smaller than the plasma frequency $\omega_p \sim c\lambda^{-1}$). We substitute into Eq. (3.26) $B_v = 4\pi M e^{-x/\lambda}$, and $\mathbf{m} \approx \mathbf{m}_2 e^{-x/\lambda} + \mathbf{m}_2^{(1)} e^{-2x/\lambda}$, where $\mathbf{m}_2^{(1)}$ is the amplitude of the first-order correction, which is to be estimated. This correction is determined from the following equations:

$$-\frac{i\omega}{\gamma M}\mathbf{m}_2^{(1)} + (K - 4\alpha\lambda^{-2})\mathbf{m}_2^{(1)} \times \mathbf{z}_0 = \left(\mathbf{b}_2^{(1)} - 4\pi\mathbf{m}_2\right) \times \mathbf{z}_0, \tag{E1}$$

$$-\frac{3}{\lambda^2}\mathbf{b}_2^{(1)} = -\frac{16\pi}{\lambda^2} m_{2y}^{(1)} \mathbf{y}_0.$$

For $\omega \approx \gamma M(K + \alpha q_1^2)$, $\alpha q_1^2 \gg 1$ we find

$$\mathbf{m}_2^{(1)} \approx \frac{4\pi}{\alpha q_1^2}\mathbf{m}_2. \tag{E2}$$

Hence, $\left|\mathbf{m}_2^{(1)}\right| \ll |\mathbf{m}_2|$, so the small correction can be neglected.

Appendix F

Derivation of equation (3.100)

To determine the force $\mathbf{f}_M$, one should calculate the variation of the free energy when all vortices are shifted by an equal vector, and the magnetization is kept fixed. To simplify the calculations we may use the fact that the free energy acquires the same variation if the vortices are kept fixed, and the magnetization is shifted in the opposite direction. Then

$$\delta F = \int \left(\frac{\delta F}{\delta \mathbf{A}} \delta \mathbf{A} + \frac{\delta F}{\delta \mathbf{M}} \delta \mathbf{M} \right) d^3\mathbf{r}.$$

According to the London equation $\delta F/\delta \mathbf{A} = 0$ the first term in the right-hand side vanishes. Also, the terms in Eq. (3.6) which depend only on $\mathbf{M}$ (e. g., the exchange energy) are not affected by the magnetization shift. Hence, only the term

$$\delta F = -\int \mathbf{B} \delta \mathbf{M} d^3\mathbf{r}, \tag{F1}$$

remains, and the force acting on a vortex is

$$(\mathbf{f}_M)_{x_i} = \frac{1}{N_v L_v} \int \mathbf{B} \frac{\partial \mathbf{M}}{\partial x_i} d^3\mathbf{r} = -\frac{1}{N_v L_v} \int \frac{\partial \mathbf{B}}{\partial x_i} \mathbf{M} d^3\mathbf{r}$$

Presenting the magnetic field as $\mathbf{B} = \mathbf{h} + \mathbf{b}_M$, we have

$$\mathbf{f}_M = \mathbf{f}_{M1} + \mathbf{f}_{M2}. \tag{F2}$$

$$(\mathbf{f}_{M1})_{x_i} = -\tfrac{1}{N_v L_v} \int \tfrac{\partial \mathbf{b}_M}{\partial x_i} \mathbf{M} d^3\mathbf{r},$$
$$(\mathbf{f}_{M2})_{x_i} = -\tfrac{1}{N_v L_v} \int \tfrac{\partial \mathbf{h}}{\partial x_i} \mathbf{M} d^3\mathbf{r}.$$

Note that the term $\mathbf{f}_{M1}$ does not depend on the vortex positions. Hence, to calculate this term we can place the vortices anywhere in the superconductor. Let us position the vortices in an area with uniform magnetization ($\mathbf{M} = \text{const}$). Then, $\mathbf{f}_{M2}$ vanishes, and $\mathbf{f}_M = \mathbf{f}_{M1}$. On the other hand, in the area with homogenous magnetization any identical displacement of all vortices does not change the free energy, hence, the whole force $\mathbf{f}_M$ vanishes. Thus, $\mathbf{f}_{M1} = 0$, and for any vortex positions $\mathbf{f}_M = \mathbf{f}_{M2}$. From this follows Eq. (3.100).

Appendix G

Evaluation of the integral in Eq. (3.128)

In this Appendix it is shown how the integral in Eq. (3.128) can be evaluated. Let us introduce the dimensionless quantities $l = L/\lambda$, $l_v = V_L/(\omega_F \lambda)$ and $\mathbf{g} = \lambda \mathbf{q}$, and direct the g_x axis along $\mathbf{V}_L$. Then $f_{My} = 0$, and

$$f_{Mx} = -\frac{\gamma M \Phi_0^2 \sin^2\theta}{4\pi\lambda^3\omega_F} \int\limits_{g<\lambda/\xi} \frac{g_x d^2\mathbf{g}}{(1+g^2)^2} \delta(1 + l^2 g^2 - l_v g_x) = -\frac{\gamma M \Phi_0^2 \sin^2\theta}{4\pi\lambda^2 V_L} \int\limits_{g<\lambda/\xi} \frac{(1+l^2g^2)\delta(1+l^2g^2-l_v g_x)}{(1+g^2)^2} d^2\mathbf{g}$$

$$= -\frac{\gamma M \Phi_0^2 \sin^2\theta}{4\pi\lambda^2 V_L} \left[l^2 \int\limits_{g<\lambda/\xi} \frac{\delta(1+l^2g^2-l_v g_x)}{1+g^2} d^2\mathbf{g} + (1-l^2) \int\limits_{g<\lambda/\xi} \frac{\delta(1+l^2g^2-l_v g_x)}{(1+g^2)^2} d^2\mathbf{g} \right]. \quad \text{(G1)}$$

We will put $V_L > V_{\rm th} \equiv 2\omega_F L$, so that $f_{Mx} \neq 0$. For simplicity, we will assume that

$$L^2\xi^{-1} > \frac{V_L}{2\omega_F} + \sqrt{\left(\frac{V_L}{2\omega_F}\right) - L^2}, \quad \text{(G2)}$$

which is possible when $\xi < L$. Then, the whole circle $1 + l^2g^2 - l_v g_x = 0$ lies in the region $g < \lambda/\xi$. Now we make a coordinate shift, redesignating $g_x - l_v/(2l^2)$ by g_x:

$$f_{Mx} = -\frac{\gamma M \Phi_0^2 \sin^2\theta}{4\pi\lambda^2 V_L} \left\{ \int \frac{\delta(g^2 - g_0^2) d^2\mathbf{g}}{1 + g_y^2 + \left(g_x + \frac{l_v}{2l^2}\right)^2} + (l^{-2} - 1) \int \frac{\delta(g^2 - g_0^2) d^2\mathbf{g}}{\left[1 + g_y^2 + \left(g_x + \frac{l_v}{2l^2}\right)^2\right]^2} \right\}, \quad \text{(G3)}$$

where

$$g_0^2 = l^{-2} \left(\frac{l_v^2}{4l^2} - 1 \right).$$

Integration over the modulus of $\mathbf{g}$ is now straightforward:

$$f_{Mx} = -\frac{\gamma M \Phi_0^2 \sin^2\theta}{8\pi\lambda^2 V_L} \left[\int_0^{2\pi} \frac{d\varphi}{1 + g_0^2 + \frac{l_v^2}{4l^4} + \frac{l_v}{l^2} g_0 \cos\varphi} + \int_0^{2\pi} \frac{(l^{-2} - 1) d\varphi}{\left(1 + g_0^2 + \frac{l_v^2}{4l^4} + \frac{l_v}{l^2} g_0 \cos\varphi\right)^2} \right], \quad \text{(G4)}$$

where φ is the polar angle in the $\mathbf{g}$-plane. Integration can be completed using standard methods or a table of integrals. The result is

$$f_{Mx} = -\frac{\gamma M \Phi_0^2 \sin^2\theta}{8\lambda^2 V_L} (l^{-2} + 1) \frac{l_v^2}{l^4} \left[(1 - l^{-2})^2 + \frac{l_v^2}{l^4} \right]^{-3/2}. \quad \text{(G5)}$$

If we return to dimensional variables and recall that $L \ll \lambda$, we obtain Eq. (3.129).

Publications of the author in refereed journals

[A1] A. A. Bespalov and A. S. Mel'nikov. Mismatch of conductivity anisotropy in the mixed and normal states of type-II superconductors. *Phys. Rev. B*, 85:174502, May 2012.

[A2] A. A. Bespalov and A. S. Melnikov. Abrikosov vortex pinning on a cylindrical cavity inside the vortex core: formation of a bound state and depinning. *Supercond. Sci. Technol.*, 26(8):085014, 2013.

[A3] A. A. Bespalov and A. I. Buzdin. Band structure of magnetic excitations in the vortex phase of a ferromagnetic superconductor. *Phys. Rev. B*, 87:094509, Mar 2013.

[A4] A. A. Bespalov, A. S. Mel'nikov, and A. I. Buzdin. Magnon radiation by moving Abrikosov vortices in ferromagnetic superconductors and superconductor-ferromagnet multilayers. *Phys. Rev. B*, 89:054516, Feb 2014.

[A5] A.A. Bespalov, A.S. Melnikov, and A.I. Buzdin. Microwave and dc response of an abrikosov vortex lattice in ferromagnetic superconductors. *Physica C: Superconductivity*, 503(0):98 – 100, 2014.

Publications in conference proceedings

[B1] Bespalov A. A. and A. S. Mel'nikov. Resistivity anisotropy of a superconductor in the mixed state. In *Nanophysics and Nanoelectronics: Proceedings of the XV-th International Symposium*, volume 1, pages 274–275, Nizhny Novgorod, 2011. IPM RAS.

[B2] Bespalov A. A. and A. S. Mel'nikov. Pinning of an Abrikosov vortex on a small cylindrical cavity. In *Nanophysics and Nanoelectronics: Proceedings of the XVI-th International Symposium*, volume 1, pages 7–8, Nizhny Novgorod, Russia, 2012. IPM RAS.

[B3] A. A. Bespalov and A. S. Mel'nikov. Pinning of an Abrikosov vortex on a small cylindrical cavity. In *Dubna-Nano2012: Book of Abstracts of the International Conference on Theoretical Physics*, page 26, Dubna, 2012. JINR.

[B4] Bespalov A. A. and Buzdin A. I. Band structure of the magnon spectrum in a ferromagnetic superconductor in the mixed state. In *Nanophysics and Nanoelectronics: Proceedings of the XVII-th International Symposium*, volume 1, pages 13–14, Nizhny Novgorod, Russia, 2013. IPM RAS.

[B5] A. A. Bespalov and A. I. Buzdin. Spin wave excitation by a moving vortex lattice in ferromagnetic superconductors and SF bilayers. In *Eight International Conference on Vortex Matter in Nanostructured Superconductors: Abstract Book*, page 105, Leuven, Belgium, 2013. KU Leuven.

[B6] A. A. Bespalov, A. S. Mel'nikov, and A. I. Buzdin. Magnon radiation by moving Abrikosov vortices in ferromagnetic superconductors and superconductor/ferromagnet multilayers. In *Nanophysics and Nanoelectronics: Proceedings of the XVIII-th International Symposium*, volume 1, pages 11–12, Nizhny Novgorod, Russia, 2014. IPM RAS.

[B7] A. A. Bespalov and A. I. Buzdin. Complex London penetration depth and vortex-vortex attraction in ferromagnet/superconductor systems. In *Nanophysics and Nanoelectronics: Proceedings of the XVIII-th International Symposium*, volume 1, pages 13–14, Nizhny Novgorod, Russia, 2014. IPM RAS.

[B8] A. Bespalov, A. Mel'nikov, and A. Buzdin. Crossover between Abrikosov vortex repulsion and attraction in superconducting and ferromagnetic hybrid systems. In

Condensed matter in Paris 2014: Conference program, keynote speakers presentations and abstracts, page 117, Paris, 2014.

Bibliography

[1] W. Meissner and R. Ochsenfeld. Ein neuer Effekt bei Eintritt der Supraleitfhigkeit. *Naturwissenschaften*, 21(44):787–788, 1933.

[2] J. Bardeen, L. N. Cooper, and J. R. Schrieffer. Theory of Superconductivity. *Phys. Rev.*, 108:1175–1204, Dec 1957.

[3] L.D. Landau, E.M. Lifshitz, and L.P. Pitaevskii. *Statistical Physics. Part 2: Theory of the condensed state*, volume 9 of *Course of Theoretical Physics Series*. Butterworth-Heinemann, Oxford, 1980.

[4] F. London and H. London. The Electromagnetic Equations of the Supraconductor. *Proceedings of the Royal Society of London. Series A - Mathematical and Physical Sciences*, 149(866):71–88, 1935.

[5] V. L. Ginzburg and Landau L. D. On the theory of superconductivity. *Zh. Eksp. Teor. Fiz*, 20:1064–1081, 1950.

[6] M. Tinkham. *Introduction to superconductivity*. McGraw-Hill, Inc., USA, second edition edition, 1996.

[7] Abrikosov A. A. On the magnetic properties of superconductors of the second group. *Zh. Eksp. Teor. Fiz*, 32:1442, 1957.

[8] P. G. de Gennes. *Superconductivity of metals and alloys*. Advanced Books Classics Series. Westview Press, USA, 1999.

[9] D. Cribier, B. Jacrot, L. Madhav Rao, and B. Farnoux. Mise en evidence par diffraction de neutrons d'une structure periodique du champ magnetique dans le niobium supraconducteur. *Physics Letters*, 9(2):106 – 107, 1964.

[10] U. Essmann and H. Träuble. The direct observation of individual flux lines in type II superconductors. *Physics Letters A*, 24(10):526 – 527, 1967.

[11] G. Blatter, M. V. Feigel'man, V. B. Geshkenbein, A. I. Larkin, and V. M. Vinokur. Vortices in high-temperature superconductors. *Rev. Mod. Phys.*, 66:1125–1388, Oct 1994.

[12] L. Civale, A. D. Marwick, T. K. Worthington, M. A. Kirk, J. R. Thompson, L. Krusin-Elbaum, Y. Sun, J. R. Clem, and F. Holtzberg. Vortex confinement by columnar defects in $YBa_2Cu_3O_7$ crystals: Enhanced pinning at high fields and temperatures. *Phys. Rev. Lett.*, 67:648–651, Jul 1991.

[13] A. Goyal, S. Kang, K. J. Leonard, P. M. Martin, A. A. Gapud, M. Varela, M. Paranthaman, A. O. Ijaduola, E. D. Specht, J. R. Thompson, D. K. Christen, S. J. Pennycook, and F. A. List. Irradiation-free, columnar defects comprised of self-assembled nanodots and nanorods resulting in strongly enhanced flux-pinning in $YBa_2Cu_3O_{7-\delta}$ films. *Superconductor Science and Technology*, 18(11):1533, 2005.

[14] Vyacheslav F. Solovyov, Qiang Li, Weidong Si, Boris Maiorov, Timothy J. Haugan, J. L. MacManus-Driscoll, H. Yao, Q. X. Jia, and E. D. Specht. Influence of defect-induced biaxial strain on flux pinning in thick $YBa_2Cu_3O_7$ layers. *Phys. Rev. B*, 86:094511, Sep 2012.

[15] B. Maiorov, T. Katase, I. O. Usov, M. Weigand, L. Civale, H. Hiramatsu, and H. Hosono. Competition and cooperation of pinning by extrinsic point-like defects and intrinsic strong columnar defects in $BaFe_2As_2$ thin films. *Phys. Rev. B*, 86:094513, Sep 2012.

[16] A. Xu, V. Braccini, J. Jaroszynski, Y. Xin, and D. C. Larbalestier. Role of weak uncorrelated pinning introduced by $BaZrO_3$ nanorods at low-temperature in $(Y, Gd)Ba_2Cu_3O_x$ thin films. *Phys. Rev. B*, 86:115416, Sep 2012.

[17] N. Haberkorn, M. Miura, J. Baca, B. Maiorov, I. Usov, P. Dowden, S. R. Foltyn, T. G. Holesinger, J. O. Willis, K. R. Marken, T. Izumi, Y. Shiohara, and L. Civale. High-temperature change of the creep rate in $YBa_2Cu_3O_{7-\delta}$ films with different pinning landscapes. *Phys. Rev. B*, 85:174504, May 2012.

[18] U. Welp, Z. L. Xiao, J. S. Jiang, V. K. Vlasko-Vlasov, S. D. Bader, G. W. Crabtree, J. Liang, H. Chik, and J. M. Xu. Superconducting transition and vortex pinning in Nb films patterned with nanoscale hole arrays. *Phys. Rev. B*, 66:212507, Dec 2002.

[19] S. Raedts, A. V. Silhanek, M. J. Van Bael, and V. V. Moshchalkov. Flux-pinning properties of superconducting films with arrays of blind holes. *Phys. Rev. B*, 70:024509, Jul 2004.

[20] G. Karapetrov, J. Fedor, M. Iavarone, D. Rosenmann, and W. K. Kwok. Direct observation of geometrical phase transitions in mesoscopic superconductors by scanning tunneling microscopy. *Phys. Rev. Lett.*, 95:167002, Oct 2005.

[21] A.M. Campbell and J.E. Evetts. Flux vortices and transport currents in type II superconductors. *Adv. Phys.*, 21(90):199–428, 1972.

[22] G. S. Mkrtchyan and V. V. Shmidt. Interaction between a cavity and a vortex in a superconductor of the second kind. *Sov. Phys. JETP*, 34:195–197, 1972.

[23] I.B. Khalfin and B.Ya. Shapiro. Relaxation of magnetic flux in a superconductor with a system of columnar defects. *Physica C: Superconductivity*, 207(34):359 – 365, 1993.

[24] A. Buzdin and D. Feinberg. Electromagnetic pinning of vortices by non-superconducting defects and their influence on screening. *Physica C*, 256:303 – 311, 1996.

[25] A. Buzdin and M. Daumens. Electromagnetic pinning of vortices on different types of defects. *Physica C*, 294:257 – 269, 1998.

[26] A. Buzdin and M. Daumens. Electrostatic analogies in the problems of vortex-defect interactions. *Physica C*, 332:108 – 114, 2000.

[27] H. Nordborg and V. M. Vinokur. Interaction between a vortex and a columnar defect in the London approximation. *Phys. Rev. B*, 62:12408–12412, Nov 2000.

[28] S. M. Maurer, N. C. Yeh, and T. A. Tombrello. Vortex pinning by cylindrical defects in type-II superconductors: Numerical solutions to the Ginzburg-Landau equations. *Phys. Rev. B*, 54:15372–15379, Dec 1996.

[29] S. M. Maurer, N. C. Yeh, and T. A. Tombrello. Numerical calculation of the vortex-columnar-defect interaction and critical currents in extreme type-II superconductors - a two-dimensional model based on the Ginzburg-Landau approximation. *J. Phys.: Condens. Matter*, 10(33):7429, 1998.

[30] D. J. Priour and H. A. Fertig. Deformation and depinning of superconducting vortices from artificial defects: A Ginzburg-Landau study. *Phys. Rev. B*, 67:054504, Feb 2003.

[31] B. Rosenstein, I. Shapiro, and B. Ya. Shapiro. Maximal persistent current in a type-II superconductor with an artificial pinning array at the matching magnetic field. *Phys. Rev. B*, 81:064507, Feb 2010.

[32] John Bardeen and M. J. Stephen. Theory of the motion of vortices in superconductors. *Phys. Rev.*, 140:A1197–A1207, Nov 1965.

[33] A. Schmid. A time-dependent Ginzburg-Landau equation and its application to the resistivity in the mixed state. *Phys. Kond. Materie*, 5:302–317, 1966.

[34] L. P. Gor'kov and N. B. Kopnin. Viscous vortex flow in superconductors with paramagnetic impurities. *Sov. Phys. JETP*, 33(6):1251–1256, 1971.

[35] N.B. Kopnin. *Theory of Nonequilibrium Superconductivity*. International Series of Monographs on Physics. Clarendon Press, 2001.

[36] Chia-Ren Hu and Richard S. Thompson. Dynamic Structure of Vortices in Superconductors. II. $H \ll H_{c2}$. *Phys. Rev. B*, 6:110–120, Jul 1972.

[37] Chia-Ren Hu. Numerical constants for isolated vortices in superconductors. *Phys. Rev. B*, 6:1756–1760, Sep 1972.

[38] M. Yu. Kupriyanov and K.K. Likharev. Viscous Motion of Vortices in Type-II Superconductors. *JETP Lett.*, 15:247–250, 1972.

[39] A. Mourachkine. *High-Temperature Superconductivity in Cuprates: The Nonlinear Mechanism and Tunneling Measurements*. Fundamental Theories of Physics. Kluwer Academic Publishers, Dordrecht, Netherlands, 2002.

[40] V. M. Genkin and A. S. Mel'nikov. Motion of Abrikosov vortices in anisotropic superconductors. *Sov. Phys. JETP*, 68:1254–1256, 1989.

[41] B. I. Ivlev and N. B. Kopnin. Flux-Flow Conductivity in Anisotropic and Layered High-T_c Superconductors. *Europhys. Lett.*, 15(3):349, 1991.

[42] G. R. Stewart. Superconductivity in iron compounds. *Rev. Mod. Phys.*, 83:1589–1652, Dec 2011.

[43] Yoo Jang Song, Jin Soo Ghim, Byeong Hun Min, Yong Seung Kwon, Myung Hwa Jung, and Jong-Soo Rhyee. Synthesis, anisotropy, and superconducting properties of LiFeAs single crystal. *Appl. Phys. Lett.*, 96(21):212508, 2010.

[44] Hang-Dong Wang, Chi-Heng Dong, Zu-Juan Li, Qian-Hui Mao, Sha-Sha Zhu, Chun-Mu Feng, H. Q. Yuan, and Ming-Hu Fang. Superconductivity at 32 K and anisotropy in $Tl_{0.58}Rb_{0.42}Fe_{1.72}Se_2$ crystals. *Europhys. Lett.*, 93(4):47004, 2011.

[45] G. F. Chen, Z. Li, J. Dong, G. Li, W. Z. Hu, X. D. Zhang, X. H. Song, P. Zheng, N. L. Wang, and J. L. Luo. Transport and anisotropy in single-crystalline $SrFe_2As_2$ and $A_{0.6}K_{0.4}Fe_2As_2$ (A=Sr, Ba) superconductors. *Phys. Rev. B*, 78:224512, Dec 2008.

[46] X. F. Wang, T. Wu, G. Wu, H. Chen, Y. L. Xie, J. J. Ying, Y. J. Yan, R. H. Liu, and X. H. Chen. Anisotropy in the Electrical Resistivity and Susceptibility of Superconducting $BaFe_2As_2$ Single Crystals. *Phys. Rev. Lett.*, 102:117005, Mar 2009.

[47] K. Shirai, H. Kashiwaya, S. Miura, M. Ishikado, H. Eisaki, A. Iyo, I. Kurosawa, and S. Kashiwaya. Local transport properties of $PrFeAsO_{0.7}$ using FIB micro-fabrication technique. *Physica C*, 470(20):1473 – 1476, 2010. Proceedings of the 22nd International Symposium on Superconductivity (ISS 2009).

[48] M. A. Tanatar, N. Ni, G. D. Samolyuk, S. L. Bud'ko, P. C. Canfield, and R. Prozorov. Resistivity anisotropy of AFe_2As_2 (A=Ca, Sr, Ba): Direct versus Montgomery technique measurements. *Phys. Rev. B*, 79:134528, Apr 2009.

[49] M. A. Tanatar, N. Ni, C. Martin, R. T. Gordon, H. Kim, V. G. Kogan, G. D. Samolyuk, S. L. Bud'ko, P. C. Canfield, and R. Prozorov. Anisotropy of the iron pnictide superconductor $Ba(Fe_{1-x}Co_x)_2As_2$ ($x = 0.074$, $T_c = 23$ K). *Phys. Rev. B*, 79:094507, Mar 2009.

[50] Z. Hao and J. R. Clem. Viscous flux motion in anisotropic type-ii superconductors in low fields. *IEEE Trans. Magn.*, 27:1086–1088, 1991.

[51] L.N. Bulaevskii, A.I. Buzdin, M.L. Kulić, and S.V. Panjukov. Coexistence of superconductivity and magnetism. Theoretical predictions and experimental results. *Advances in Physics*, 34(2):175–261, 1985.

[52] Peter Fulde and Richard A. Ferrell. Superconductivity in a strong spin-exchange field. *Phys. Rev.*, 135:A550–A563, Aug 1964.

[53] A. I. Larkin and Yu. N. Ovchinnikov. Inhomogeneous state of superconductors. *Sov. Phys. JETP*, 20:762, 1964.

[54] Alexandre Buzdin and Jacques Flouquet. Ferromagnetic superconductors. *Phys. World*, 15:41–46, Jan 2002.

[55] S. S. Saxena, P. Agarwal, K. Ahilan, F. M. Grosche, R. K. W. Haselwimmer, M. J. Steiner, E. Pugh, I. R. Walker, S. R. Julian, P. Monthoux, G. G. Lonzarich, A. Huxley, I. Sheikin, D. Braithwaite, and J. Flouquet. Superconductivity on the border of itinerant-electron ferromagnetism in UGe_2. *Nature (London)*, 406:587–592, 2000.

[56] Dai Aoki, Andrew Huxley, Daniel Ressouche, Eric Braithwaite, Jacques Flouquet, Jean-Pascal Brison, Elsa Lhotel, and Carley Paulsen. Coexistence of superconductivity and ferromagnetism in URhGe. *Nature (London)*, 413:613–616, 2001.

[57] N. T. Huy, A. Gasparini, D. E. de Nijs, Y. Huang, J. C. P. Klaasse, T. Gortenmulder, A. de Visser, A. Hamann, T. Görlach, and H. v. Löhneysen. Superconductivity on the Border of Weak Itinerant Ferromagnetism in UCoGe. *Phys. Rev. Lett.*, 99:067006, Aug 2007.

[58] C. Paulsen, D. J. Hykel, K. Hasselbach, and D. Aoki. Observation of the Meissner-Ochsenfeld Effect and the Absence of the Meissner State in UCoGe. *Phys. Rev. Lett.*, 109:237001, Dec 2012.

[59] S. Nandi, W. T. Jin, Y. Xiao, Y. Su, S. Price, D. K. Shukla, J. Strempfer, H. S. Jeevan, P. Gegenwart, and Th. Brückel. Coexistence of superconductivity and ferromagnetism in P-doped $EuFe_2As_2$. *Phys. Rev. B*, 89:014512, Jan 2014.

[60] S. V. Vonsovskii. *Ferromagnetic Resonance*. Israel Program for Scientific Translations, Jerusalem, 1964.

[61] A. I. Buzdin. Spin-wave spectrum of antiferromagnetic superconductors. *JETP Letters*, 40(5):956–958, 1985.

[62] T. K. Ng and C. M. Varma. Spin and vortex dynamics and electromagnetic propagation in the spontaneous vortex phase. *Phys. Rev. B*, 58:11624–11630, Nov 1998.

[63] V. Braude and E. B. Sonin. Excitation of spin waves in superconducting ferromagnets. *Phys. Rev. Lett.*, 93:117001, Sep 2004.

[64] L. N. Bulaevskii, M. Hruška, and M. P. Maley. Spectroscopy of magnetic excitations in magnetic superconductors using vortex motion. *Phys. Rev. Lett.*, 95:207002, Nov 2005.

[65] A. Shekhter, L. N. Bulaevskii, and C. D. Batista. Vortex viscosity in magnetic superconductors due to radiation of spin waves. *Phys. Rev. Lett.*, 106:037001, Jan 2011.

[66] Lev N. Bulaevskii and Shi-Zeng Lin. Prediction of Polaronlike Vortices and a Dissociation Depinning Transition in Magnetic Superconductors: The Example of $ErNi_2B_2C$. *Phys. Rev. Lett.*, 109:027001, Jul 2012.

[67] Lev N. Bulaevskii and Shi-Zeng Lin. Self-induced pinning of vortices in the presence of ac driving force in magnetic superconductors. *Phys. Rev. B*, 86:224513, Dec 2012.

[68] Shi-Zeng Lin and Lev N. Bulaevskii. Measuring spectrum of spin wave using vortex dynamics. *Phys. Rev. B*, 85:134508, Apr 2012.

[69] Shi-Zeng Lin, Lev N. Bulaevskii, and Cristian D. Batista. Vortex dynamics in ferromagnetic superconductors: Vortex clusters, domain walls, and enhanced viscosity. *Phys. Rev. B*, 86:180506, Nov 2012.

[70] Shi-Zeng Lin and Lev N. Bulaevskii. Enhancement of critical current density in superconducting/magnetic multilayers with slow magnetic relaxation dynamics and large magnetic susceptibility. *Phys. Rev. B*, 86:064523, Aug 2012.

[71] Lev N. Bulaevskii and Shi-Zeng Lin. Polaron-like vortices, dissociation transition, and self-induced pinning in magnetic superconductors. *Sov. Phys. JETP*, 144:475, Sep 2013.

[72] T.L. Gilbert. A phenomenological theory of damping in ferromagnetic materials. *IEEE Trans. Magn.*, 40(6):3443–3449, Nov 2004.

[73] E. V. Thuneberg, J. Kurkijärvi, and D. Rainer. Pinning of a Vortex Line to a Small Defect in Superconductors. *Phys. Rev. Lett.*, 48:1853–1856, Jun 1982.

[74] Mark Friesen and Paul Muzikar. Microscopic theory of vortex pinning: Impurity terms in the Ginzburg-Landau free energy. *Phys. Rev. B*, 53:R11953–R11956, May 1996.

[75] A. S. Mel'nikov, A. V. Samokhvalov, and M. N. Zubarev. Electronic structure of vortices pinned by columnar defects. *Phys. Rev. B*, 79:134529, Apr 2009.

[76] A.S. Melnikov and A.V. Samokhvalov. Abrikosov vortex escape from a columnar defect as a topological electronic transition in a vortex core. *JETP Letters*, 94(10):759–763, 2012.

[77] L. P. Gorkov and N. B. Kopnin. Vortex motion and resistivity of type-ll superconductors in a magnetic field. *Sov. Phys. Usp.*, 18(7):496–513, 1975.

[78] A.N. Tikhonov and A.A. Samarskii. *Equations of Mathematical Physics*. Dover Books on Physics. Dover Publications, New York, 1990.

[79] D. Vasyukov, Y. Anahory, L. Embon, D. Halbertal, J. Cuppens, L. Neeman, A. Finkler, Y. Segev, Y. Myasoedov, M. L. Rappaport, M. E. Huber, and E. Zeldov. A scanning superconducting quantum interference device with single electron spin sensitivity. *Nature Nanotechnology*, 8:639–644, Sep 2013.

[80] J. E. Villegas, Sergey Savel'ev, Franco Nori, E. M. Gonzalez, J. V. Anguita, R. García, and J. L. Vicent. A superconducting reversible rectifier that controls the motion of magnetic flux quanta. *Science*, 302(5648):1188–1191, 2003.

[81] R. Wördenweber, P. Dymashevski, and V. R. Misko. Guidance of vortices and the vortex ratchet effect in high-T_c superconducting thin films obtained by arrangement of antidots. *Phys. Rev. B*, 69:184504, May 2004.

[82] J. Van de Vondel, C. C. de Souza Silva, B. Y. Zhu, M. Morelle, and V. V. Moshchalkov. Vortex-rectification effects in films with periodic asymmetric pinning. *Phys. Rev. Lett.*, 94:057003, Feb 2005.

[83] T. C. Wu, Lance Horng, J. C. Wu, R. Cao, Jan Koláček, and T. J. Yang. Vortex ratchet effect in a niobium film with spacing-graded density of pinning sites. *Journal of Applied Physics*, 102(3):033918, 2007.

[84] B. B. Jin, B. Y. Zhu, R. Wördenweber, C. C. de Souza Silva, P. H. Wu, and V. V. Moshchalkov. High-frequency vortex ratchet effect in a superconducting film with a nanoengineered array of asymmetric pinning sites. *Phys. Rev. B*, 81:174505, May 2010.

[85] Clécio C. de Souza Silva, J. Van de Vondel, B. Y. Zhu, M. Morelle, and V. V. Moshchalkov. Vortex ratchet effects in films with a periodic array of antidots. *Phys. Rev. B*, 73:014507, Jan 2006.

[86] M. Tinkham. Viscous flow of flux in type-ii superconductors. *Phys. Rev. Lett.*, 13:804–807, Dec 1964.

[87] I. Prigogine. *Introduction to thermodynamics of irreversible processes.* Interscience Publishers, 1968.

[88] R.J. Watts-Tobin, Y. Krähenbühl, and L. Kramer. Nonequilibrium theory of dirty, current-carrying superconductors: phase-slip oscillators in narrow filaments near T_c. *J. Low. Temp. Phys.*, 42(5-6):459–501, 1981.

[89] V. Braude. Microwave response and spin waves in superconducting ferromagnets. *Phys. Rev. B*, 74:054515, Aug 2006.

[90] N. A. Logoboy and E. B. Sonin. Two-dimensional domain-wall magnon waves in superconducting ferromagnets. *Phys. Rev. B*, 75:153206, Apr 2007.

[91] V. Braude and E. B. Sonin. Surface spin waves in superconducting and insulating ferromagnets. *Europhys. Lett.*, 72(1):124, 2005.

[92] L. D. Landau, L. P. Pitaevskii, and E. M. Lifshitz. *Electrodynamics of Continuous Media, Second Edition*, volume 8 of *Course of Theoretical Physics.* Butterworth-Heinemann, 2 edition, 1984.

[93] J. A. Osborn. Demagnetizing factors of the general ellipsoid. *Phys. Rev.*, 67:351–357, Jun 1945.

[94] Vu Hung Dao, Sébastien Burdin, and Alexandre Buzdin. Size of stripe domains in a superconducting ferromagnet. *Phys. Rev. B*, 84:134503, Oct 2011.

[95] Alexander B. Shick. Electronic and magnetic structure of URhGe. *Phys. Rev. B*, 65:180509, Apr 2002.

[96] N. T. Huy, D. E. de Nijs, Y. K. Huang, and A. de Visser. Unusual upper critical field of the ferromagnetic superconductor UCoGe. *Phys. Rev. Lett.*, 100:077002, Feb 2008.

[97] Robert M White. *Quantum Theory of Magnetism: Magnetic Properties of Materials*. Springer Series in SOLID-STATE SCIENCES. Springer, Dordrecht, 3 edition, 2007.

[98] A. I. Buzdin. Proximity effects in superconductor-ferromagnet heterostructures. *Rev. Mod. Phys.*, 77:935–976, Sep 2005.

[99] N. Kokubo, T. Nishizaki, B. Shinozaki, and P.H. Kes. Lattice orientations of driven vortex matter in amorphous MoGe films. *Physica C*, 470(1):43 – 47, 2010.

[100] S. Okuma, H. Imaizumi, D. Shimamoto, and N. Kokubo. Quantum melting and lattice orientation of driven vortex matter. *Phys. Rev. B*, 83:064520, Feb 2011.

[101] D. Charalambous, P. G. Kealey, E. M. Forgan, T. M. Riseman, M. W. Long, C. Goupil, R. Khasanov, D. Fort, P. J. C. King, S. L. Lee, and F. Ogrin. Vortex motion in type-II superconductors probed by muon spin rotation and small-angle neutron scattering. *Phys. Rev. B*, 66:054506, Aug 2002.

[102] Albert Schmid and Wolfgang Hauger. On the theory of vortex motion in an inhomogeneous superconducting film. *J. Low Temp. Phys.*, 11(5-6):667–685, 1973.

[103] Dingping Li, Andrey M. Malkin, and Baruch Rosenstein. Structure and orientation of the moving vortex lattice in clean type-II superconductors. *Phys. Rev. B*, 70:214529, Dec 2004.

[104] Hans Fangohr, Simon J. Cox, and Peter A. J. de Groot. Vortex dynamics in two-dimensional systems at high driving forces. *Phys. Rev. B*, 64:064505, Jul 2001.

[105] Mahesh Chandran, R. T. Scalettar, and G. T. Zimányi. Dynamic transition in driven vortices across the peak effect in superconductors. *Phys. Rev. B*, 67:052507, Feb 2003.

[106] D. Y. Vodolazov and F. M. Peeters. Rearrangement of the vortex lattice due to instabilities of vortex flow. *Phys. Rev. B*, 76:014521, Jul 2007.

[107] N. Nakai, N. Hayashi, and M. Machida. Simulation study for the orientation of the driven vortex lattice in an amorphous superconductor. *Physica C*, 469(1520):1106 – 1109, 2009. Proceedings of the 21st International Symposium on Superconductivity (ISS 2008).

[108] H. Kawano-Furukawa, C. J. Bowell, J. S. White, R. W. Heslop, A. S. Cameron, E. M. Forgan, K. Kihou, C. H. Lee, A. Iyo, H. Eisaki, T. Saito, H. Fukazawa, Y. Kohori, R. Cubitt, C. D. Dewhurst, J. L. Gavilano, and M. Zolliker. Gap in KFe_2As_2 studied by small-angle neutron scattering observations of the magnetic vortex lattice. *Phys. Rev. B*, 84:024507, Jul 2011.

[109] A. I. Larkin. Effect of inhomogeneities on the structure of the mixed state of superconductors. *Sov. Phys. JETP*, 31:784, 1970.

[110] M. Iavarone, R. Di Capua, G. Karapetrov, A. E. Koshelev, D. Rosenmann, H. Claus, C. D. Malliakas, M. G. Kanatzidis, T. Nishizaki, and N. Kobayashi. Effect of magnetic impurities on the vortex lattice properties in $NbSe_2$ single crystals. *Phys. Rev. B*, 78:174518, Nov 2008.

[111] M. Laver, C. J. Bowell, E. M. Forgan, A. B. Abrahamsen, D. Fort, C. D. Dewhurst, S. Mühlbauer, D. K. Christen, J. Kohlbrecher, R. Cubitt, and S. Ramos. Structure and degeneracy of vortex lattice domains in pure superconducting niobium: A small-angle neutron scattering study. *Phys. Rev. B*, 79:014518, Jan 2009.

[112] M. R. Eskildsen, L. Ya. Vinnikov, T. D. Blasius, I. S. Veshchunov, T. M. Artemova, J. M. Densmore, C. D. Dewhurst, N. Ni, A. Kreyssig, S. L. Bud'ko, P. C. Canfield, and A. I. Goldman. Vortices in superconducting $Ba(Fe_{0.93}Co_{0.07})_2As_2$ studied via small-angle neutron scattering and Bitter decoration. *Phys. Rev. B*, 79:100501, Mar 2009.

[113] H. A. Hanson, X. Wang, I. K. Dimitrov, J. Shi, X. S. Ling, B. B. Maranville, C. F. Majkrzak, M. Laver, U. Keiderling, and M. Russina. Structural evidence for an edge-contaminated vortex phase in a Nb crystal using neutron diffraction. *Phys. Rev. B*, 84:014506, Jul 2011.

[114] M. Yu. Kupriyanov and K. K. Likharev. Microwave impedance of superconductors in the mixed state. *Sov. Phys. JETP*, 41(4):755 – 758, 1975.

[115] E. D. Bauer, R. P. Dickey, V. S. Zapf, and M. B. Maple. Coexistence of superconductivity and ferromagnetism in polycrystalline UGe_2. *J. Phys.: Condens. Matter*, 13(33):L759, 2001.

[116] Dai Aoki, Ilya Sheikin, Tatsuma D. Matsuda, Valentin Taufour, Georg Knebel, and Jacques Flouquet. First Observation of Quantum Oscillations in the Ferromagnetic Superconductor UCoGe. *J. Phys. Soc. Jpn.*, 80(1):013705, 2011.

[117] E. A. Yelland, J. M. Barraclough, W. Wang, K. V. Kamenev, and A. D. Huxley. High-field superconductivity at an electronic topological transition in URhGe. *Nat. Phys.*, 7:890 – 894, 2011.

[118] A. S. Mel'nikov. Dynamics of two-dimensional pancake vortices in layered superconductors. *Phys. Rev. B*, 53:449–456, Jan 1996.

[119] A. S. Mel'nikov. Inertial mass and viscosity of tilted vortex lines in layered superconductors. *Phys. Rev. Lett.*, 77:2786–2789, Sep 1996.

[120] H.-U. Habermeier, G. Cristiani, R.K. Kremer, O. Lebedev, and G. van Tendeloo. Cuprate/manganite superlattices: A model system for a bulk ferromagnetic superconductor. *Physica C: Superconductivity*, 364–365(0):298–304, 2001.

[121] Z. Sefrioui, D. Arias, V. Peña, J. E. Villegas, M. Varela, P. Prieto, C. León, J. L. Martinez, and J. Santamaria. Ferromagnetic/superconducting proximity effect in $La_{0.7}Ca_{0.3}MnO_3/YBa_2Cu_3O_{7-\delta}$ superlattices. *Phys. Rev. B*, 67:214511, Jun 2003.

[122] Todd Holden, H.-U. Habermeier, G. Cristiani, A. Golnik, A. Boris, A. Pimenov, J. Humlíček, O. I. Lebedev, G. Van Tendeloo, B. Keimer, and C. Bernhard. Proximity induced metal-insulator transition in $YBa_2Cu_3O_7La_{2/3}Ca_{1/3}MnO_3$ superlattices. *Phys. Rev. B*, 69:064505, Feb 2004.

[123] V. Peña, Z. Sefrioui, D. Arias, C. Leon, J. Santamaria, J. L. Martinez, S. G. E. te Velthuis, and A. Hoffmann. Giant magnetoresistance in ferromagnet/superconductor superlattices. *Phys. Rev. Lett.*, 94:057002, Feb 2005.

[124] V. K. Malik, I. Marozau, S. Das, B. Doggett, D. K. Satapathy, M. A. Uribe-Laverde, N. Biskup, M. Varela, C. W. Schneider, C. Marcelot, J. Stahn, and C. Bernhard. Pulsed laser deposition growth of heteroepitaxial $YBa_2Cu_3O_7/La_{0.67}Ca_{0.33}MnO_3$ superlattices on $NdGaO_3$ and $Sr_{0.7}La_{0.3}Al_{0.65}Ta_{0.35}O_3$ substrates. *Phys. Rev. B*, 85:054514, Feb 2012.

[125] J. Hoppler, J. Stahn, Ch. Niedermayer, V. K. Malik, H. Bouyanfif, A. J. Drew, M. Rssle, A. Buzdin, G. Cristiani, H.-U. Habermeier, B. Keimer, and C. Bernhard. Giant superconductivity-induced modulation of the ferromagnetic magnetization in a cuprate-manganite superlattice. *Nat. Mater.*, 8:315–319, 2009.

[126] J. Stahn, J. Chakhalian, Ch. Niedermayer, J. Hoppler, T. Gutberlet, J. Voigt, F. Treubel, H-U. Habermeier, G. Cristiani, B. Keimer, and C. Bernhard. Magnetic proximity effect in perovskite superconductor/ferromagnet multilayers. *Phys. Rev. B*, 71:140509, Apr 2005.

[127] A. Hoffmann, S. G. E. te Velthuis, Z. Sefrioui, J. Santamaría, M. R. Fitzsimmons, S. Park, and M. Varela. Suppressed magnetization in $La_{0.7}Ca_{0.3}MnO_3/YBa_2Cu_3O_{7-\delta}$ superlattices. *Phys. Rev. B*, 72:140407, Oct 2005.

[128] D. K. Satapathy, M. A. Uribe-Laverde, I. Marozau, V. K. Malik, S. Das, Th. Wagner, C. Marcelot, J. Stahn, S. Brück, A. Rühm, S. Macke, T. Tietze, E. Goering, A. Frañó, J. H. Kim, M. Wu, E. Benckiser, B. Keimer, A. Devishvili, B. P. Toperverg, M. Merz, P. Nagel, S. Schuppler, and C. Bernhard. Magnetic Proximity Effect in $YBa_2Cu_3O_7/La_{2/3}Ca_{1/3}MnO_3$ and $YBa_2Cu_3O_7/LaMnO_{3+\delta}$ Superlattices. *Phys. Rev. Lett.*, 108:197201, May 2012.

[129] M. A. Uribe-Laverde, D. K. Satapathy, I. Marozau, V. K. Malik, S. Das, K. Sen, J. Stahn, A. Rühm, J.-H. Kim, T. Keller, A. Devishvili, B. P. Toperverg, and C. Bernhard. Depth profile of the ferromagnetic order in a $YBa_2Cu_3O_7/La_{2/3}Ca_{1/3}MnO_3$ superlattice on a LSAT substrate: A polarized neutron reflectometry study. *Phys. Rev. B*, 87:115105, Mar 2013.

[130] N. D. Mathur, M.-H. Jo, J. E. Evetts, and M. G. Blamire. Magnetic anisotropy of thin film $La_{0.7}Ca_{0.3}MnO_3$ on untwinned paramagnetic $NdGaO_3$ (001). *J. Appl. Phys.*, 89(6):3388–3392, 2001.

[131] S. J. Lloyd, N. D. Mathur, J. C. Loudon, and P. A. Midgley. Magnetic domain-wall width in $La_{0.7}Ca_{0.3}MnO_3$ thin films measured using Fresnel imaging. *Phys. Rev. B*, 64:172407, Oct 2001.

[132] Nir Mass, D. Ilzycer, G. Deutscher, G. Desgardin, I. Monot, and M. Weger. Sharp gap edge and determination of the fermi velocity in $Y_1Ba_2Cu_3O_{7-\delta}$ by point contact spectroscopy. *J. Supercond.*, 5(2):191–194, 1992.

[133] A. I. Larkin and Yu. N. Ovchinnikov. Nonlinear conductivity of superconductors in the mixed state. *Sov. Phys. JETP*, 41(5):960 – 965, 1975.

[134] D. Babić, J. Bentner, C. Sürgers, and C. Strunk. Flux-flow instabilities in amorphous $Nb_{0.7}Ge_{0.3}$ microbridges. *Phys. Rev. B*, 69:092510, Mar 2004.

[135] Milind N. Kunchur. Unstable flux flow due to heated electrons in superconducting films. *Phys. Rev. Lett.*, 89:137005, Sep 2002.

[136] S. G. Doettinger, R. P. Huebener, and A. Kühle. Electronic instability during vortex motion in cuprate superconductors. Regime of low and high magnetic fields. *Physica C*, 251(34):285 – 289, 1995.

[137] W. Klein, R. P. Huebener, S. Gauss, and J. Parisi. Nonlinearity in the flux-flow behavior of thin-film superconductors. *J. Low Temp. Phys.*, 61(5-6):413–432, 1985.

[138] K. Torokhtii, N. Pompeo, C. Meneghini, C. Attanasio, C. Cirillo, E.A. Ilyina, S. Sarti, and E. Silva. Microwave Properties of Nb/PdNi/Nb Trilayers. *J. Supercond. Nov. Magn.*, 26(3):571–574, 2013.

[139] Y. Shapira and L. J. Neuringer. Magnetoacoustic attenuation in high-field superconductors. *Phys. Rev.*, 154:375–385, Feb 1967.

[140] E. B. Sonin and K. B. Traito. Surface impedance of a type-ii superconductor in dc magnetic fields parallel and tilted to the superconductor border. *Phys. Rev. B*, 50:13547–13556, Nov 1994.

[141] R. A. Klemm. *Layered Superconductors*, volume 1. Oxford University Press, Oxford, 2012.

[142] A. E. Jacobs. Interaction of Vortices in Type-II Superconductors near T_c. *Phys. Rev. B*, 4:3029–3034, Nov 1971.

[143] Lorenz Kramer. Interaction of vortices in type II superconductors and the behavior near H_{c1} at arbitrary temperature. *Z. Phys.*, 258(5):367–380, 1973.

[144] M.C. Leung. Attractive interaction between vortices in type-ii superconductors at arbitrary temperatures. *J. Low Temp. Phys.*, 12(1-2):215–235, 1973.

[145] E. H. Brandt. Microscopic theory of clean type-II superconductors in the entire field-temperature plane. *Phys. Status Solidi B*, 77(1):105–119, 1976.

[146] U. Klein. Microscopic calculations on the vortex state of type II superconductors. *J. Low Temp. Phys.*, 69(1-2):1–37, 1987.

[147] U. Kumpf. Magnetisierungskurven von Supraleitern zweiter Art mit kleinen Ginzburg-Landau-Parametern. *Phys. Status Solidi (b)*, 44(2):829–843, 1971.

[148] J. Auer and H. Ullmaier. Magnetic Behavior of Type-II Superconductors with Small Ginzburg-Landau Parameters. *Phys. Rev. B*, 7:136–145, Jan 1973.

[149] Ernst Helmut Brandt and Mukunda P. Das. Attractive vortex interaction and the intermediate-mixed state of superconductors. *J. Supercond. Nov. Magn.*, 24(1-2):57–67, 2011.

[150] Victor Moshchalkov, Mariela Menghini, T. Nishio, Q. H. Chen, A. V. Silhanek, V. H. Dao, L. F. Chibotaru, N. D. Zhigadlo, and J. Karpinski. Type-1.5 superconductivity. *Phys. Rev. Lett.*, 102:117001, Mar 2009.

[151] Julien Garaud, Daniel F. Agterberg, and Egor Babaev. Vortex coalescence and type-1.5 superconductivity in Sr_2RuO_4. *Phys. Rev. B*, 86:060513, Aug 2012.

[152] Egor Babaev and Martin Speight. Semi-Meissner state and neither type-I nor type-II superconductivity in multicomponent superconductors. *Phys. Rev. B*, 72:180502, Nov 2005.

[153] A. E. Koshelev and A. A. Golubov. Mixed State of a Dirty Two-Band Superconductor: Application to MgB_2. *Phys. Rev. Lett.*, 90:177002, Apr 2003.

[154] A. I. Buzdin and A. Y. Simonov. Penetration of inclined vortices into layered superconductors. *JETP Letters*, 51(3):191–195, Feb 1990.

[155] V. G. Kogan, N. Nakagawa, and S. L. Thiemann. Interaction of vortices in uniaxial superconductors. *Phys. Rev. B*, 42:2631–2634, Aug 1990.

[156] A. M. Grishin, A. Yu. Martinovich, and S. V. Yampol'skiy. Magnetic field inversion and vortex chains in anisotropic superconductors. *Sov. Phys. JETP*, 70:1089, 1990.

[157] A.I. Buzdin and A.Yu. Simonov. Magnetization of anisotropic superconductors in the tilted magnetic field. *Physica C*, 175(12):143 – 155, 1991.

[158] A.I. Buzdin, S.S. Krotov, and D.A. Kuptsov. Attraction of inclined vortices in magnetic superconductors. *Physica C: Superconductivity*, 175(1 - 2):42 – 46, 1991.

[159] Simon J Bending and Matthew J W Dodgson. Vortex chains in anisotropic superconductors. *J. Phys.: Condens. Matter*, 17(35):R955, 2005.

[160] K. Dichtel. A nonlocal model of a single flux line. *Phys. Lett. A*, 35(4):285 – 286, 1971.

[161] Gert Eilenberger and Helmut Büttner. The structure of single vortices in type II superconductors. *Z. Phys.*, 224(4):335–352, 1969.

[162] X. B. Xu, H. Fangohr, S. Y. Ding, F. Zhou, X. N. Xu, Z. H. Wang, M. Gu, D. Q. Shi, and S. X. Dou. Phase diagram of vortex matter of type-II superconductors. *Phys. Rev. B*, 83:014501, Jan 2011.

[163] X. B. Xu, H. Fangohr, Z. H. Wang, M. Gu, S. L. Liu, D. Q. Shi, and S. X. Dou. Vortex dynamics for low-κ type-II superconductors. *Phys. Rev. B*, 84:014515, Jul 2011.

[164] Shi-Zeng Lin and Xiao Hu. Vortex states and the phase diagram of a multiple-component Ginzburg-Landau theory with competing repulsive and attractive vortex interactions. *Phys. Rev. B*, 84:214505, Dec 2011.

[165] H. J. Zhao, V. R. Misko, and F. M. Peeters. Analysis of pattern formation in systems with competing range interactions. *New Journal of Physics*, 14(6):063032, 2012.

[166] C. Reichhardt, J. Drocco, C.J. Olson Reichhardt, and A.R. Bishop. Statics and dynamics of vortex matter with competing repulsive and attractive interactions. *J. Supercond. Nov. Magn.*, 26(5):2041–2044, 2013.

[167] Jeff E. Sonier, Jess H. Brewer, and Robert F. Kiefl. μSR studies of the vortex state in type-II superconductors. *Rev. Mod. Phys.*, 72:769–811, Jul 2000.

[168] V. E Koronovskyy. Non linear electromagneto-optical effect in epitaxial films of yttrium iron garnet. *Functional materials*, 13:515–518, 2006.

[169] T. Trunk, M. Redjdal, A. Kákay, M. F. Ruane, and F. B. Humphrey. Domain wall structure in Permalloy films with decreasing thickness at the Bloch to Néel transition. *J. Appl. Phys.*, 89(11):7606–7608, 2001.

[170] A. I. Gubin, K. S. Il'in, S. A. Vitusevich, M. Siegel, and N. Klein. Dependence of magnetic penetration depth on the thickness of superconducting Nb thin films. *Phys. Rev. B*, 72:064503, Aug 2005.